ECMWF COPERNICUS REPORT

Copernicus Atmosphere Monitoring Service

Validation report for the CAMS global reanalyses, year 2003

Issued by: KNMI / Henk Eskes

Date: 12/05/2017, draft

Ref: CAMS84_2015SC2_D84.7.1.1_Y1_v0.2

IMPLEMENTED BY ECMWF

Validation report for the CAMS global reanalyses, year 2003

EDITORS:
H.J. ESKES (KNMI), H. CLARK (CNRS-LA), M. SCHULZ (METNO),
Y. CHRISTOPHE (BIRA-IASB), M. RAMONET (LSCE)

AUTHORS:
S. BASART (BSC), A. BENEDICTOW (METNO), A.-M. BLECHSCHMIDT (IUP-UB),
S. CHABRILLAT (BIRA-IASB), E. CUEVAS (AEMET), H. FLENTJE (DWD),
K. M. HANSEN (AU), U. IM (AU), J. KAPSOMENAKIS (AA),
B. LANGEROCK (BIRA-IASB), K. PETERSEN (MPG), A. RICHTER (IUP-UB),
N. SUDARCHIKOVA (MPG), V. THOURET (CNRS-LA), A. WAGNER (MPG),
T. WARNEKE (UBC), C. ZEREFOS (AA)

REPORT OF THE COPERNICUS ATMOSPHERE MONITORING SERVICE, VALIDATION SUBPROJECT.

AVAILABLE AT:
HTTP://ATMOSPHERE.COPERNICUS.EU/

CITATION:
VALIDATION REPORT OF THE CAMS GLOBAL REANALYSIS, YEAR 2003.
H.J. ESKES, H. CLARK, M. SCHULZ, Y. CHRISTOPHE, M. RAMONET, S. BASART, A. BENEDICTOW, A.-M. BLECHSCHMIDT, S. CHABRILLAT, E. CUEVAS, H. FLENTJE, K.M. HANSEN, U. IM, J. KAPSOMENAKIS, B. LANGEROCK, K. PETERSEN, A. RICHTER, N. SUDARCHIKOVA, V. THOURET, A. WAGNER, T. WARNEKE, C. ZEREFOS,
COPERNICUS ATMOSPHERE MONITORING SERVICE (CAMS) REPORT,
CAMS84_2015SC2_D84.7.1.1_Y1_v1.pdf, MAY 2017.

STATUS:
DRAFT, VERSION 0.2 (12 MAY)

DATE:
31/05/2016

1 Executive Summary

The Copernicus Atmosphere Monitoring Service (http://atmosphere.copernicus.eu, CAMS) is a component of the European Earth Observation programme Copernicus. The CAMS system was developed by a series of MACC research projects (MACC I-II-III) until July 2015.

As one of the service products, CAMS will produce a global reanalysis of reactive trace gases, greenhouse gases and aerosol concentrations. The production of the reanalysis has started early 2017, and will be completed in 2018. The CAMS reanalysis will cover the period 2003-2017.

This document presents the validation results for the first year of the reanalysis run, 2003. Updates of this document will appear during the production: there will be updates after year 2 (2004), year 5 (2007), year 10 (2012) and year 15 (2017).

This summary is split according to areas of interest to users: Climate forcing, regional air quality, and stratospheric ozone. Specific attention is given to the ability of the CAMS system to capture events. We furthermore assess the impact of the assimilation of the composition observations by comparing the validation results from the reanalysis to a 'control' configuration without assimilation. The CAMS reanalysis is compared to the previous MACC reanalysis, 2003-2012.

In this report we report biases in ozone. Part of these biases have been attributed to the assimilation of a new 21-layer SBUV satellite product. A new reanalysis run has been initiated using the previous 6-layer SBUV data. This new dataset will be the one that will be publicly available.

Climate forcing

Global Aerosol

The first year of the CAMS reanalysis has been evaluated along with the CAMS control experiment for the year 2003. Detailed results are displayed on a subsection of the AeroCom/CAMS website. Taking the old MACC reanalysis as reference, the following changes with respect to aerosol optical depth (AOD) can be found in the CAMS reanalysis: AOD reductions (-25%) are seen both in Northern hemisphere pollution regions, sea salt and dust regions. Quite a big change in composition is found such as a +90% increase in organic aerosol along with a -36% decrease in sulphate. The sum of sulphate and organic AOD is increased by 5% in CAMS, but the decrease in sea salt (-42%) and dust (-68%) is contributing to the overall reduction in AOD.

Despite the composition change the RMS error against daily Aeronet in 2003 is similar in the CAMS and MACC reanalysis for 2003. The spatial distribution of AOD bias has become more evenly distributed with few spots sticking out. Volcanic aerosol hot spots near Hawaii seem to be responsible for high model outliers. The dust AOD may be too small, showing up in a high bias of the Angstrom coefficient in cases of low Angstrom coefficient. 84% of the Angstrom coefficient values are within a factor of two.

The quality of the CAMS reanalysis, despite or because of the significant shift in the aerosol composition is similar as in the previous MACC reanalysis or the operational CAMS forecast system (o-suite). Globally, no major issues have been found. See section 3.1.1 for more details.

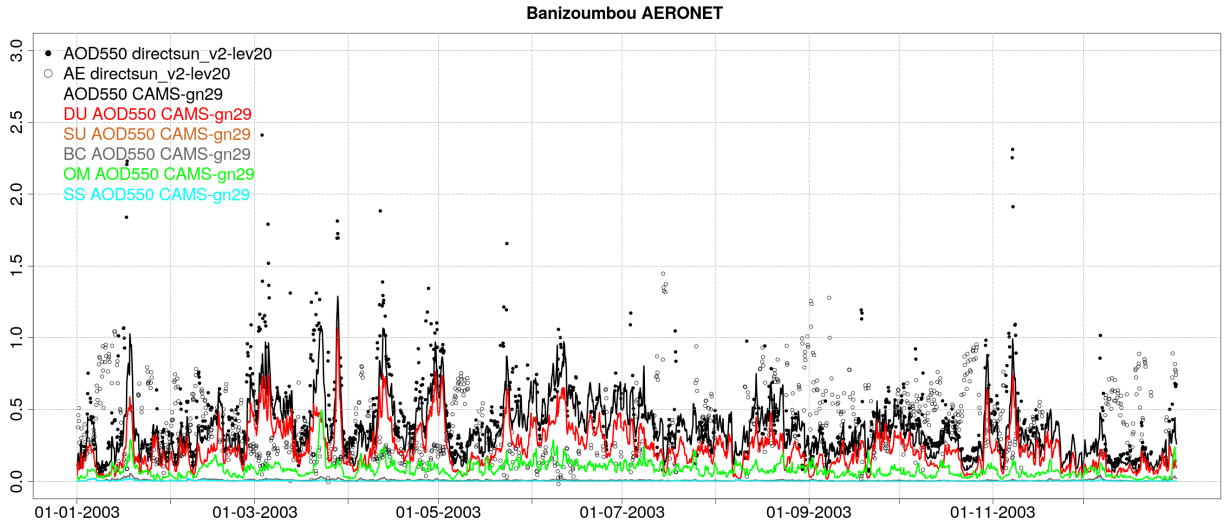

Figure S1. 3-houly AOD and AE Level 2.0 AERONET observations (dots), as well as CAMS AOD compounds (DU: desert dust, SU: sulphate, BC: black carbon, OM: organic matter, SS: sea-salt) over Banizoumbou (Sahel).

Dust

The seasonal dust optical depth (DOD) fields from CAMS reanalysis (gn29) show a distinct seasonal pattern linked to the spatial distribution of dust emissions and transport throughout the year 2003, in good qualitative agreement with ground-based satellite (MODIS and MISR) observations. However, DOD appears underestimated. The DOD comparison with AERONET observations shows that the reanalysis reproduces the annual variability showing an annual correlation coefficient of 0.85 in average for all the AERONET sites. However, the CAMS reanalysis tends to underestimate DOD with an MB of -0.10, RMSE of 0.21 and FGE of 1.34 in average for all the AERONET sites.

Differences between AOD and DOD observed over North Africa and the Middle East, are relatively large and indicate DOD underestimations, which may be linked to enhanced organic matter AOD from biomass burning during wintertime and possibly also to overestimation of secondary organics over heavily populated areas during summertime (see figure S1). This, coupled with low DOD obtained in the control run, makes organic matter a bit too preponderant through the assimilation step.

Tropospheric ozone (O_3)

A positive bias in ozone is observed in the tropics, by comparing with ozone sondes in the free troposphere and GAW observations at the surface. This may be related to the assimilation of the SBUV profiles (to be confirmed). On average the bias against GAW stations is small, but the variation between stations is considerable, with time correlations ranging between 0.3 and 0.9. The models compare well with IAGOS ozone observations in the surface layer and boundary layer. During the period of the 2003 heatwave, the model shows clear enhancements in ozone with a good timing, but the highest ozone values are underestimated (Fig. S2). The results during the heat wave are improved compared to the MACC reanalysis. In the upper troposphere the models overestimate the amount of ozone, with the control generally performing better. Comparisons

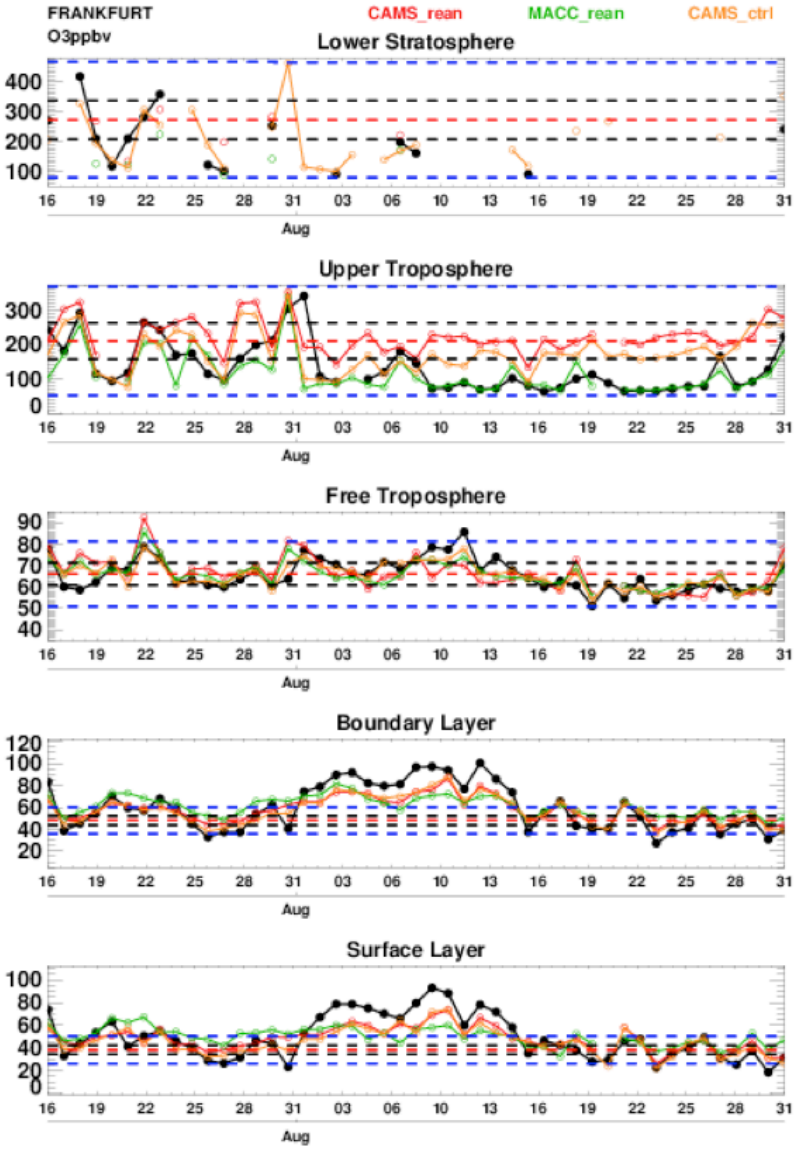

Figure S2. Timeseries of ozone over Frankfurt for the period of the intense heatwave over Europe 16 July- 31 August. Observations are in black, the CAMS reanalysis is in red, the CAMS control in orange and the MACC reanalysis in green. The red dashed line is the mean of the observations from 2003-2012 the black dashed line is 1 sigma from the mean, and the blue dashed line is 3 sigma from the mean.

against European EMEP surface observations confirm the overall improvement of the ozone concentrations (bias, correlations and seasonality) as compared to the MACC reanalysis.

Tropospheric Carbon Monoxide (CO)

Times series of CO total columns from MOPITT v6 and v7 and the 2003 reanalysis over eight selected regions have been compared. The CO total column seasonality in the different regions is in general well reproduced by the reanalysis model, with the exception of May 2003 in the Siberian fire region, where the CAMS reanalysis is higher than the satellite retrievals by ~15%.

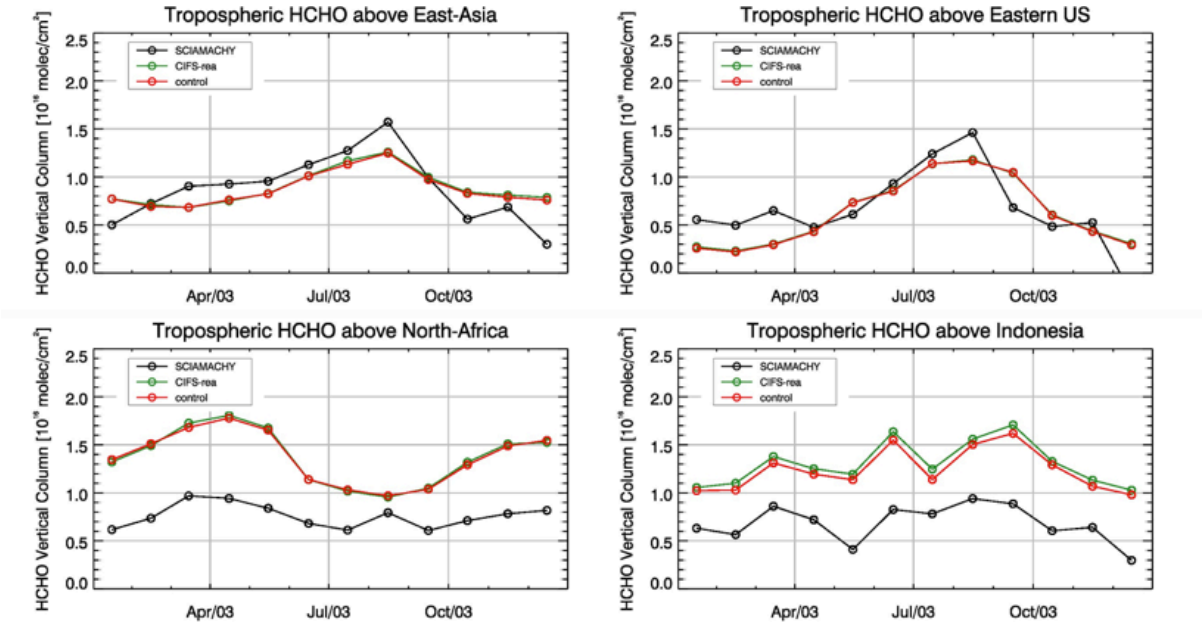

Figure S3. Comparison of time series of tropospheric HCHO columns from SCIAMACHY and model results over selected regions. The regions differ from those used for NO_2 to better focus on HCHO hotspots: East Asia (25-40°N, 110-125°E), Eastern US (30-40°N, 75-90°W), Northern Africa (0-15°N, 15°W-25°E) and Indonesia (5°S-5°N, 100-120°E). Negative satellite retrieved values over Eastern US are due to a lack of data during Northern Hemisphere winter months for this region.

Surface CO for GAW stations is mostly slightly underestimated (with MNMBs between -16% and 12%) by the reanalysis. Similarly, IAGOS data shows that the models underestimate CO in the surface layer, boundary layer and free troposphere. The CAMS reanalysis appears to be better than the MACC reanalysis at capturing the high concentrations of CO in the surface layer over European airports (Frankfurt, Paris, Vienna, Munich) during winter 2003.

Tropospheric Nitrogen dioxide (NO_2)

The CAMS reanalysis performs reasonably well regarding magnitude and seasonality, with the exception of East-Asia, where the reanalysis fails to reproduce observed seasonality. Apart from this, we see similar features as for the operational CAMS system, i.e. stronger shipping signals and overestimation of boreal forest fire emissions (the latter is also the case for HCHO).

Formaldehyde

HCHO concentrations over East-Asia and Eastern-US show a good agreement with SCIAMACHY satellite observations, see Fig. S3. Values over North-Africa and Indonesia are overestimated by a factor of about 2.

Greenhouse gases

(to be added).

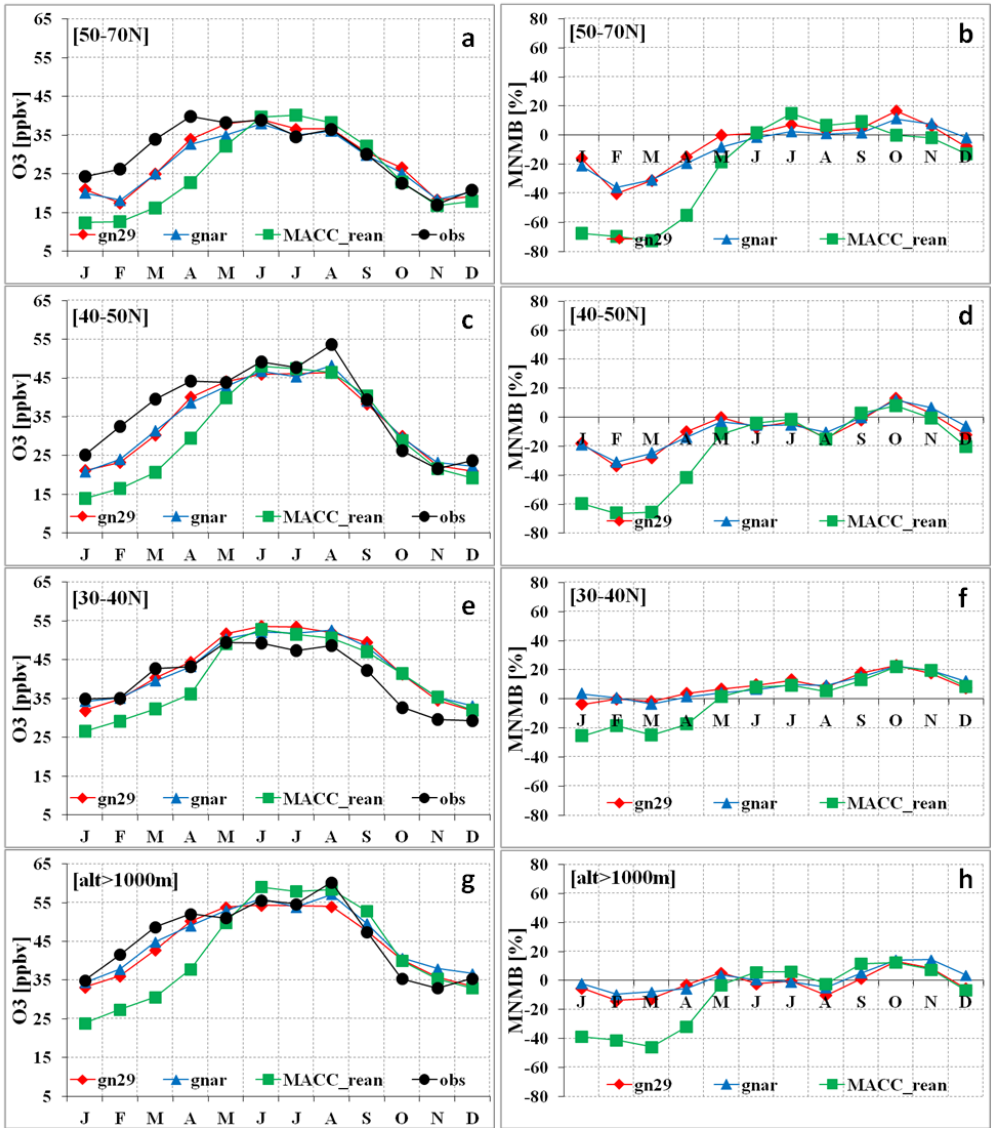

Figure S4. Mean monthly ozone variability for the year 2003 (left) and the MNMBs (right) of the new Reanalysis experiment gn29 (red robs) the control Reanalysis experiment gnar (blue triangles), the MACC reanalysis (green squares), and the EMEP observations (black circles) over Northern Europe (1st row, a and b), Central Europe (2nd row, c and d), Southern Europe (3rd row, e and f) as well as for stations with altitude greater than 1000m a.s.l. (4rd row, g and h)

System performance in the Arctic

Over the three IASOA Arctic surface sites, the simulations are on average in good agreement with the observations apart from the spring ozone depletion events related to halogen chemistry reactions that are not represented in the model simulations. O_3 mixing ratios are slightly overestimated between -5 and 14 % (calculated over the whole period for the GAW arctic sites. The overestimation appears mostly during spring when ozone depletion events are not captured by the model. During fall and winter, the model tends to underestimate O_3. The model shows good correlation during the winter period, whereas during spring and summer, correlation is low. The overall correlation is relatively low, due to the ozone depletion events, between 0.3 and 0.57.

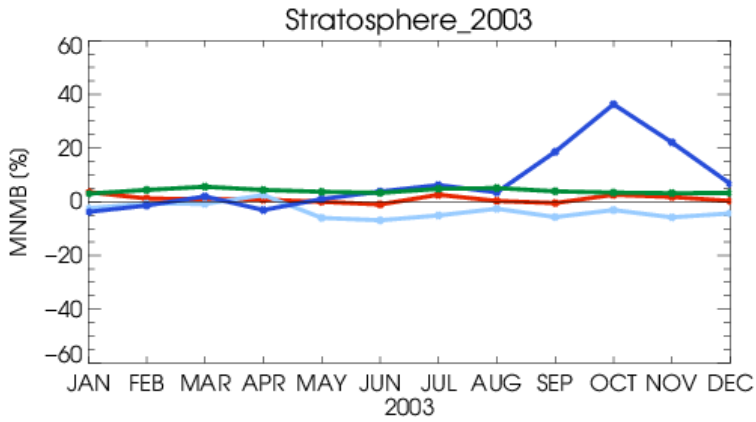

Figure S5: Normalised bias of the reanalysis versus ozone sondes, for 4 regions in the stratosphere (dark blue: Antarctica, light blue: Arctic, red: Northern midlatitudes, green: Tropics). The comparisons are averaged between 90 and 10hPa (for the Tropics 60 and 10hPa).

System performance in the Mediterranean

Aerosol over the Mediterranean

Over the Mediterranean, CAMS reanalysis is able to reproduce the Saharan long-range transport of dust with correlation coefficients of 0.73, 0.78 and 0.82 for Eastern, Central and Western Mediterranean, respectively, in the AOD AERONET comparison. Meanwhile the model tends to underestimate the AOD observations in Northern Mediterranean sites; it overestimates in Southern sites. These overestimations are mainly linked to organic matter production of secondary organics over heavily populated areas during summertime. At surface level, the lack of representative background-rural sites makes qualitative the comparison with PM10 Airbase observations. Relatively close stations (distance less than 100 km) show, in many cases, completely different PM10 behaviour indicating that they are strongly influenced by local factors. Despite these limitations, the comparison highlights the ability of the global reanalysis to detect the impact of desert dust long-range dust transport at ground level and underestimations in the Western Mediterranean during summertime.

Regional air quality

Ozone, CO and aerosol boundary conditions

The comparison of ozone against EMEP surface observations shows a clear improvement as compared to the MACC reanalysis, see Fig. S4.

Ozone layer

Ozone partial columns and vertical profiles

Ozone columns and profiles have been compared with the following observations: vertical profiles from balloon-borne ozonesondes; ground-based remote-sensing observations from the NDACC (Network for the Detection of Atmospheric Composition Change, http://www.ndacc.org); and satellite observations by several limb profiling instruments. Furthermore, the reanalyses are compared with the MACC reanalysis of global atmospheric composition.

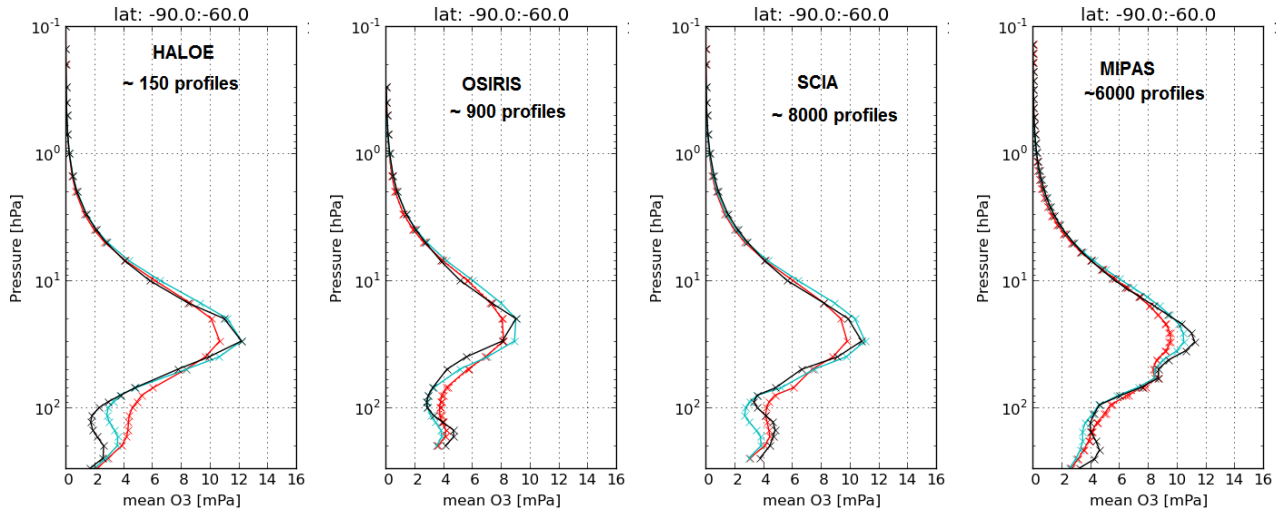

Figure S6: Mean profiles for October 2003 over the South Pole latitude band (90°S-60°S): reanalysis gn29 (red) and MACC (cyan) versus satellite observations (black) using, from left to right: HALOE, OSIRIS, SCIAMACHY and MIPAS.

Compared to ozone sondes the model O_3 partial pressures are within 10% for the whole year, except in the Antarctic during the ozone hole period: in the layer between 90 and 10 hPa during the month of October, ozone is overestimated by 36% on average, see Fig. S5. The sonde comparisons, and a comparison of mean profiles during the ozone hole with 4 satellite datasets (Fig. S6) shows that the disagreement is due to smoother vertical profiles in the reanalysis gn29, which was not the case with the MACC reanalysis. This holds also in the comparison with MIPAS, even though that dataset was assimilated.

Apart from the ozone hole period, the comparison with independent satellite observations is generally in good agreement compared to the spread observed between the instruments.

Other stratospheric trace gases

Due to the lack of stratospheric chemistry in the C-IFS-CB05 scheme, the only useful product in the stratosphere is ozone. Other species, like NO_2, have also been evaluated but the results are only indicative.

Table of Contents

1. Introduction

The Copernicus Atmosphere Monitoring Service (CAMS, http://atmosphere.copernicus.eu/) is a component of the European Earth Observation programme Copernicus. The CAMS global near-real time (NRT) service provides daily analyses and forecasts of trace gas and aerosol concentrations. Apart from these daily analyses, CAMS will produce a global reanalysis covering 15 years (2003-2017). The CAMS system was originally developed by a series of MACC research projects (MACC I-II-III) until it became operational in 2015. The CAMS near-real time and reanalysis services consist of daily analysis and forecasts with the Composition-IFS system with data assimilation of trace gas concentrations and aerosol properties. A second component of CAMS consists of the provision of air-quality forecasts and reanalyses over Europe, based on an ensemble of European air quality models.

This document presents the validation of the global reanalysis during production. The validation methodology and measurement datasets are discussed in Eskes et al. (2015). In this report the performance of the system is assessed in two ways: both the longer-term mean performance (seasonality) as well as its ability to capture events are documented. Table 1.1 provides an overview of the trace gas species and aerosol aspects discussed in this CAMS reanalysis validation report. The reanalysis results are compared with results for a free model run without assimilation, to document the improvements by using the (satellite) observations.

Key CAMS products and their users are: Boundary conditions for regional air quality models (e.g. AQMEII, air quality models not participating in CAMS); Long range transport of air pollution (e.g. LRTAP); Stratospheric ozone column and UV (e.g. WMO, DWD); 3D ozone fields (e.g. SPARC).

As outlined in the MACC-II Atmospheric Service Validation Protocol (2013) and MACC O-INT document (2011), relevant user requirements are quick looks of validation scores, and quality flags and uncertainty information along with the actual data. This is further stimulated by QA4EO (Quality Assurance Framework for Earth Observation, http://www.qa4eo.org) who write that “all earth observation data and derived products is associated with it a documented and fully traceable quality indicator (QI)”. It is our long-term aim to provide such background information. The user is seen as the driver for any specific quality requirements and should assess if any supplied information, as characterised by its associated QI, are "fit for purpose" (QA4EO task team, 2010).

CAMS data are made available to users as data products (grib or netcdf files) and graphical products from ECMWF, http://atmosphere.copernicus.eu/. The stratospheric ozone service is provided by BIRA-IASB at http://copernicus-stratosphere.eu.

A summary of the reanalysis system is given in section 2. Section 3 gives an overview of the performance of the system for various species. Section 4 describes the performance of the system concerning greenhouse gases, and section 5 describes several events. Extended validation for the CAMS forecasts and reanalysis fields can be found online via regularly updated verification pages, http://atmosphere.copernicus.eu/user-support/validation/verification-global-services.
Table 1.2 lists all specific validation websites that can also be found through this link.

Table 1.1: Overview of the trace gas species and aerosol aspects discussed in this CAMS reanalysis validation report. Shown are the datasets assimilated in the CAMS reanalysis (second column) and the datasets used for validation, as shown in this report (third column). Green colors indicate that substantial data is available to either constrain the species in the analysis, or substantial data is available to assess the quality of the analysis. Yellow boxes indicate that measurements are available, but that the impact on the analysis is not very strong or indirect (second column), or that only certain aspects are validated (third column).

Species, vertical range	Assimilation	Validation
Aerosol, optical properties	MODIS Aqua/Terra AOD, AATSR	AOD, Ångström: AERONET, GAW, Skynet, MISR, OMI, lidar, ceilometer
Aerosol mass (PM10, PM2.5)	-	European AirBase stations
O_3, stratosphere	MIPAS, MLS, GOME, SCIAMACHY, GOME-2A, GOME-2B, OMI, SBUV-2	Sonde, lidar, MWR, FTIR, HALOE, GOMOS, OSIRIS, SCIAMACHY, SAGE II
O_3, UT/LS	Indirectly constrained by limb and nadir sounders	MOZAIC, IAGOS, ozone sonde
O_3, free troposphere	Indirectly constrained by limb and nadir sounders	MOZAIC, IAGOS, ozone sonde
O_3, PBL / surface	-	Surface ozone: WMO/GAW, NOAA/ESRL-GMD, AIRBASE, EMEP
CO, UT/LS	-	MOZAIC, IAGOS
CO, free troposphere	MOPITT	MOZAIC, IAGOS, MOPITT, IASI, TCCON
CO, PBL / surface	Indirectly constrained by satellite IR sounders	Surface CO: WMO/GAW, NOAA/ESRL
NO_2, troposphere	SCIAMACHY, OMI, GOME-2A, GOME-2B	SCIAMACHY, GOME-2, MAX-DOAS
HCHO	-	SCIAMACHY, GOME-2, MAX-DOAS
SO_2	GOME-2A, GOME-2B (Volcanic eruptions)	-
Stratosphere, other than O_3	-	SCIAMACHY, GOME-2 (NO_2 column)
CO_2, surface, PBL		ICOS
CO_2, column	SCIAMACHY, IASI, TANSO	TCCON
CH_4, surface, PBL		ICOS
CH_4, column	SCIAMACHY, IASI, TANSO	TCCON

Table 1.2: Overview of quick-look validation websites of the CAMS system.

Reactive gases – Troposphere
GAW surface ozone and carbon monoxide: **http://macc.copernicus-atmosphere.eu/d/services/gac/verif/grg/gaw/gaw_station_ts/** IAGOS tropospheric ozone and carbon monoxide: **http://www.iagos.fr/cams/** Surface ozone from EMEP (Europe) and NOAA-ESRL (USA): **http://www.academyofathens.gr/cams** Tropospheric nitrogen dioxide and formaldehyde columns against satellite retrievals: **http://www.doas-bremen.de/macc/macc_veri_iup_home.html** Tropospheric CO columns against satellite retrievals: **http://cams.mpimet.mpg.de**
Reactive gases - Stratosphere
Stratospheric composition: **http://www.copernicus-stratosphere.eu** NDACC evaluation in stratosphere and troposphere (the NORS server) **http://nors-server.aeronomie.be**
Aerosol
Evaluation against selection of Aeronet stations: **http://www.copernicus-atmosphere.eu/d/services/gac/verif/aer/nrt/** Aerocom evaluation: **http://aerocom.met.no/cgi-bin/aerocom/surfobs_annualrs.pl?PROJECT=MACC&MODELLIST=MACC-VALreports&** WMO Sand and Dust Storm Warning Advisory and Assessment System (SDS-WAS) model intercomparison and evaluation: **http://sds-was.aemet.es/forecast-products/models**
Satellite data monitoring
Monitoring of satellite data usage in the Reanalysis and Near-Real-Time production: **http://copernicus-atmosphere.eu/d/services/gac/monitor/**

The CAMS validation reports are accompanied by the "Observations characterization and validation methods" report, Eskes et al. (2016), which describes the observations used in the comparisons, and the validation methodology. This report can also be found on the global validation page, http://atmosphere.copernicus.eu/user-support/validation/verification-global-services.

2. System summary and model background information

The specifics of the CAMS reanalysis model versions are given (section 2.1). An overview of products derived from this system is given in section 2.3. Several external products used for validation and intercomparison are listed in section 2.4. Timeliness and availability of the CAMS products is given in section 2.5.

2.1 System based on the ECMWF IFS model

Key model information is given on the CAMS reanalysis data-assimilation and its control experiment. Further details on the different model runs and their data usage can be found at http://atmosphere.copernicus.eu/documentation-global-systems and http://atmosphere.copernicus.eu/user-support/operational-info

2.1.1 CAMS reanalysis system

The reanalysis system consists of the C-IFS-CB05 chemistry combined with the CAMS bulk aerosol model. The chemistry is described in Flemming et al. (2015) and Flemming et al. (2017), aerosol is described by Morcrette et al. (2009). The data is stored under experiment ID "**gn29**". The model resolution is T255 with 60 vertical layers. Here a summary of the main specifications of the CAMS reanalysis system is given.

- The meteorological model is based on IFS version cy42r1, with interactive ozone and aerosol in radiation scheme, see also http://www.ecmwf.int/en/forecasts/documentation-and-support/changes-ecmwf-model; the model resolution is T255L60.
- The modified CB05 tropospheric chemistry is used (Williams et al., 2013), originally taken from the TM5 chemistry transport model (Huijnen et al., 2010)
- Stratospheric ozone during the forecast is computed from the Cariolle scheme (Cariolle and Teyssèdre, 2007) as already available in IFS, while stratospheric NOx is constrained through a climatological ratio of HNO_3/O_3 at 10 hPa.
- Monthly mean dry deposition velocities are based on the SUMO model provided by the MOCAGE team.
- Data assimilation is described in Inness et al. (2015) and Benedetti et al. (2009) for chemical trace gases and aerosol, respectively.
- Anthropogenic and biogenic reactive gas emissions are based on MACCity (Granier et al., 2011) and a climatology of the MEGAN-MACC emission inventories (Sindelarova et al., 2014). CO_2 emission are from EDGAR v4.2 (anthropogenic), CHTESSEL (ecosystem), ACCMIP/EDGAR (aviation), Takahashi 2009 (ocean). CH_4 emissions are from LPJ-HYMN (wetland, natural), Bergamaschi 2013 (chemical sinks) and EDGAR v4.2 (anthropogenic).
- NRT fire emissions are taken from GFASv1.2 (Kaiser et al. 2012).

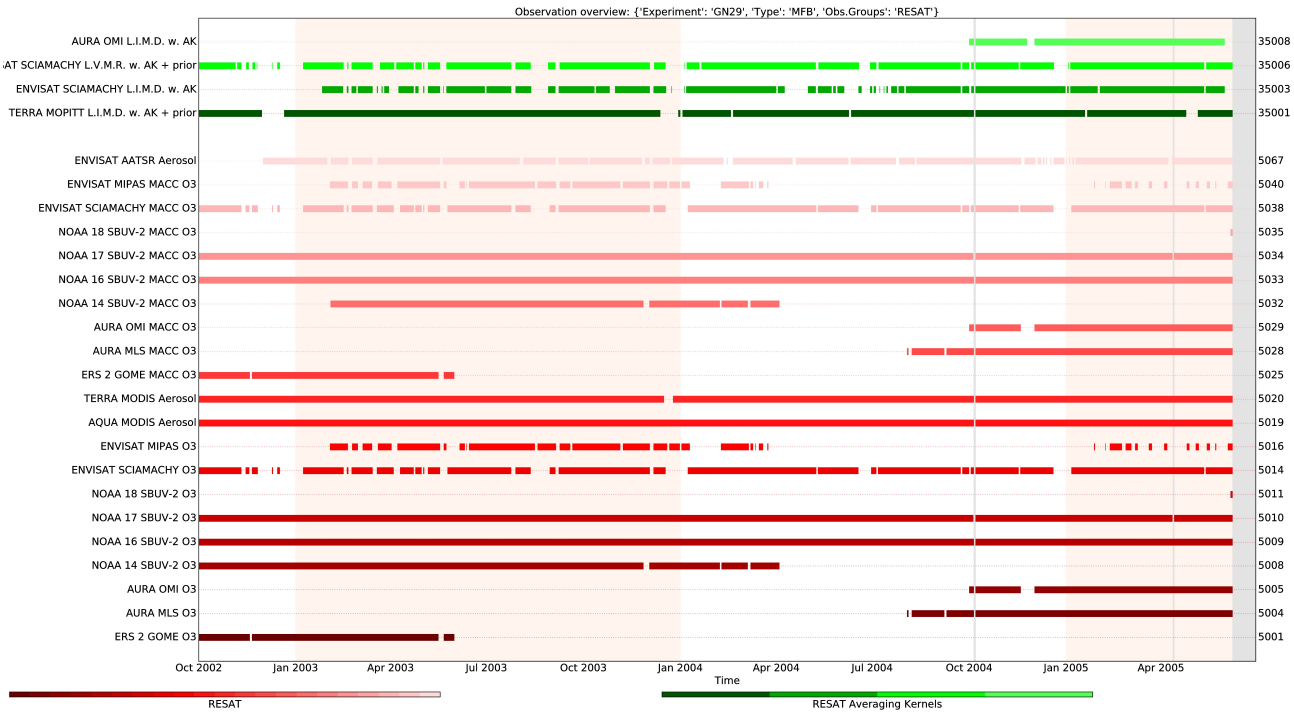

Figure 2.1: Satellite observation usage in the reanalysis, from Oct. 2002 onwards. The top three rows correspond to OMI NO2 (no data for 2003), SCIAMACHY CO2 and CH4, SCIAMACHY NO2.

The following updates were applied to the chemistry:

- update of heterogeneous rate coefficients for N2O5 and HO2 based on clouds and aerosol
- modification of photolysis rates by aerosol
- dynamic tropopause definition based on T profile for coupling to stratosphere and tropospheric mass diagnostics
- Monthly mean VOC emissions calculated by the MEGAN model for all VOCs and for whole period 2003-2015 period.
- bugfixes, in particular for diurnal cycle of dry deposition whose correction has decreased ozone dry deposition (about 15-20%)

The model configuration for GHG is based on the specification of the following components documented in the listed papers below:

- Emissions for CO2 are documented in Agusti-Panareda et al. (2014), Massart et al. (2016).
- Bias correction for CO2 ecosystem fluxes based on the Biogenic Flux Adjustement Scheme is documented by Agusti-Panareda et al. (2016)
- Emissions and loss rate for CH4 is documented in Massart et al. (2014)
- Mass fixer configuration for CO2 and CH4 is documented by Agusti-Panareda et al. (2017)

The aerosol model includes 12 prognostic variables, which are 3 bins for sea salt and desert dust, hydrophobic and hydrophilic organic matter and black carbon, sulphate aerosols and its precursor trace gas SO_2 (Morcrette et al., 2009). Aerosol total mass is constrained by the assimilation of MODIS AOD (Benedetti et al. 2009). A variational bias correction for the MODIS AOD is in place based on the approach used also elsewhere in the IFS (Dee and Uppala, 2009).

Table 2.2: Satellite retrievals of reactive gases, greenhouse gases and aerosol optical depth that are actively assimilated in the reanalysis.

Variable	Instrument	Satellite	Product	Period	AK
O3	SCIAMACHY	Envisat	TC	CCI: 20020803-20120408	no
O3	MIPAS	Envisat	PROF	ESA NRT: 20030127- 20030720 MARS ESA NRT: 20030721-20040326 CCI: 20050127-20120331	no
O3	GOME	ERS2	PROF	20021001-20030531	no
O3	MLS	Aura	PROF	V4: 20040803-20151231 NRT: 20160101 -	no
O3	OMI	Aura	TC	KNMI reproc: 20041001-20150531 NRT:	no
O3	GOME-2	Metop-A	TC	BIRA CCI or GDP 4.8	no
O3	GOME-2	Metop-B	TC	BIRA CCI or GDP 4.8	no
O3	SBUV/2	NOAA-16	PC 21L	v8.6 ODB2	no
O3	SBUV/2	NOAA-17	PC 21L	v8.6 ODB2	no
O3	SBUV/2	NOAA-18	PC 21L	v8.6 ODB2	no
O3	SBUV/2	NOAA-19	PC 21L	NRT: 20130829 -	no
CO	MOPITT	Terra	TC	V6: 20020101-20151231 NRT: 20160101-	yes
NO2	SCIAMACHY	Envisat	TRC	v1p: 20030101-20101231 v2:20110101-20120409	yes
NO2	OMI	Aura	TRC	COL3: 20041001-20101231 DOM: 20110101-20121231 NRT: 20130101 -20140430 NRT SAPP: 20140501 -	yes
NO2	GOME-2	Metop-A	TRC		yes
NO2	GOME-2	Metop-B	TRC		yes
AOD	AATSR	Envisat	TC	CCI: 20021201-20120331	no
AOD	MODIS	Terra	TC	COL6: 20021001-20151231	no
AOD	MODIS	Aqua	TC	COL6: 20021001-20151231	no
CO2	SCIAMACHY	Envisat	TC	CCI: 20021001	yes
CO2	IASI	Metop-A	TC		yes
CO2	Tanso	GOSAT	TC		yes
CH4	SCIAMACHY	Envisat	TC		yes
CH4	IASI	MetoP-A	TC		yes
CH4	IASI	Metop-B	TC		yes
CH4	Tanso	GOSAT	TC		yes

2.1.2 Control

The control run (expver="**gnar**") applies the same settings as the reanalysis, based on the coupled C-IFS-CB05 system with CAMS aerosol for cy42r1, except that data assimilation is not switched on. It consists of 24h cycling forecasts.

2.2 Other systems

2.2.1 The MACC reanalysis and CAMS forecasts

The previous reanalysis was produced during the MACC project. This reanalysis is available through the CAMS website, or ECMWF archive with EXP='rean', CLASS='mc'.

In a few places the performance of the reanalysis is compared with the CAMS operational forecasts/analyses. This system is sometimes referred to as CAMS "o-suite".

2.2.2 BASCOE

The NRT analyses and forecasts of ozone and related species for the stratosphere, as delivered by the Belgian Assimilation System for Chemical ObsErvations (BASCOE) of BIRA-IASB (Lefever et al., 2014; Errera et al., 2008), are used as an independent model evaluation of the CAMS products. The NRT BASCOE product is the ozone analysis of Aura/MLS-SCI level 2 standard products, run in the following configuration (version 05.07):

- The following species are assimilated: O_3, H_2O, HNO_3, HCl, HOCl, N_2O and ClO.
- It lags by typically 4 days, due to latency time of 4 days for arrival of non-ozone data from Aura/MLS-SCI (i.e. the scientific offline Aura/MLS dataset).
- Global horizontal grid with a 3.75° longitude by 2.5° latitude resolution.
- Vertical grid is hybrid-pressure and consists in 86 levels extending from 0.01 hPa to the surface.
- Winds, temperature and surface pressure are interpolated in the ECMWF operational 6-hourly analyses.
- Time steps of 20 minutes, output every 3 hours

See the stratospheric ozone service at http://www.copernicus-stratosphere.eu/.
It delivers graphical products dedicated to stratospheric composition and allows easy comparison between the results of o-suite, BASCOE and TM3DAM. The BASCOE data products (HDF4 files) are also distributed from this webpage. Other details and bibliographic references on BASCOE can be found at http://bascoe.oma.be/. A detailed change log for BASCOE can be found at http://www.copernicus-stratosphere.eu/4_NRT_products/3_Models_changelogs/BASCOE.php.

2.2.3 TM3DAM and the multi-sensor reanalysis

One of the MACC products was a 30-year reanalysis, near-real time analysis and 10-day forecast of ozone column amounts performed with the KNMI TM3DAM data assimilation system, the Multi-Sensor Reanalysis (MSR) system (van der A et al., 2010, 2015),
http://www.temis.nl/macc/index.php?link=o3_msr_intro.html.
The corresponding validation report can be found at
http://www.copernicus-atmosphere.eu/services/gac/global_verification/validation_reports/.

The NRT TM3DAM product used for the validation of the CAMS NRT streams is the ozone analysis of Envisat/SCIAMACHY (until April 2012), AURA/OMI, and MetOp-A/GOME-2, run in the following configuration:

- total O_3 columns are assimilated
- Global horizontal grid with a 3° longitude by 2° latitude resolution.
- Vertical grid is hybrid-pressure and consists in 44 levels extending from 0.1 hPa to 100 hPa.
- Dynamical fields from ECMWF operational 6-hourly analysis.

An update of the MSR (MSR-2) was presented in van der A et al. (2015), which extended the record to 43 years based on ERA-interim reanalysis meteo and with an improved resolution of 1x1 degree.

2.2.4 SDS-WAS multimodel ensemble

The World Meteorological Organization's Sand and Dust Storm Warning Advisory and Assessment System (WMO SDS-WAS) for Northern Africa, Middle East and Europe (NAMEE) Regional Center (http://sds-was.aemet.es/) started its activities in 2012. During this period, the Regional Center has established a protocol to routinely exchange products from dust forecast models and observations (i.e. ground-based and satellite aerosol products) as the basis for both near-real-time and delayed common model evaluation.

Global and regional dust models for international operational and research institutions are currently providing daily operational dust forecasts (i.e. dust optical depth, DOD, and dust surface concentration). Different multi-model products are generated from the different prediction models. Two products describing centrality (multi-model median and mean) and two products describing spread (standard deviation and range of variation) are daily computed. In order to generate them, the model outputs are bi-linearly interpolated to a common grid mesh of 0.5º x 0.5º. The SDS-WAS multi-model DOD (at 550 nm) Median from available dust prediction models participating in the SDS-WAS Regional Center is used for the validation of the CAMS NRT streams. The updated list of dust models participating in the model intercomparison can be found at https://sds-was.aemet.es/forecast-products/forecast-evaluation/model-inter-comparison-and-forecast-evaluation/

The current routine evaluation of dust predictions is focused on total-column dust optical depth (DOD) and uses remote-sensing retrievals from sun-photometric (AERONET) and satellite (MODIS) measurements.

2.3 CAMS reanalysis product

The CAMS 3D reanalysis products are stored as 3-hourly fields and will update the MACC global reanalysis which is also available on the CAMS website, http://atmosphere.copernicus.eu/. The new reanalysis will also be made available through this CAMS website. The following fields are archived:

- Forecast fields: From 0z, 3-hourly, step=0,3,.., 48
- Analysis fields: Every 3 hours, e.g. 0z, 3z,...21z
- Surface forecast fields: From 0z, 1-hourly, step=0,1,2,...,48

3. Validation results for reactive gases and aerosol

This section describes the validation results of the CAMS global reanalysis for aerosols and reactive gases for the year 2003 (the first year of the CAMS reanalysis). Naming and color-coding conventions predominantly follow the scheme as given in Table 3.1.

Table 3.1 Naming and color conventions.

Name in figs	experiment	Color
{obs name}	{obs}	black
CAMS reanalysis	0001	red
Control	geuh, gjjh	blue
MACC reanalysis	rean, class=mc	green

3.1 Aerosol

3.1.1 Global aerosol distribution

The global aerosol fields are analysed both for the reanalysis and a control simulation. For comparison the previous MACC reanalysis is used. More detailed results can be found on the AeroCom/CAMS website (http://aerocom.met.no/cgi-bin/aerocom/surfobs_annualrs.pl?PROJECT=CAMS&MODELLIST=CAMS-reanalysis) in the CAMS reanalysis section.

The evaluation in table 3.1.1 shows the average global AOD and speciated AOD for the three experiments in 2003 and illustrates a shift from MACC to CAMS in aerosol composition. The control experiment shows the lowest AOD, consistently with the current CAMS operational model version (o-suite), indicating a model version which is gaining aerosol mass and AOD through assimilation, not in balance with the emissions. Changes in total AOD are relatively smaller than the increase in organic AOD and the decrease in dust AOD. The decrease in total AOD is due to reductions in dust, sulphate and seasalt AOD. Figure 3.1.1 and 3.1.2. show where the changes occur. Volcanic eruptions add sulphate near Hawaii and Middle America, seen as little hot spots on the map. These high values in GN29 near Hawaii lead to some outliers in figure 3.1.3., where Aeronet measures much smaller values on average, indicating an overestimation of the volcanic derived sulphate. The scatterplots in figure 3.1.3 show all possible comparisons for 2003, as daily and monthly aggregates. CAMS AOD at Aeronet sites is larger than MACC, while it is smaller on global average. The aerosol dispersion is less pronounced in CAMS, which is also visible in smaller AOD at polar locations (figure 3.1.1) than in MACC. Overall performance of the CAMS and MACC reanalysis is very good and rather similar, despite significant changes in aerosol composition. Figure 3.1.4 shows the regional bias with reduced bias over North America. Figures 3.1.5 and 3.1.6 further illustrate a shift to finer particles, with more organic aerosol, less dust and sea salt, leading to similar total AOD distribution as in the MACC reanalysis.

Table 3.1.1: Mean annual, global total and speciated aerosol optical depth (AOD) in the IFS experiment GN29 (new CAMS reanalysis), the CNTRL experiment GNAR and MACC reanalysis experiment (FBOV) for year 2003.

	CAMS rean	Control	MACC rean
AOD@550	0.144	0.110	0.168
BC-OD@550	0.006	0.004	0.008
Dust-OD@550	0.018	0.023	0.036
OA-OD@550	0.052	0.032	0.024
SO4-OD@550	0.034	0.022	0.044
SS-OD@550	0.034	0.029	0.055

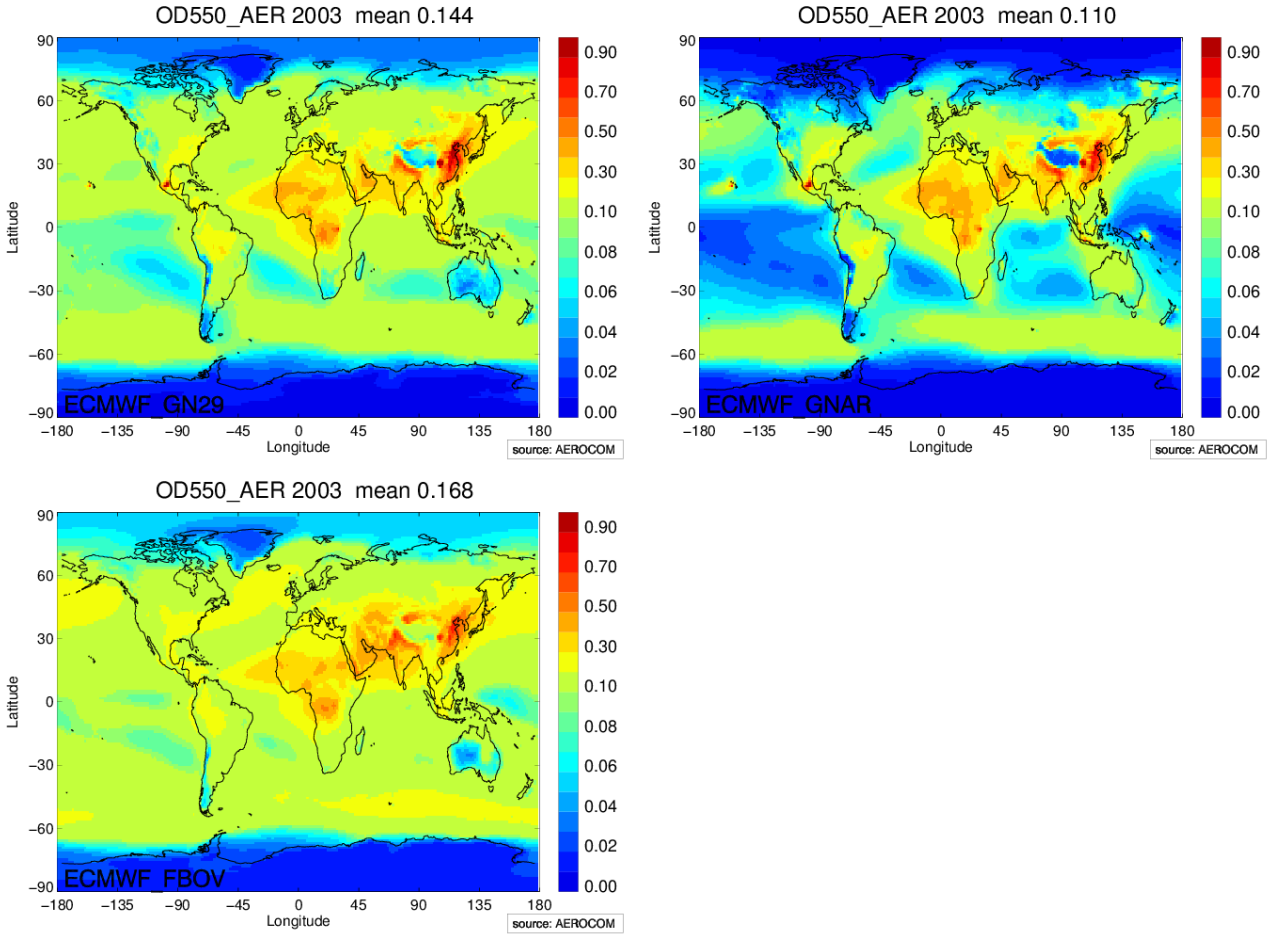

Figure 3.1.1: Averaged aerosol optical depth (AOD) from IFS experiments CAMS GN29 (left), GNAR (cntrl run) (right) and MACC FBOV (bottom) for the year 2003. Mean AOD in GN29 is at 0.144, which is 16% less than what was in the earlier MACC reanalysis FBOV. Reductions are seen both in Northern hemisphere pollution regions and dust regions.

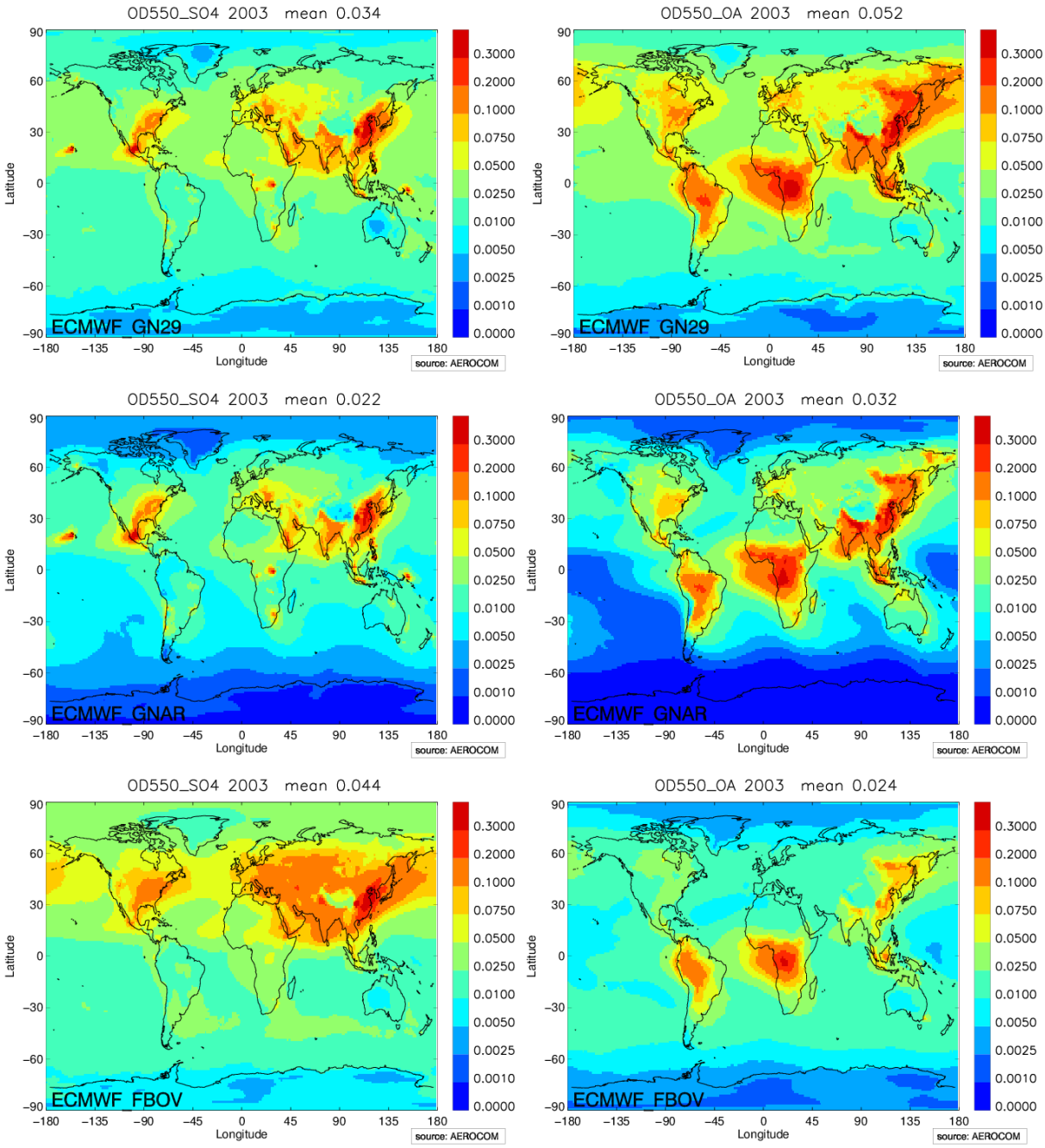

Figure 3.1.2: Averaged sulfate optical depth in left column (GN29 (top), cntrl run GNAR (middle) and MACC (bottom)) and organic aerosol optical depth (right column), for the year 2003. While sulphate AOD was dominating over organic aerosol AOD in the MACC reanalysis, mean AODs of the two components are opposite in the GLS8 reanalysis (sulphate AOD: 0.034, organic AOD: 0.048). An important shift in aerosol composition appears when comparing GN29 and MACC. The sum of sulphate and organic AOD has increased by 25% in GN29, but a larger decrease in dust and sea salt is finally contributing to the overall decrease in AOD.

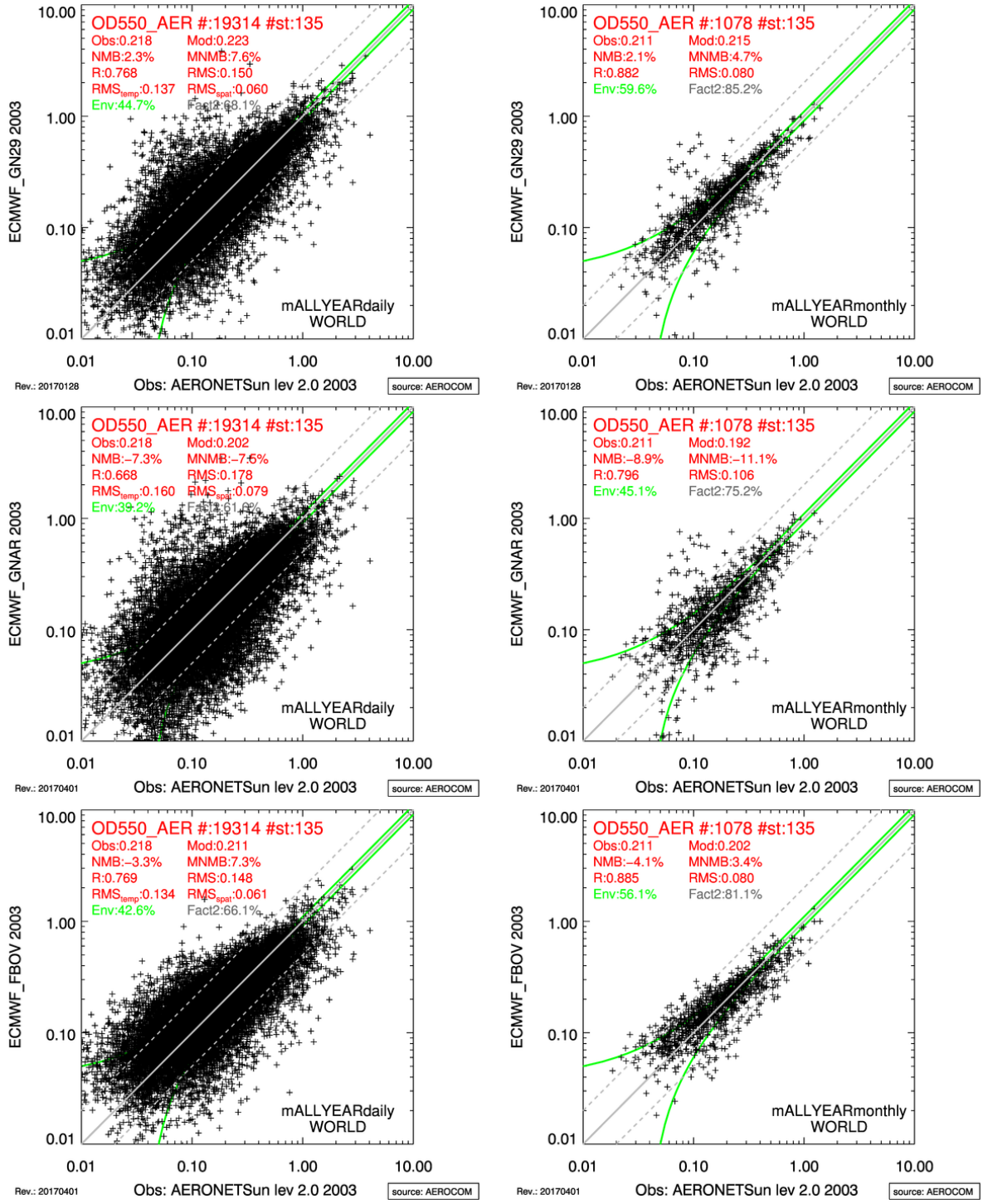

Figure 3.1.3: Evaluation of simulated daily (left column) and monthly (right column) AOD against Aeronet level 2.0 sun photometer measurements in GN29 (top), cntrl run GNAR (middle) and MACC (FBOV, bottom) for the year 2003. Statistics shown in the figure show very similar results for MACC and GN29, except a small negative bias in MACC has become a small positive bias in GN29. The quality of the IFS GN29 experiment, despite or because of the significant shift in the aerosol composition is as good as MACC. The CNTRL run GNAR has lower bias and the temporal-spatial RMS errors are larger.

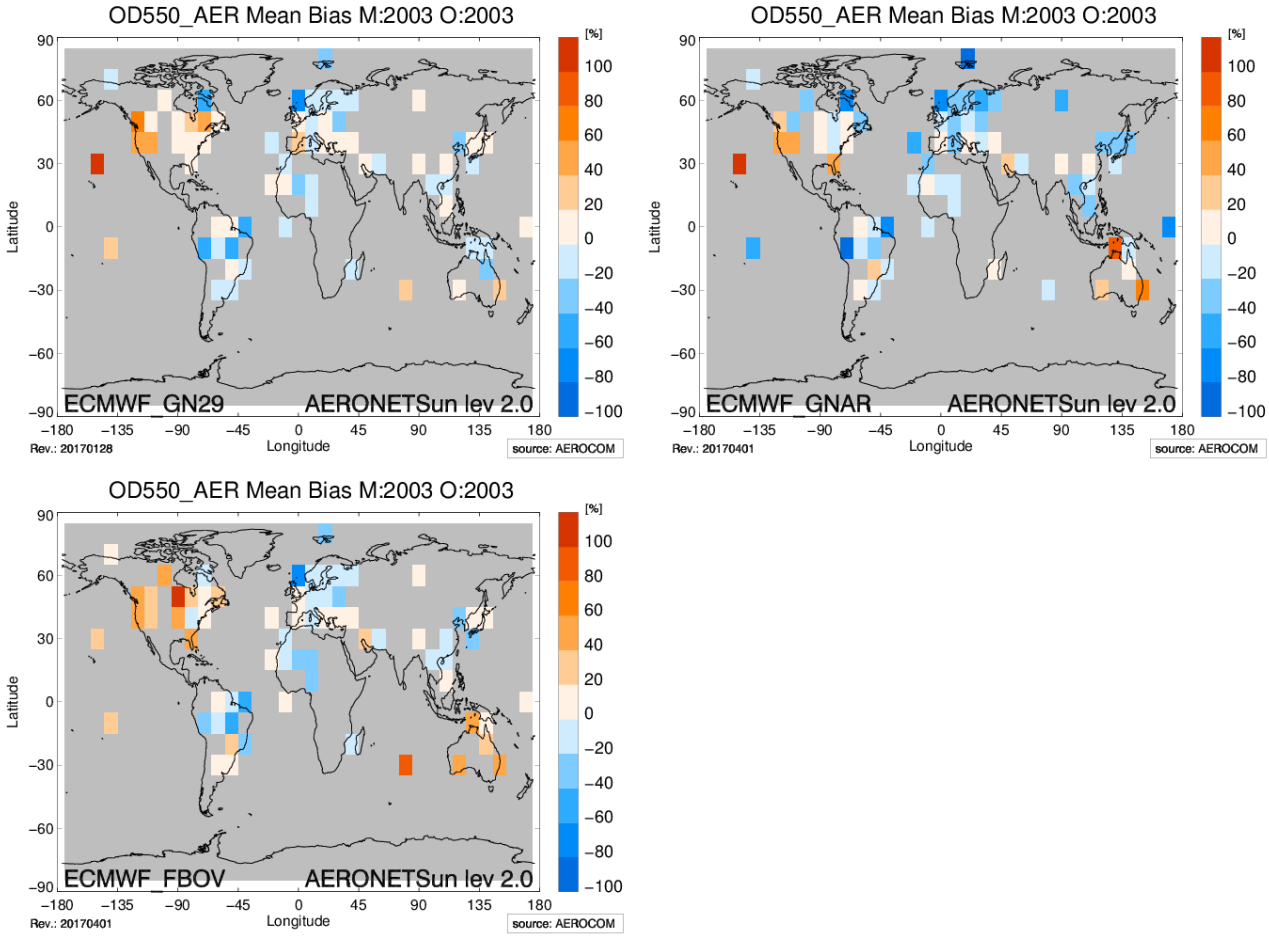

Figure 3.1.4: Regional relative mean bias of simulated daily AOD against Aeronet sun level 2.0 sun photometer measurements in GN29 (left), cntrl run GNAR (right) and MACC (bottom) for the year 2003. The regions with positive bias are reduced in the GN29 and GNAR experiments. More regions exhibit a bias of only +-20%, supporting that the GN29 experiment, despite or because of the significant shift in the aerosol composition is better than both MACC and GNAR.

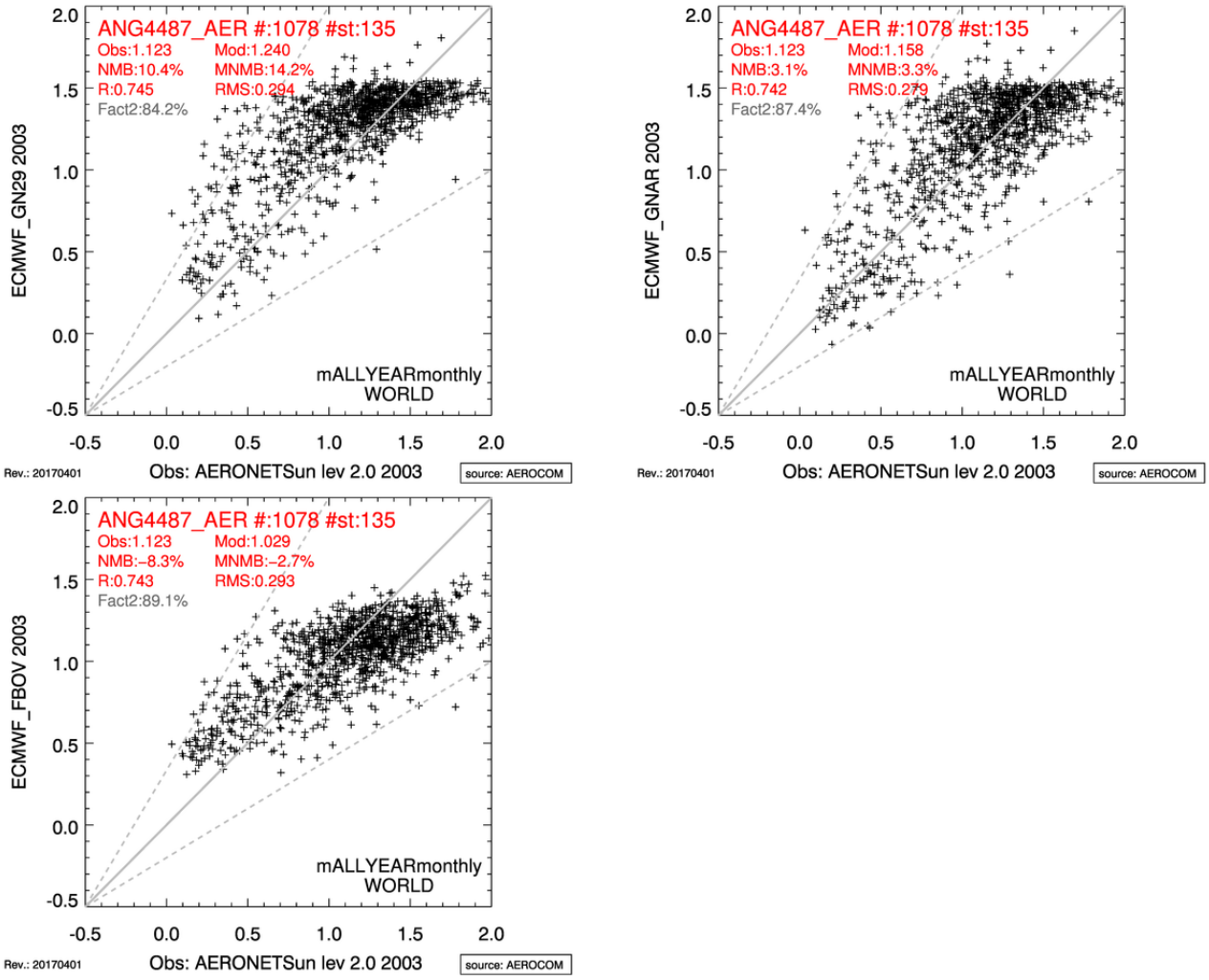

Figure 3.1.5: Evaluation of simulated daily Angstroem Coefficient against Aeronet sun level 2.0 photometer measurements in GN29 (left), cntrl run GNAR (right) and FBOV (bottom) for the year 2003. Statistics shown in the figure show a similar temporal-spatial RMS error reduction in both FBOV and GN29. The MNMB-bias increased from -2.7% in FBOV to +14.2% in GN29.

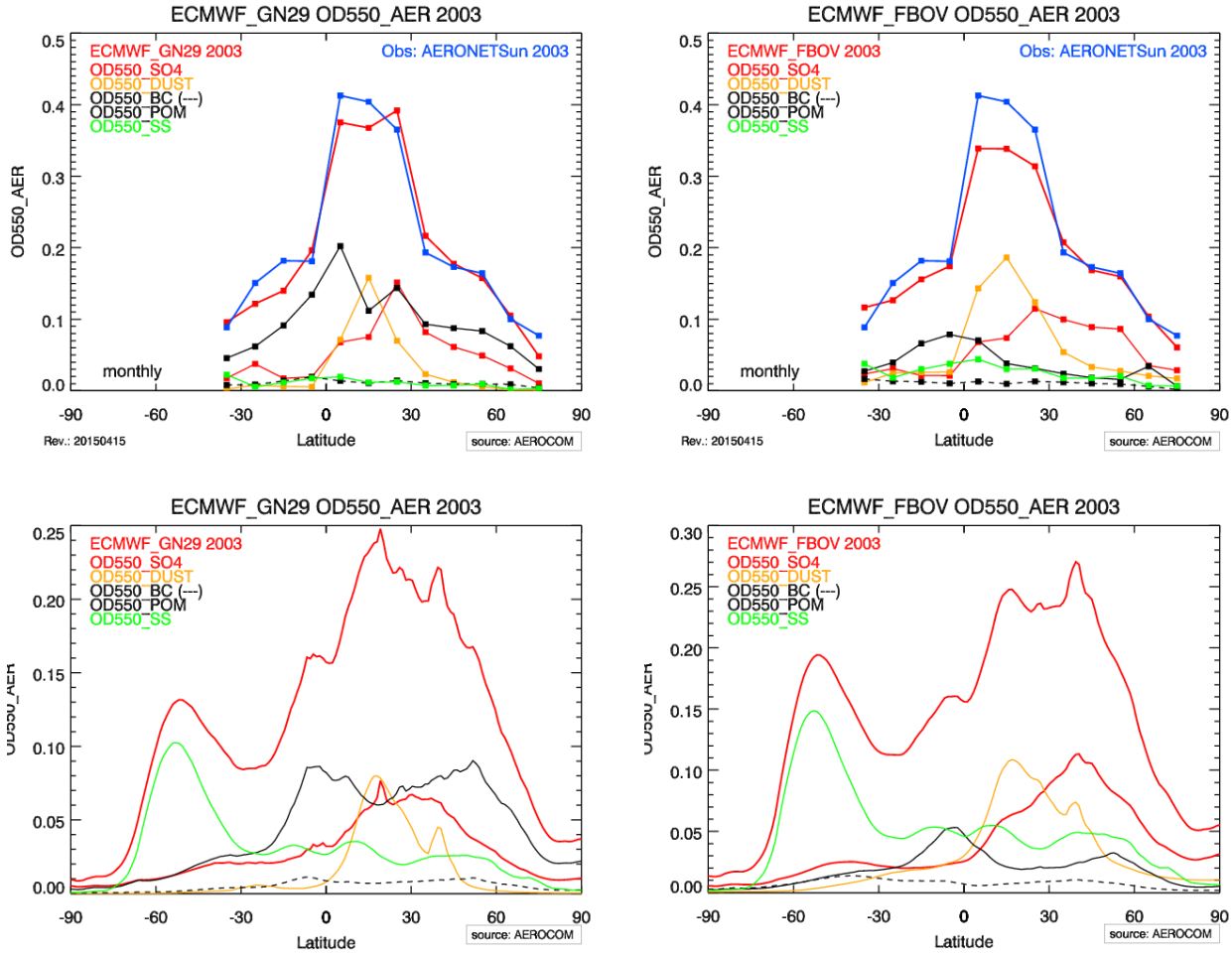

Figure 3.1.6: Upper row: Evaluation of latitudinal distribution of AOD in GN29 (left) and previous MACC reanalysis FBOV (right) for the year 2003. Total AOD from model (dark red upper curve) at Aeronet sites against total AOD from Aeronet (dark blue curve), aggregated as mean for 10 degree latitude bands, AOD speciation at Aeronet sites split in sulphate (red), dust (brown), black carbon (black dashed), organic (black) and sea salt (green); Lower row: Mean AOD in model against latitude. Total AOD (upper red curve), speciation as in upper row figures.

3.1.2 Dust model intercomparison over North Africa, Middle East and Europe

The seasonal DOD fields from CAMS reanalysis (gn29) show a distinct seasonal pattern linked to the spatial distribution of dust emissions and transport throughout the year 2003, in good qualitative agreement with both the MODIS Terra/Aqua and MISR AOD observations (Figure 3.1.7). The Bodéle, as well as the desert dust sources in Mauritania, Maghreb, Saudi Arabia and Oman, are systematically underestimated throughout the year. However, this new experiment also tends to underestimate AOD in comparison with observations, particularly over the subtropical and tropical North Atlantic (see Figure 3.1.7 and Capo Verde in Figure 3.1.8) as well as over the Red Sea, the Gulf of Oman and the Arabian Sea (see Figure 3.1.7). The most striking result is the big difference between AOD and DOD from CAMS precisely in desert areas (i.e. the Sahara and the Middle East) where mineral dust aerosol unambiguously dominates.

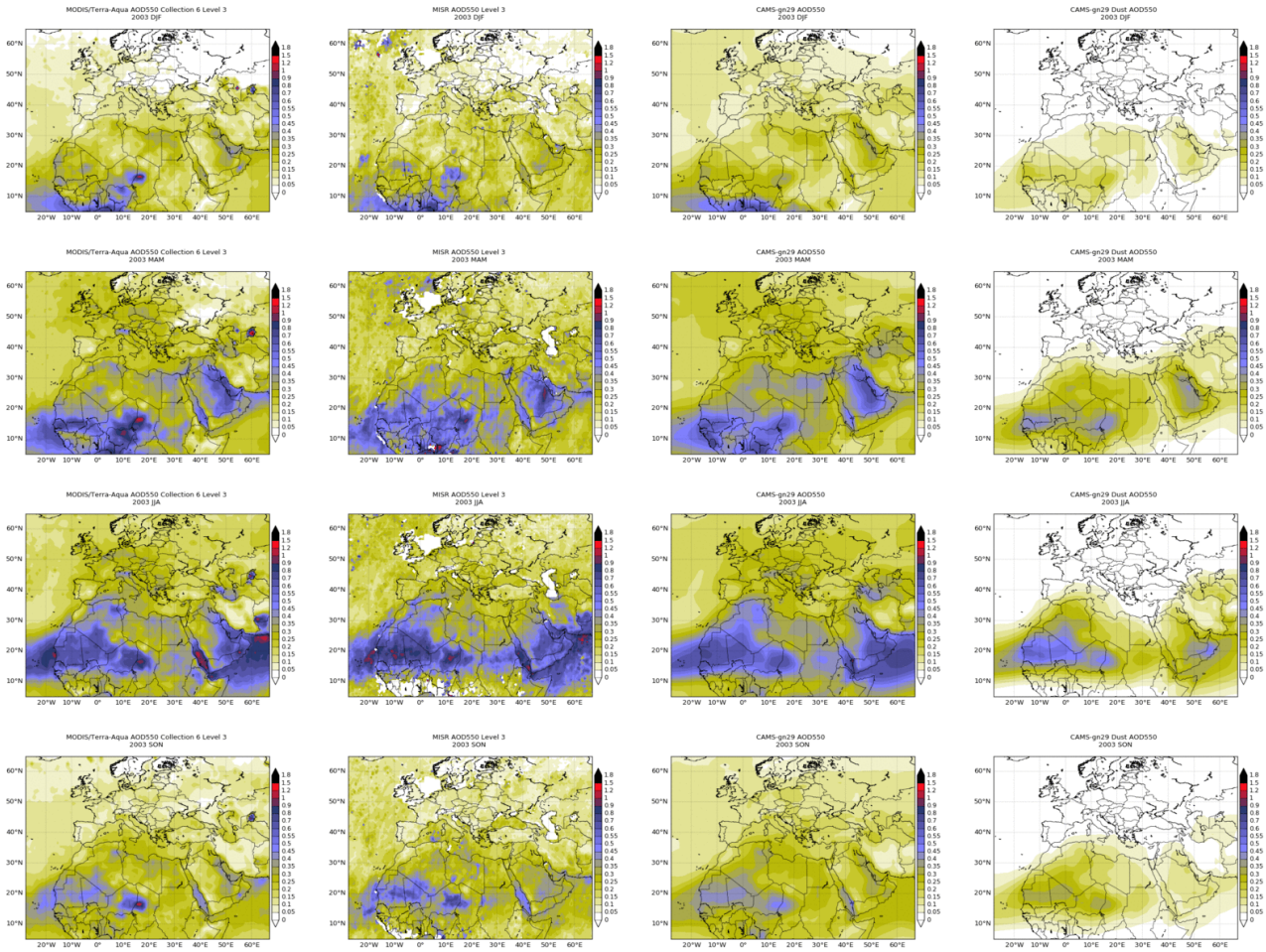

Figure 3.1.7: Seasonal averaged AOD from MODIS Collection 6 Terra/Aqua merged Dark target and Deep Blue Level 3 daily 1º x 1º global product (first column), MISR monthly Level 3 monthly 0.5º x 0.5º global product (second column) as well as AOD (third column) and DOD from CAMS-gn29 reanalysis (fourth column)(on 3-hourly basis) for the year 2003. Winter (DJF), spring (MAM), summer (JJA) and autumn (SON) from upper to lower rows.

The DOD comparison with AERONET quality-assured dust-filtered AOD Version 2 observations (i.e. DOD, on *3-hourly basis*, see selected available sites for 2003 in Figure 3.1.8) shows that the reanalysis reproduces rather well the annual variability showing an annual correlation coefficient of 0.85, in average, for all the AERONET sites, with maximum of 0.88 in Tropical North Atlantic and minimum of 0.71 in the Sahel and Western Mediterranean. However, CAMS reanalysis tends to underestimate DOD with an MB of -0.10, RMSE of 0.21 and FGE of 1.34 in average for all the AERONET sites. The south-to-north gradient observed in the RMSE and FGE (see Figure 3.1.8) is associated with the lower DOD values towards northern latitudes.

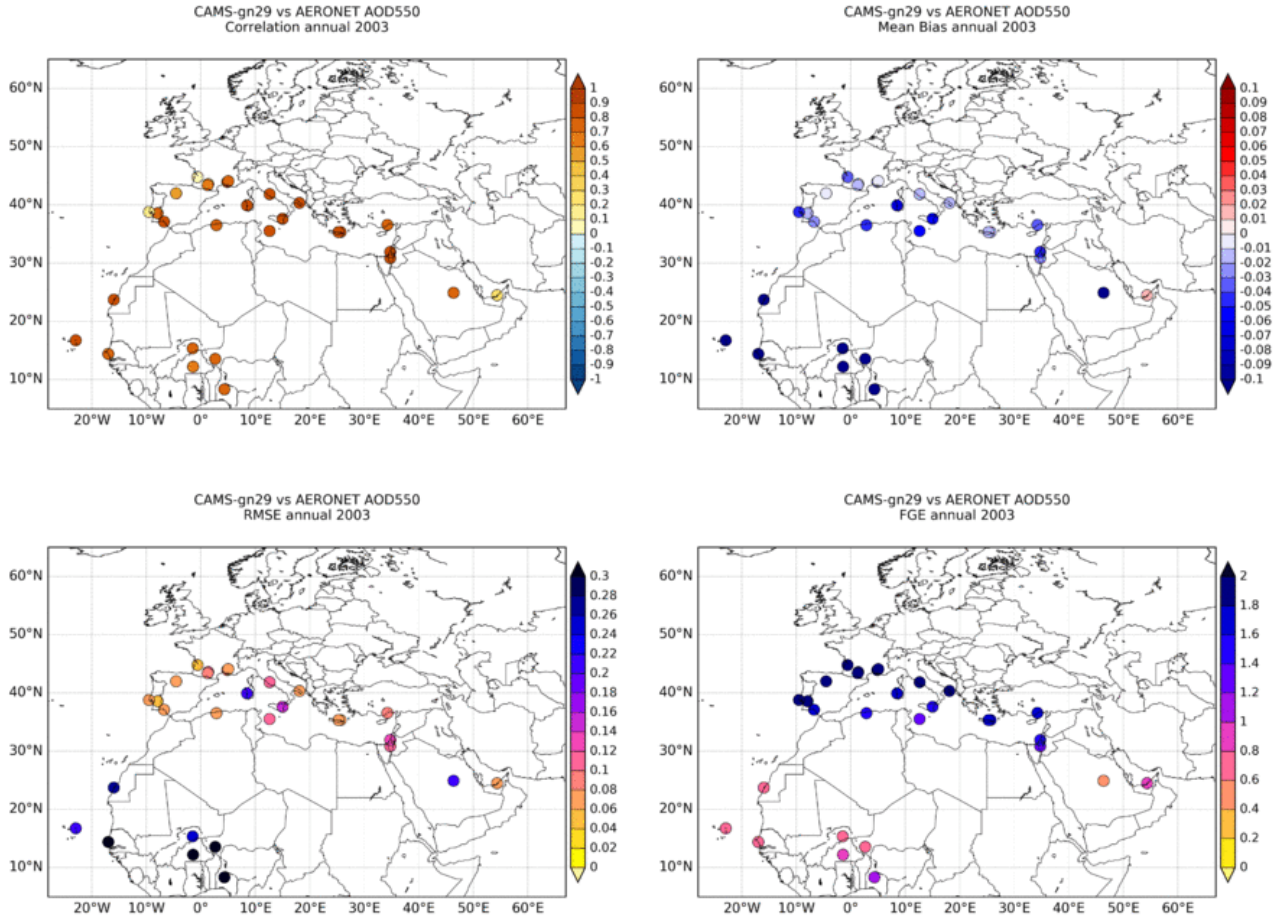

Figure 3.1.8: Skill scores (MB, FGE, RMSE and r) of DOD CAMS reanalysis (on 3-hourly basis) for the year 2003. DOD from AERONET Version 2 quality-assured is obtained applying a filter for dust; i.e. when the Angström exponent (AE) is less or equal to 0.75. All data with AE larger than 1.2 are considered free of dust (DOD = 0 is assumed). Values of AE between 0.75 and 1.2 are associated with mixed aerosols and are not included in the evaluation.

The comparison with AERONET (see Figure 3.1.9) shows that differences between AOD and DOD observed over the North Africa and Middle East (causing strong DOD underestimations) are linked to an overestimation of organic matter (OM) from biomass burning during wintertime and also to overestimation of secondary organics over heavily populated areas during summertime. This, coupled with low DOD obtained in the control run (not shown here), makes OM a bit too preponderant through the assimilation step and hence, providing low DOD values which are clearly underestimated.

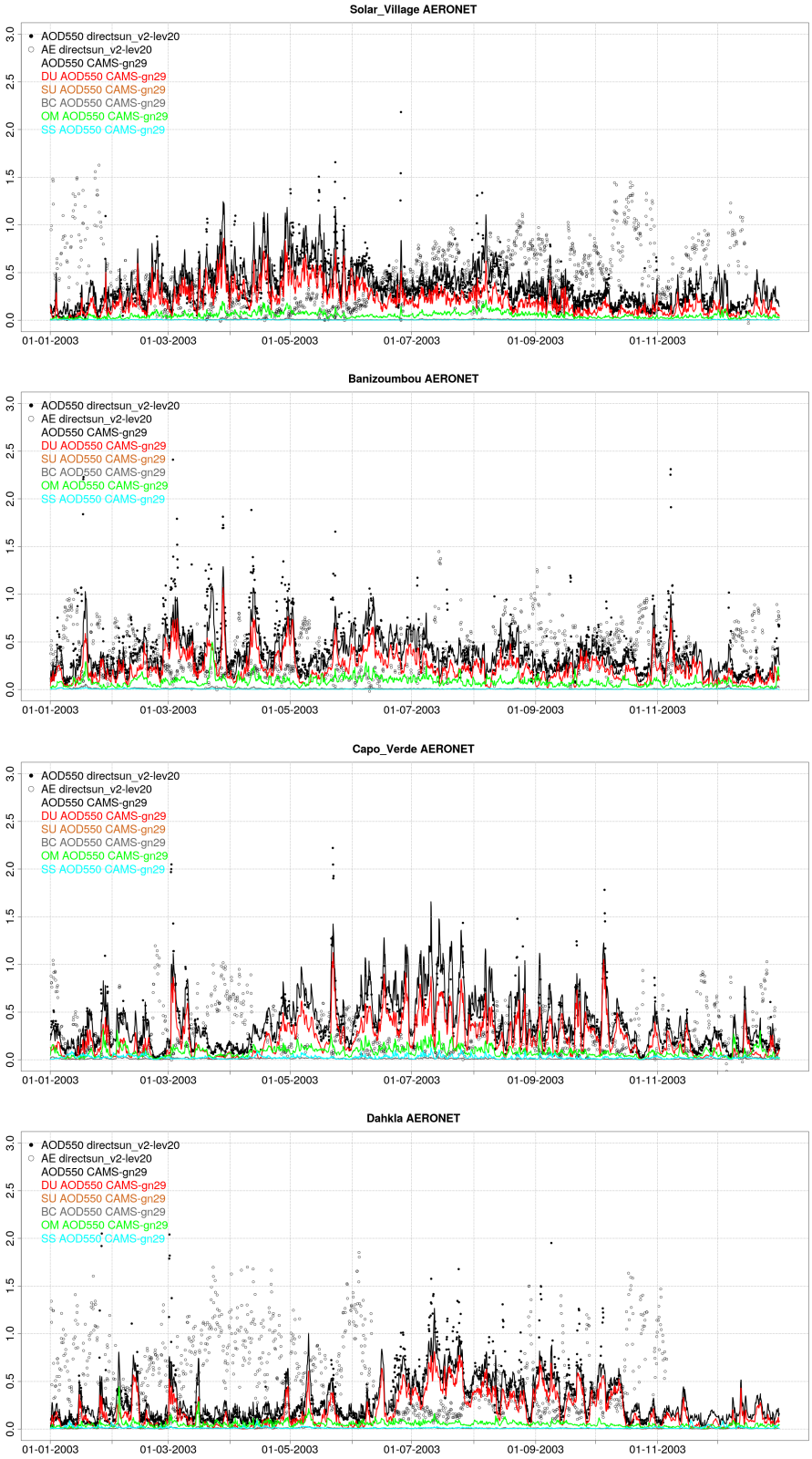

Figure 3.1.9: 3-houly AOD and AE Level 2.0 AERONET observations (dots), as well as CAMS AOD compounds (DU: desert dust, SU: sulphate, BC: black carbon, OM: organic matter, SS: sea-salt) over Solar Village (Middle East), Banizoumbou (Sahel), Capo Verde (Tropical North Atlantic) and Dahkla (NW Maghreb).

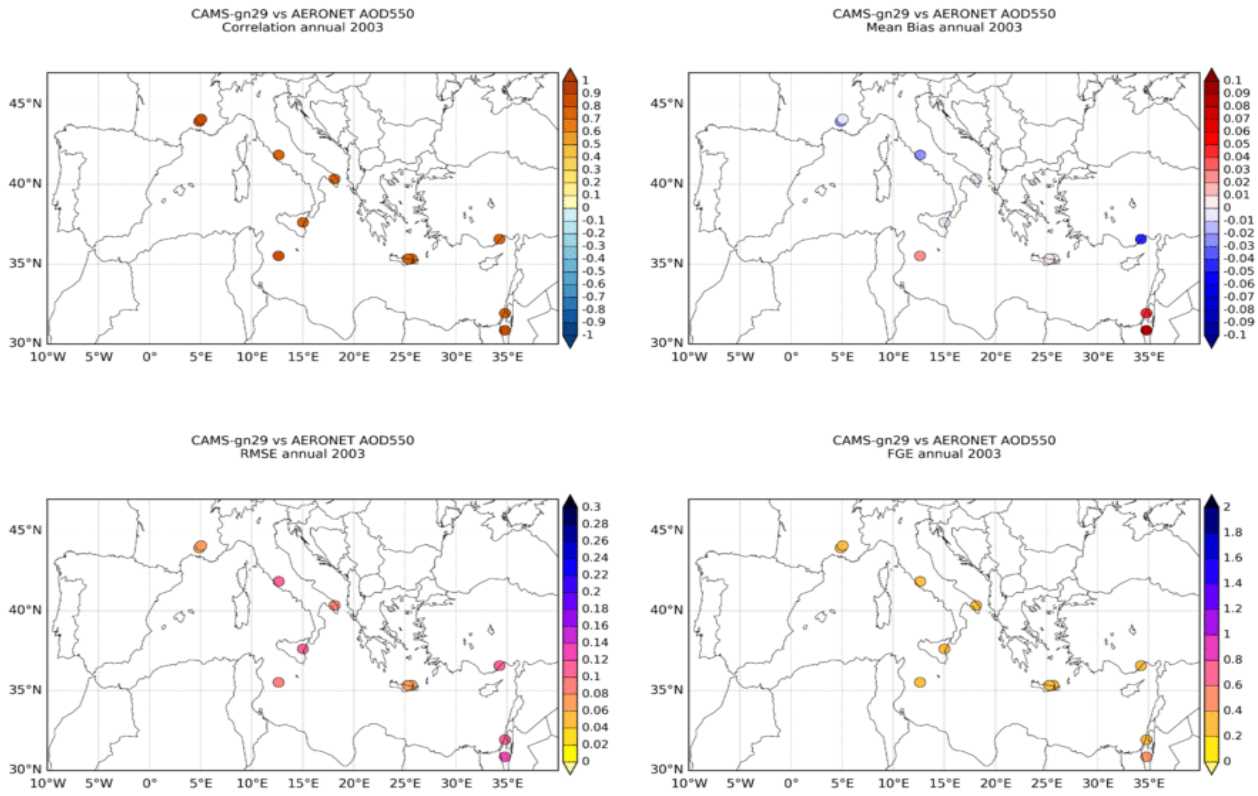

Figure 3.1.10: Skill scores (MB, FGE, RMSE and r) of CAMS reanalysis (on 3-hourly basis) for the year 2003 using AOD from AERONET Version 2 quality-assured is the reference.

3.1.3 Aerosol validation over the Mediterranean

Over the Mediterranean, CAMS reanalysis matches well the 3-hourly AOD variability of AERONET quality-assured observations (see Figure 3.1.10) with a correlation coefficient of 0.73, 0.78 and 0.82 for Eastern, Central and Western Mediterranean, respectively. In general, the model reproduces the highest AOD peaks, which are associated with desert dust intrusions (see Figure 3.1.11) although it underestimates their magnitude. While the model tends to underestimate the AOD observations in Northern Mediterranean sites, it overestimates in Southern sites (see MB in Figure 3.1.10). These overestimations are mainly linked to OM production of secondary organics over heavily populated areas during summertime when secondary processes are favoured (see Sede Boker in Figure 3.1.11).

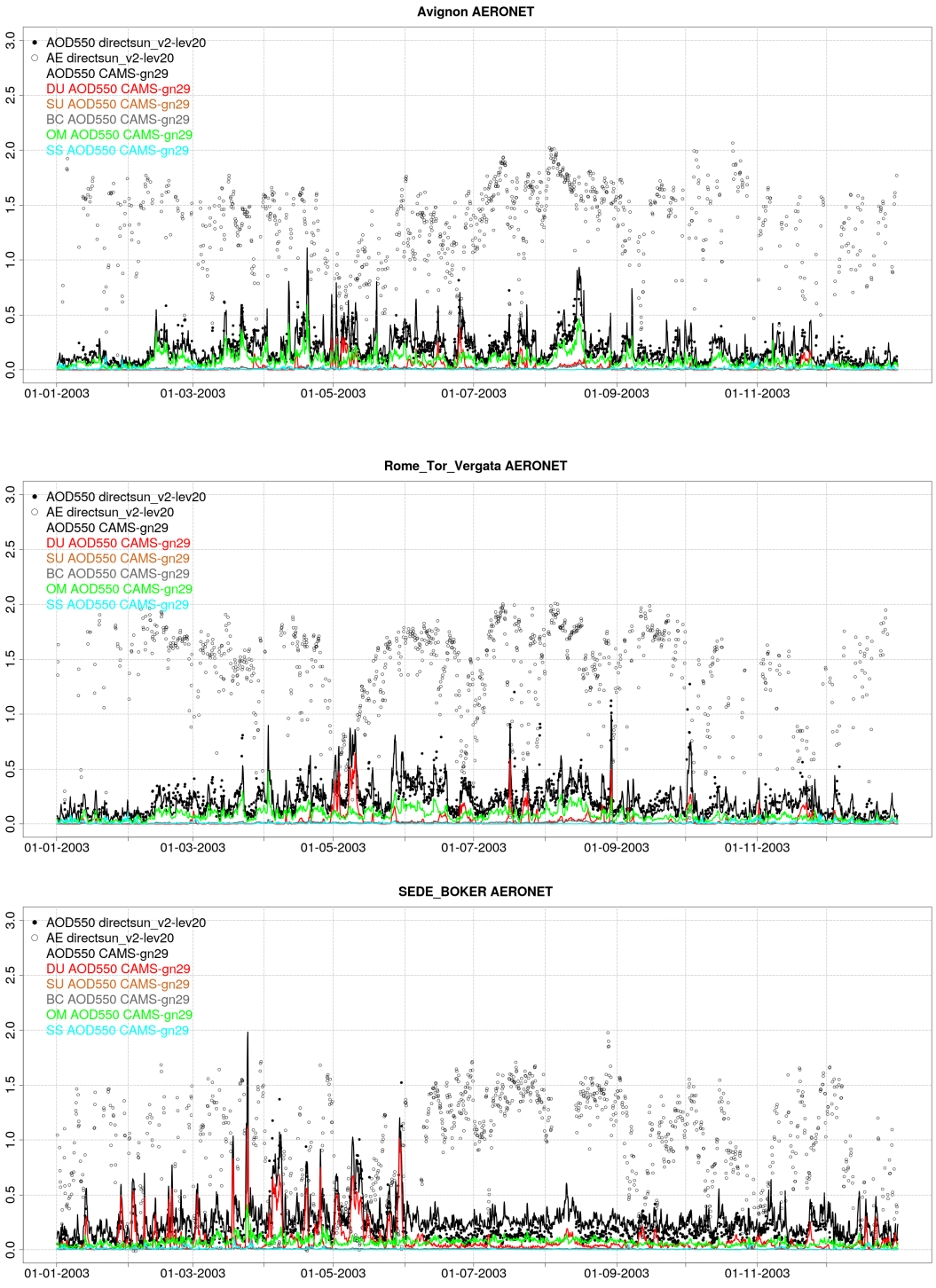

Figure 3.1.11: 3-houly AOD and AE Level 2.0 Direct-Sun AERONET observations (dots), as well as CAMS AOD compounds (DU: desert dust, SU: sulphate, BC: black carbon, OM: organic matter, SS: sea-salt) over Avignon (Western Mediterranean), Rome Tor Vergata (Central Mediterranean) and Forth Crete (Eastern Mediterranean).

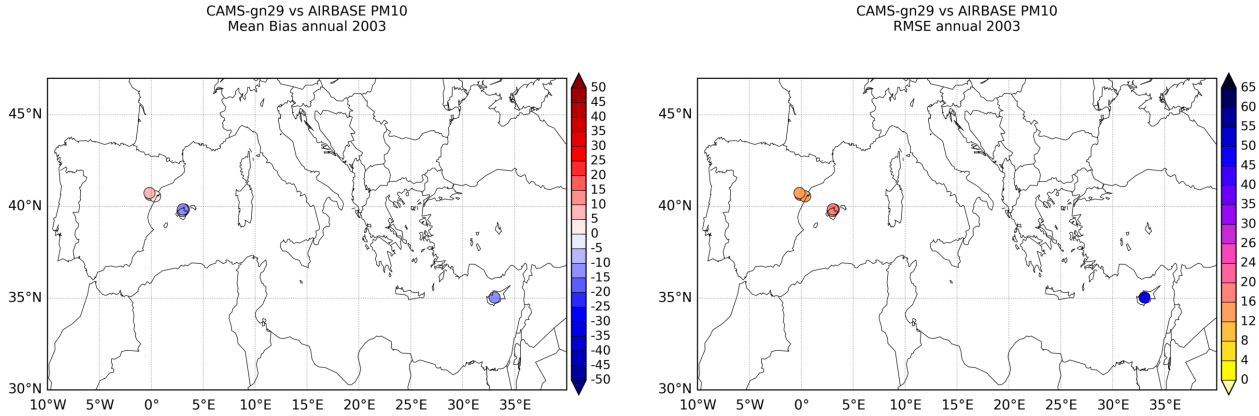

Figure 3.1.12: Skill scores (MB and RMSE) of PM10 from the CAMS reanalysis (on daily basis) for the year 2003 using Airbase observations (from the Openaire project). Only background available suburban and rural stations are displayed.

The CAMS reanalysis is compared against 7 Airbase background-rural sites (on daily basis) provided within the Openair project (www.openair-project.org/). The comparison is based on PM10 observations because no PM2.5 dataset is available for 2003. At surface level, CAMS reanalysis tends to underestimate the Airbase observations (with a MB of -6.73 µg/m3 in average for all available sites) although overestimations are observed in Eastern Iberian Peninsula sites (see MB in Figure 3.1.12 throughout the whole year (see Zorita station in Figure 3.1.13). Otherwise, negative MB values are observed over Majorca in the Balearic Islands (see Figure 3.1.12). Although these sites are categorized as background-rural sites in the Airbase catalogue, they are under the influence of anthropogenic emissions. One of them is close to the city harbor, and the other two are quite near to urban areas. Despite of this, the comparison of the model with this set of sites shows higher underestimations during summertime (see Sa Pobla station in Figure 3.1.13) when secondary processes are favoured and the maritime traffic in the region is enhanced. In Eastern Mediterranean, stronger underestimations are also observed during summertime, although CAMS reanalysis reproduces the maximum daily PM10 peaks of Airbase observations associated to desert dust outbreaks (see early-April of Ayia Marina site in Eastern Mediterranean in Figure 3.1.13).

Figure 3.1.13: Daily PM10 Airbase observations (black dots), as well as CAMS PM10 and PM2.5 over Ayia Marina (Cyprus, Eastern Mediterranean), Sa Pobla (Mallorca, Balearic Islands) and Zorita (Eastern Iberian Peninsula) sites for the year 2003.

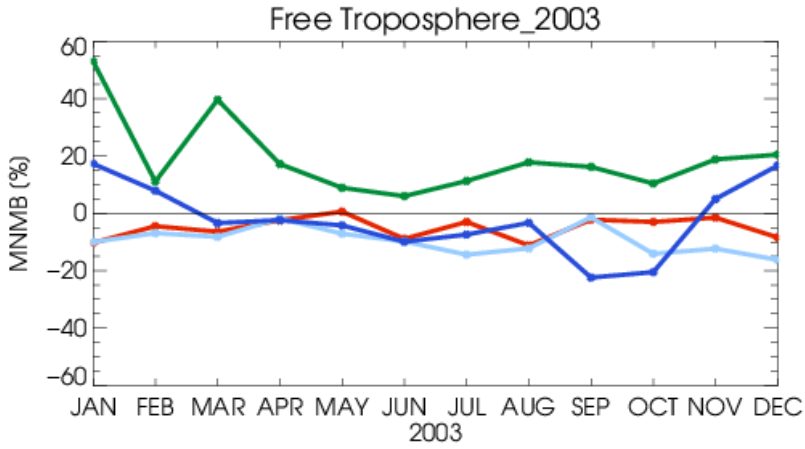

Figure 3.2.1. Ozone MNMBs (model minus ozone sondes, for all 4 regions in the free troposphere, averaged between 750 and 350 hPa (tropics: 750 and 200 hPa) (dark blue: Antarctica, light blue: Arctic, red: Northern mid-latitudes, green: Tropics)

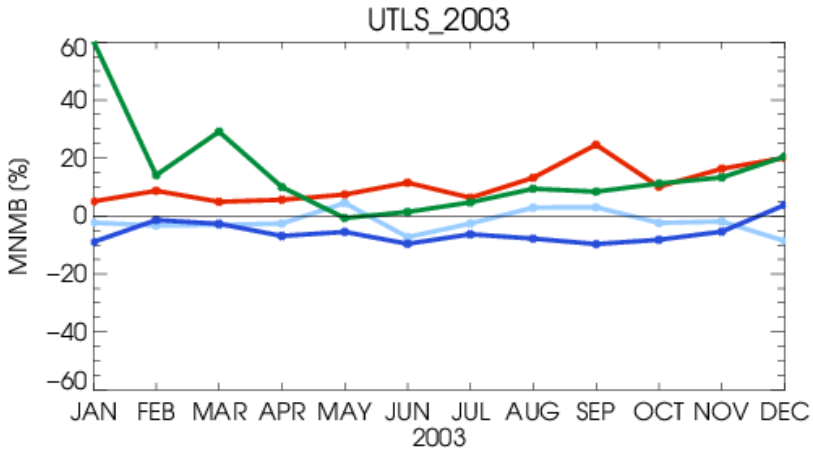

Figure 3.2.2. Ozone MNMBs, model minus ozone sonde, for all 4 regions in the UTLS, averaged between 300 and 100 hPa (tropics: 100 and 60 hPa) (dark blue: Antarctica, light blue: Arctic, red: Northern mid-latitudes, green: Tropics)

3.2 Tropospheric Ozone

3.2.1 Validation with sonde data in the free troposphere

In the **free troposphere**, Fig. 3.2.1, ozone mixing ratios are slightly underestimated over all regions except for the Tropics and Antarctica during Jan, Feb, Nov, and Dec 2003. Modified normalized mean bias (MNMB) for the Northern mid-latitudes and the Arctic range between 0.6 and -16%. For the Antarctic, larger negative MNMBs appear in the period Sep and Oct (up to -22%). MNMBs for the Tropics are mostly within 20%, with exception of Jan and Mar where positive MNMBs range up to 53%.

In the **UTLS**, Fig. 3.2.2, MNMBs are between -8 and 25% for the Arctic and the Northern mid-latitudes. For the latter ozone mixing ratios are mostly slightly overestimated, whereas for the Arctic, there is an underestimation of ozone mixing ratios in the UTLS region. For Antarctica,

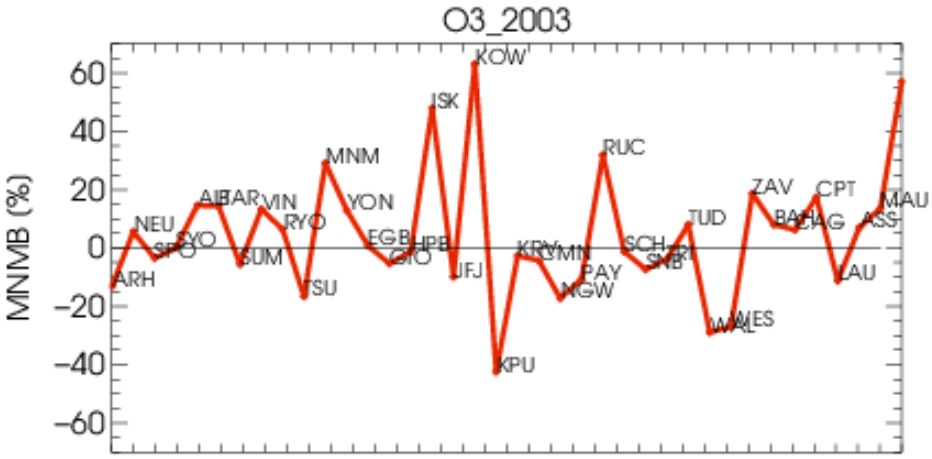

Figure 3.2.3. MNMBs for GAW stations calculated over the whole year 2003

MNMBs range between 4 and -10%. For the Tropics, MNMBs are mostly below 30%, except in Jan, where biases reach 60%.

3.2.2 Validation with GAW surface ozone observations

Antarctica

The reanalysis could well reproduce O_3 for stations in Antarctica with MNMBs between -13 and 5%. Ozone during winter and spring is generally slightly overestimated, while during the summer the model underestimates the observations. Monthly correlations are extremely low during ozone depletion events in Antarctic spring, which are not reproduced in the model, see Figure 3.2.7. Apart from that, the model shows good overall correlation with Rs between 0.68 and 0.90.

Arctic

In the Arctic, O_3 mixing ratios are mostly slightly overestimated between -5 and 14 % (calculated over the whole period). The overestimation appears mostly during spring when ozone depletion events are not captured by the model, see Fig. 3.2.8. During fall and winter, the model tends to underestimate O_3. The model shows good correlation during the winter period, whereas during spring and summer, correlation is low. The overall correlation is relatively low, due to the ozone depletion events, between 0.3 and 0.57.

Asia

For stations located in Asia, the model shows an underestimation of O_3 mixing ratios during winter (around -10%) and an overestimation during summer (around 40%). Monthly correlation coefficients are generally high, but depend on the station, see Fig. 3.2.9. The overall MNMBs are between -17% and 29%. Overall correlation is between 0.46 and 0.88.

Europe

Apart from single stations that show a strong overestimation of O_3 especially during summer and fall, most stations show a slight underestimation of O_3 for most of the year. Especially the more remote mountain stations show mostly slightly negative MNMBs. This is mostly due to summer ozone peaks that are not captured in the model, see Fig. 3.2.10. Correlation coefficients are between 0.35 and 0.86.

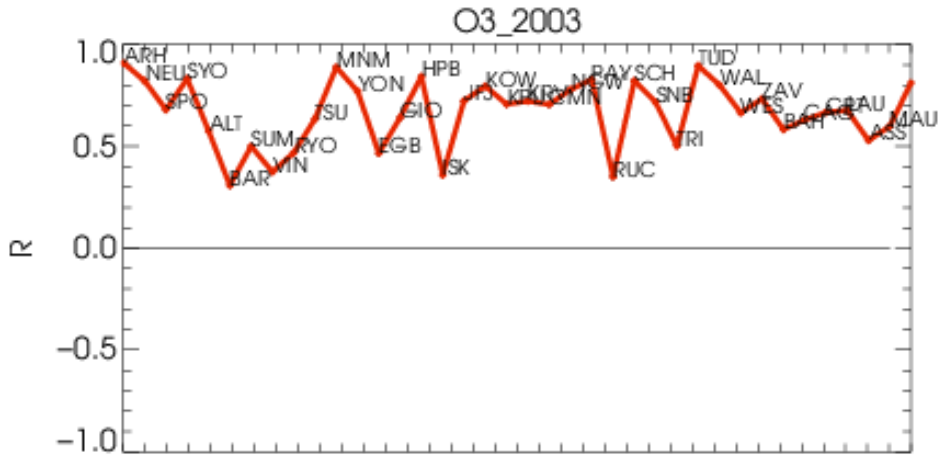

Figure 3.2.4. R for GAW stations calculated over the whole year 2003

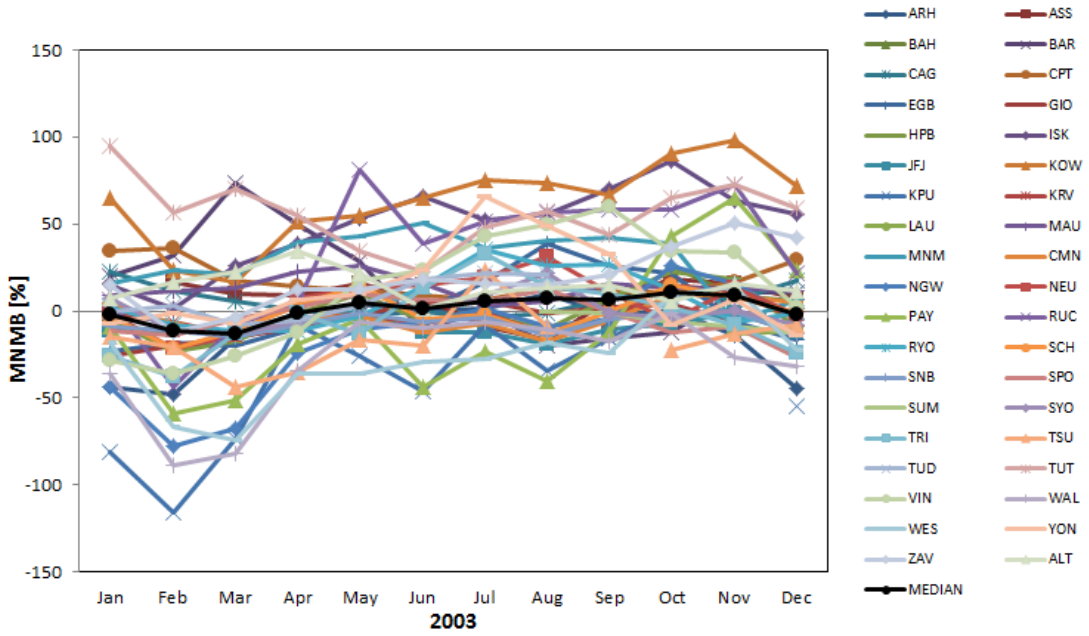

Figure 3.2.5. MNMBs for GAW stations calculated for each month in 2003

Tropics

The model shows an overestimation for O_3 mixing ratios in the tropics with MNMBs between 6 % and 57%. Correlation coefficients are between 0.52 and 0.81.

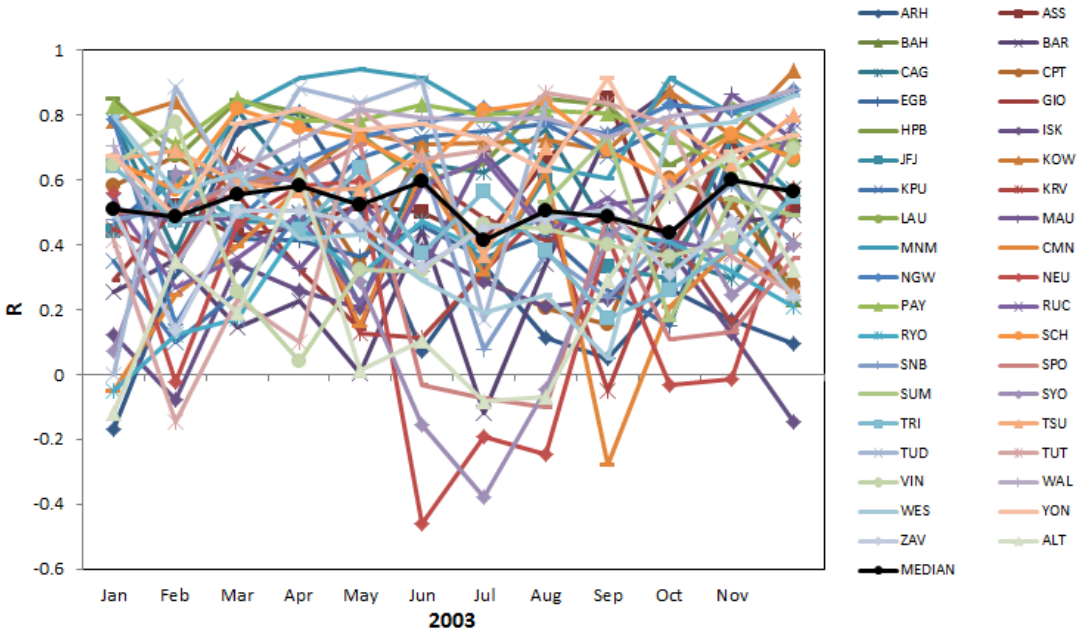

Figure 3.2.6. R for GAW stations calculated for each month and in 2003

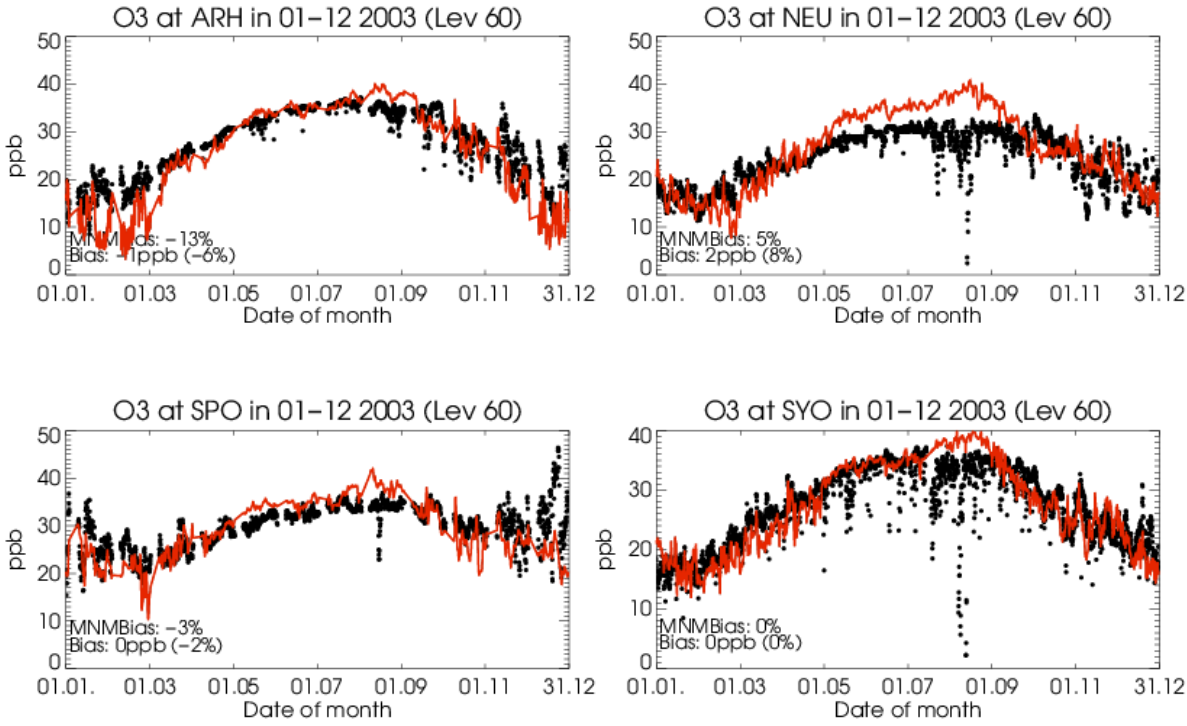

Figure 3.2.7. Timeseries for O3 in the period 01-12 2003 for GAW stations in Antarctica

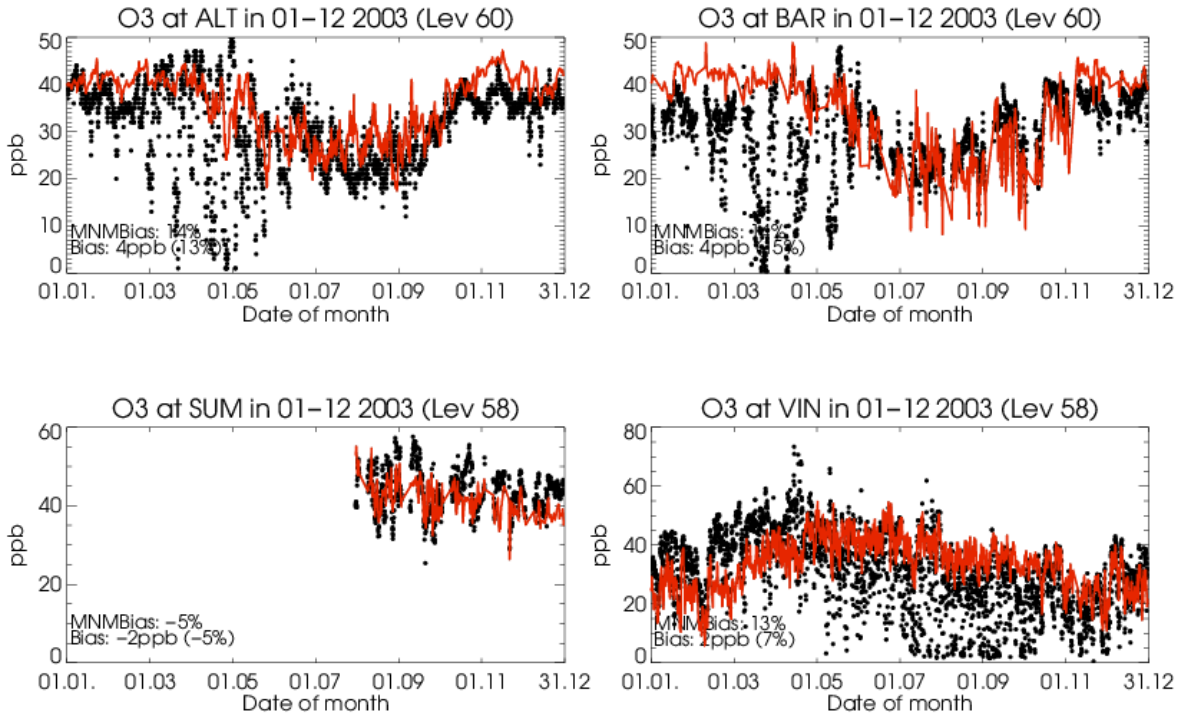

Figure 3.2.8 Timeseries for O_3 in the period 01-12 2003 for GAW stations in the Arctic

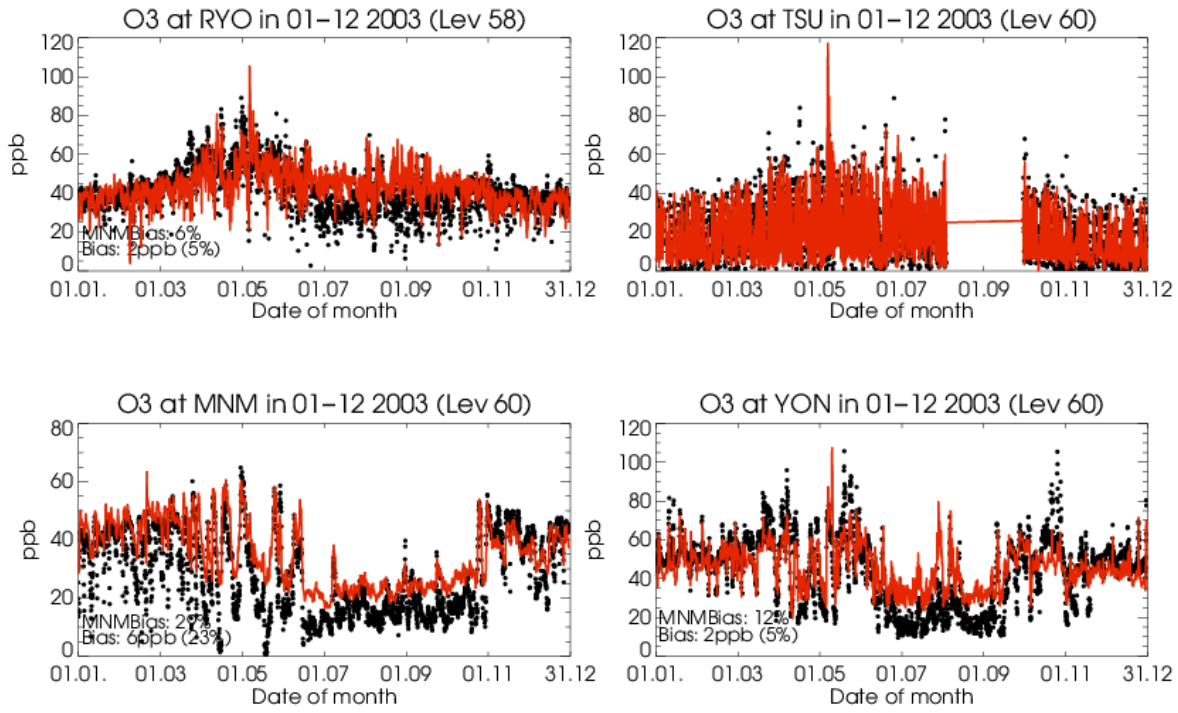

Figure 3.2.9 Timeseries for O3 in the period 01-12 2003 for GAW stations in Asia

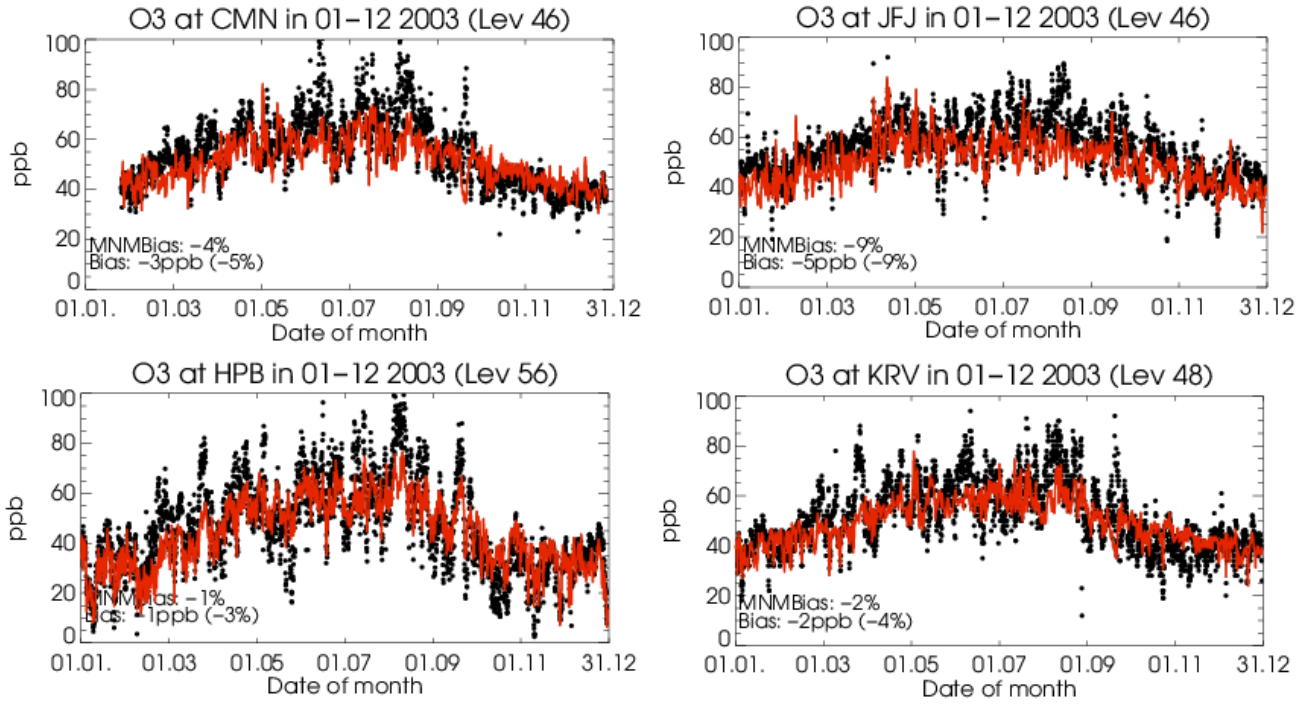

Figure 3.2.10. Timeseries for O3 in the period 01-12 2003 for GAW stations in Europe

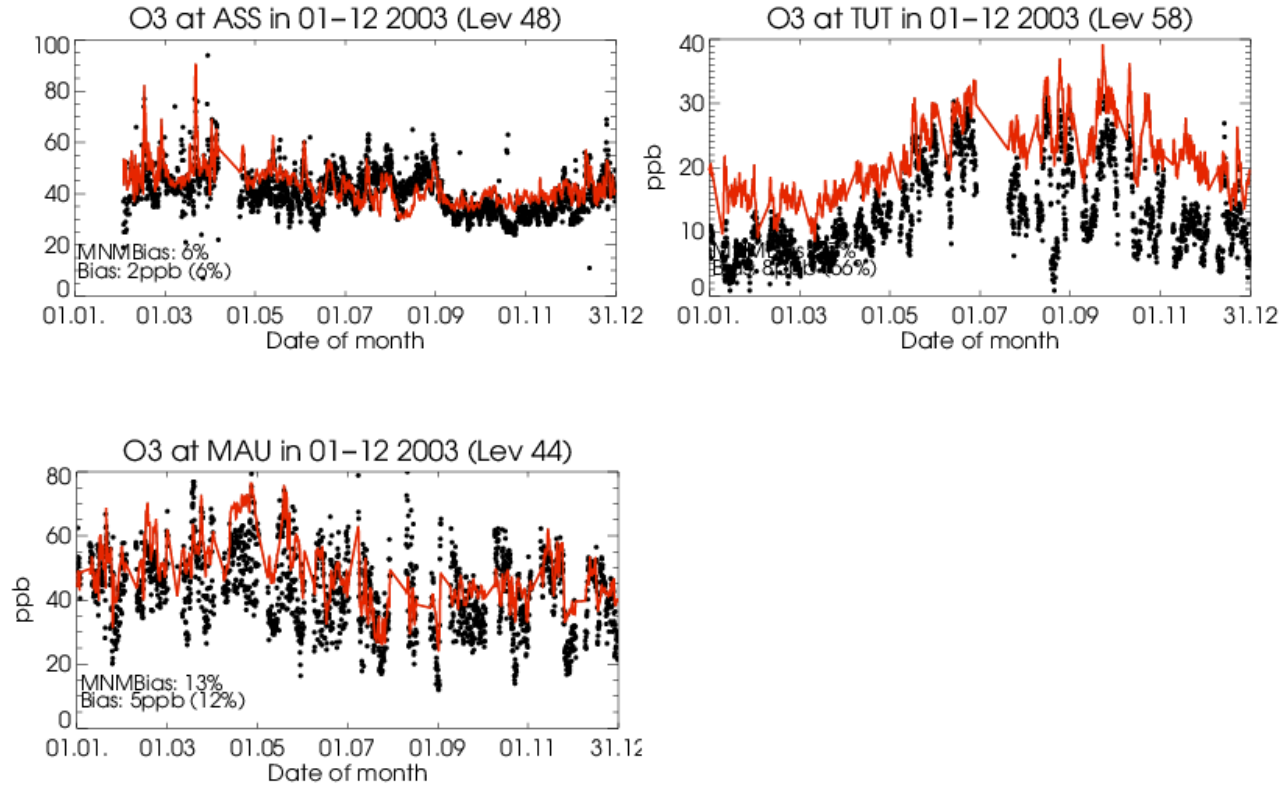

Figure 3.2.11 Timeseries for O3 in the period 01-12 2003 for GAW stations in the Tropics

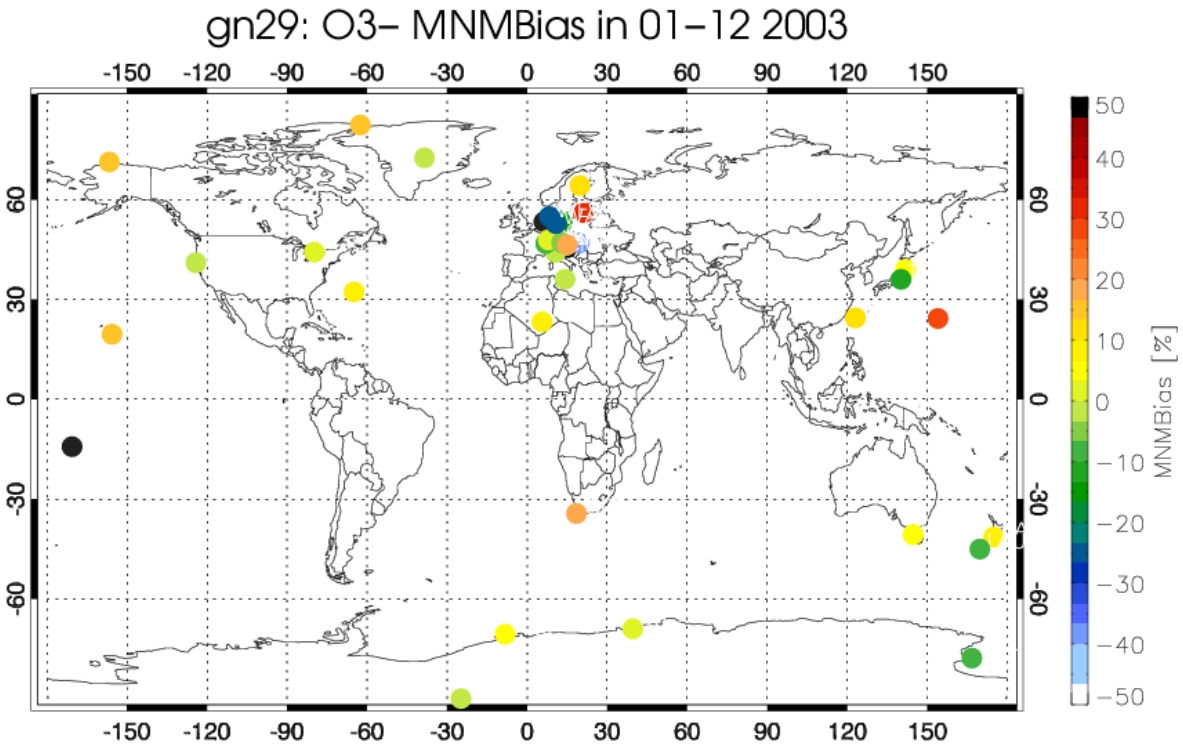

Figure 3.2.12. Map of MNMBs over the time period 01-12 2003.

3.2.3 Verification with European EMEP surface ozone observations

The CAMS reanalysis experiment gn29 as well as the CAMS control reanalysis experiment gnar and the MACC reanalysis were compared to the surface EMEP and AirBase background rural observations on a seasonal basis for the latitudinal zones of 30°N-40°N, 40°N-50°N and 50°N-70°N; these latitudinal zones denote the zonal monthly averages of surface ozone of the period 2003 over Southern, Central and Northern Europe respectively (Fig. 3.2.13).

Over Southern Europe, the CAMS reanalysis experiments (gn29 and gnar) reproduce well the mean ozone concentrations during the first half of the year (MNMBs<5%) while systematically overestimating ozone mixing ratios during the second half of the year with the highest positive amplitudes being observed during autumn (MNMBs up to 20%). It should be noted that the strong negative offset (down to 50%) which appears in the MACC Reanalysis during the period January to April 2003 is corrected in the new reanalysis.

Over Central Europe the modelled surface ozone values in all three reanalysis experiments agree well with observations for the 2nd half of the year whilst during the 1st half of the year a large negative bias is observed (down to -10 ppbv, MNMBs≈-40% for the gn29 and gnar experiments and down to -15 ppbv, MNMBs≈-60% for the MACC reanalysis).

Lastly, over Northern Europe, the CAMS reanalysis underestimates O_3 levels during winter and spring seasons (MNMBs down to -40% during February), overestimates O_3 during autumn (MNMBs up to 20%) and reproduces well mean concentrations of ozone during summer season. It should be noted again that the negative offset during the cold part of the year is lower in the new reanalysis

compared with the MACC reanalysis. It seems also that over Northern Europe the data assimilation reduces the biases during April and May. The same analysis was repeated for the high altitude stations (stations with altitude higher than 1000 m a.s.l.) and it was found that the CAMS reanalysis experiments underestimate slightly ozone mean concentrations during January to March 2003 (MNMBs down to -10%), overestimate it slightly during autumn (MNMBs up to 10%) and reproduces well O_3 levels during the rest of 2003. Again the CAMS reanalysis experiments performers better than the MACC reanalysis in terms of biases especially for the period January to April 2003.

Similar results are found from Fig. 3.2.14 which shows the spatial distribution of the Modified Normalised Mean Biases (MNMBs) calculated for the CAMS Reanalysis experiment gn29 and the MACC Reanalysis over the 262 background rural European EMEP and AirBase stations in a seasonal base (winter months, spring, summer and autumn seasons).

Finally Fig. 3.2.15 shows the spatial distribution of the temporal correlations between modelled and observed surface ozone values calculated for the CAMS Reanalysis experiment gn29 and the MACC Reanalysis over the 262 individual EMEP and AirBase stations in a seasonal base. Correlations between gn29 simulated ozone values and observations are highly significant for the majority of the stations and the higher correlations are observed during summer and autumn seasons ($0.5<r<0.9$); relatively lower correlations are observed during winter season particularly at the southern Europe stations ($0.0<r<0.4$ depending on the station) and during spring over stations northern the 60°N ($0.0<r<0.5$ depending on the station). It should be noted that the CAMS Reanalysis experiments performers better than the MACC reanalysis in terms of biases particularly during winter and spring 2003.

To summarize we conclude that, although the bias is improving, there is still a seasonal dependence of the bias and MNMB. The amplitude of the seasonality of MNMB is very much reduced in the latitudinal zones of 30°N-40°N as well as for the high altitude stations (stations with altitude higher than 1000 m a.s.l.).

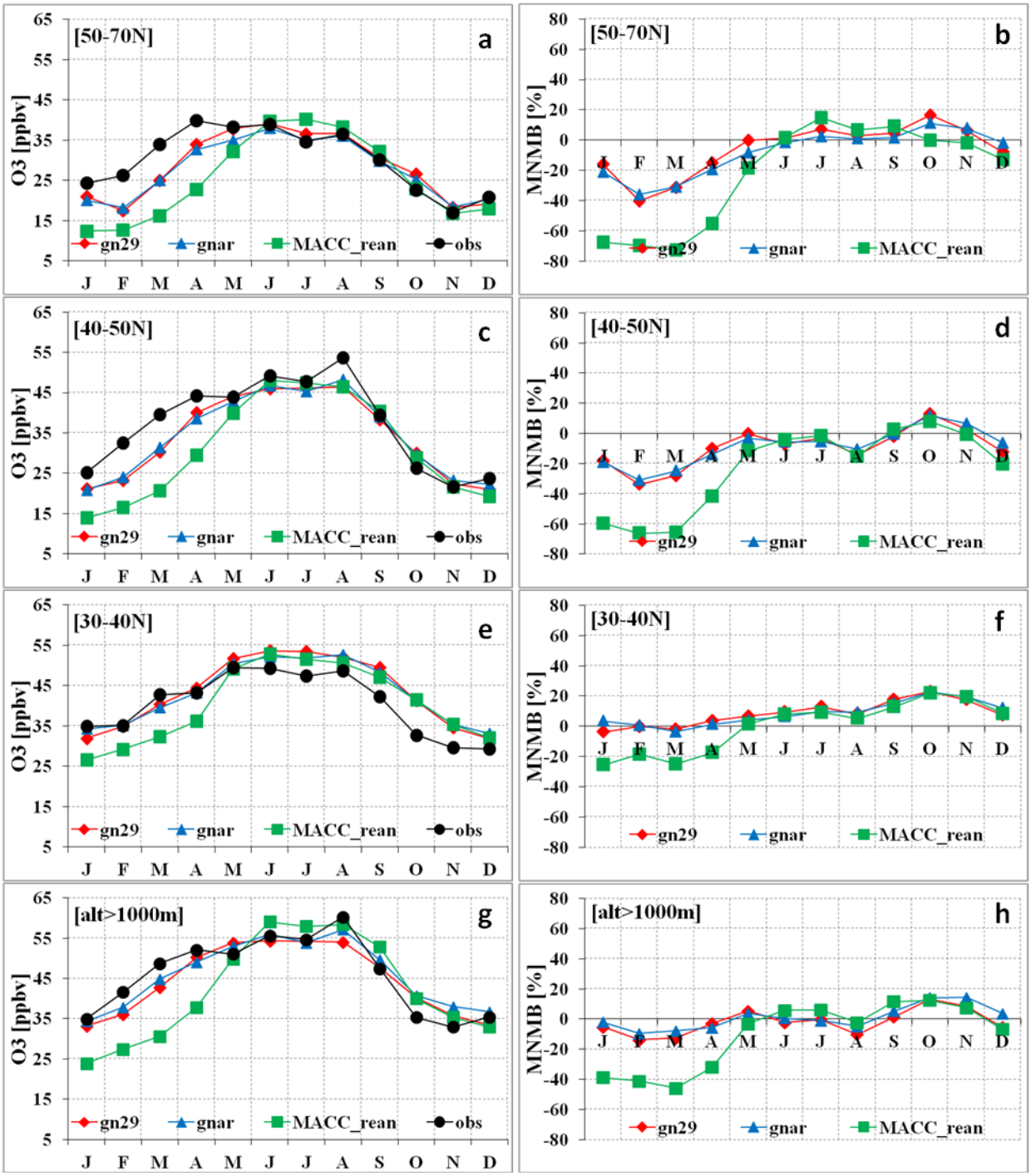

Figure 3.2.13. Mean monthly ozone variability for the year 2003 (left) and the MNMBs (right) of the new Reanalysis experiment gn29 (red robs) the control Reanalysis experiment gnar (blue triangles), the MACC reanalysis (green squares), and the EMEP observations (black circles) over Northern Europe (1st row, a and b), Central Europe (2nd row, c and d), Southern Europe (3rd row, e and f) as well as for stations with altitude greater than 1000m a.s.l. (4rd row, g and h)

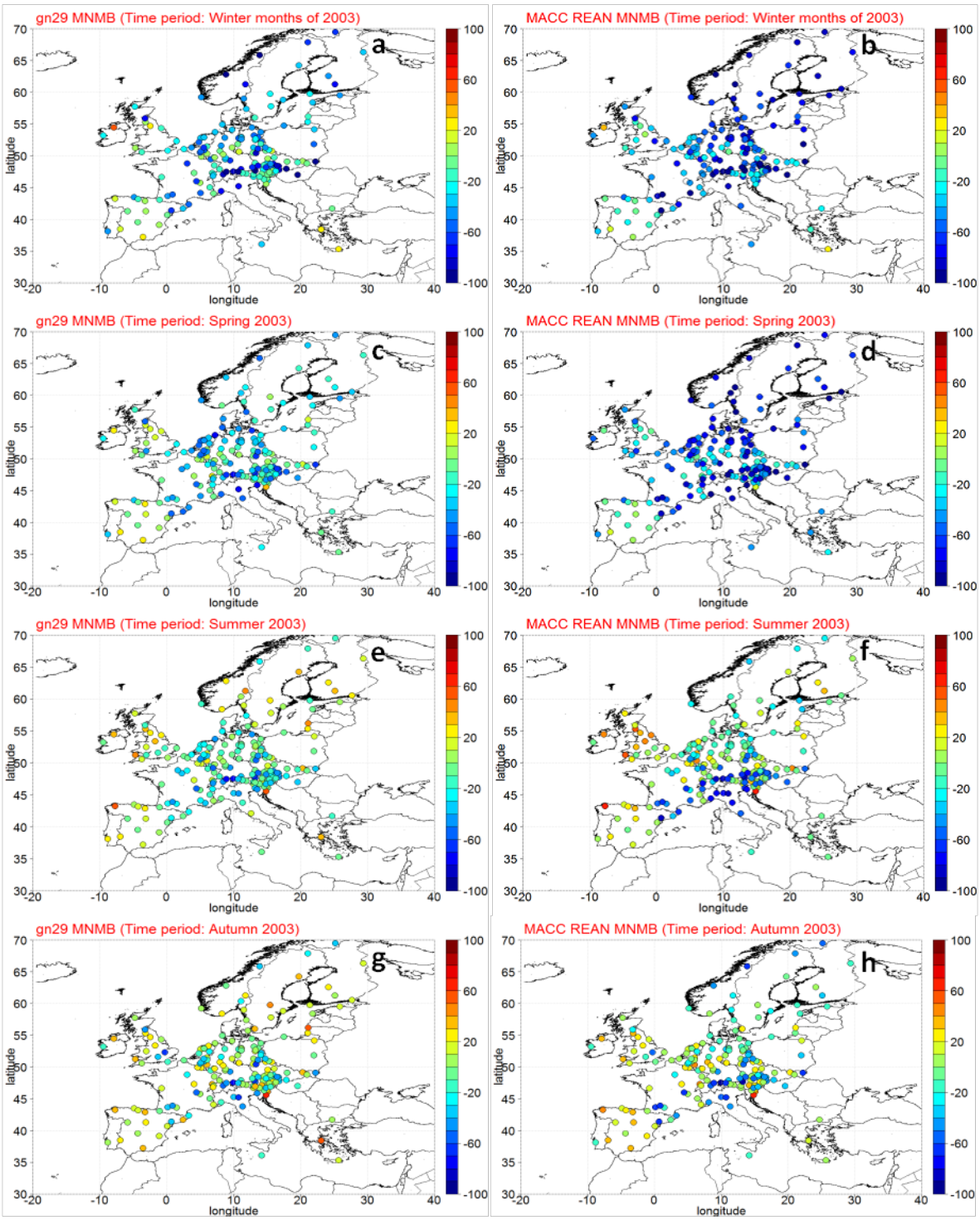

Figure 3.2.14. Modified Normalised Mean Biases (MNMBs) during Winter months of 2003 (1st row, a and b), Spring 2003 (2nd row, c and d), Summer 2003 (3rd row, e and f) and Autumn 2003 (4rd row, g and h) for the new Reanalysis experiment gn29 (left) and the MACC reanalysis (right).

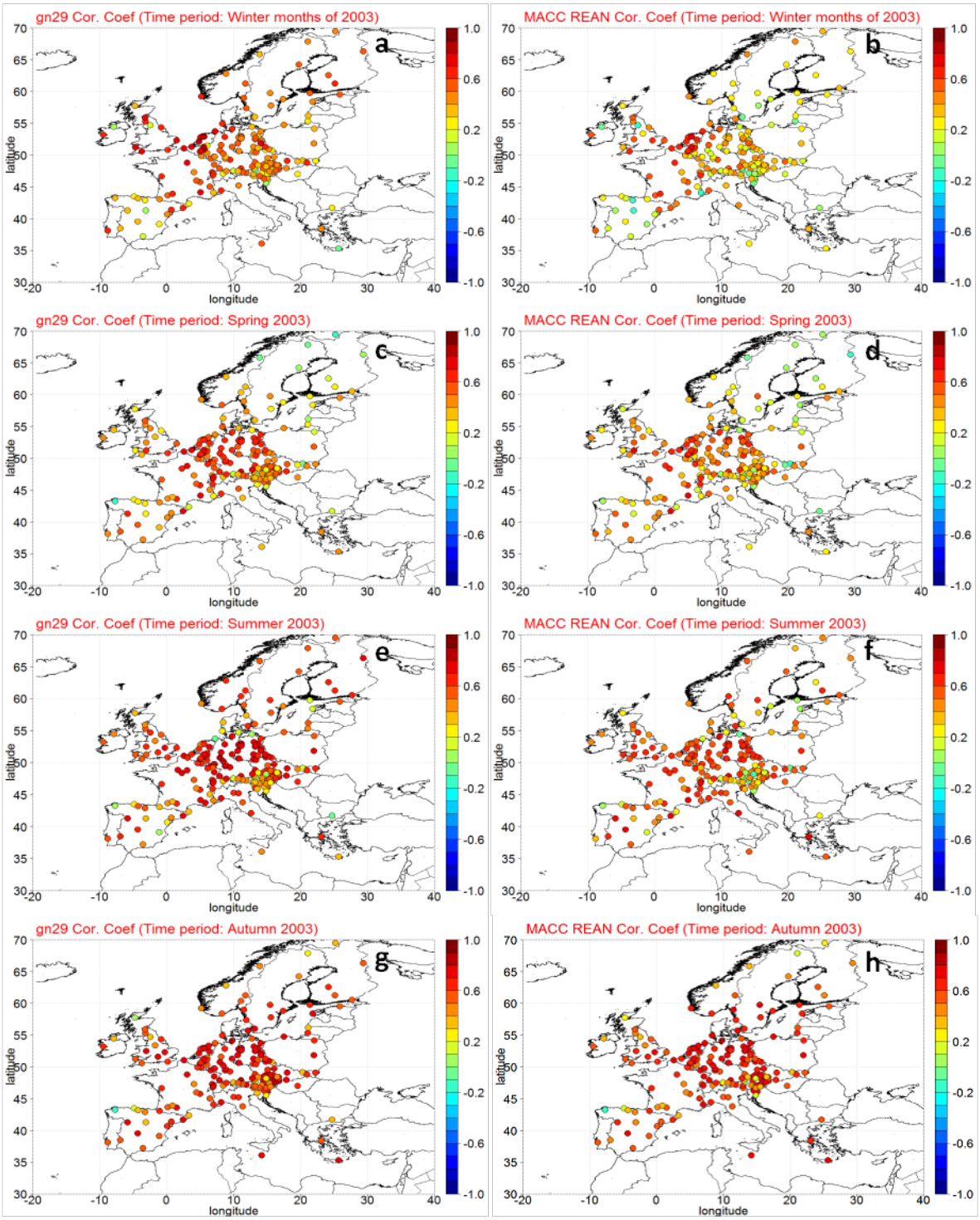

Figure 3.2.15. Correlation Coefficients (r) during Winter months of 2003 1st row, a and b), Spring 2003 (2nd row, c and d), Summer 2003 (3rd row, e and f) and Autumn 2003 (4rd row, g and h) for the new Reanalysis experiment gn29 (left) and the MACC reanalysis (right).

3.2.4 Verification with IAGOS ozone observations

Figure 3.2.16 presents a timeseries of ozone from the reanalysis and the control for 2003 at Frankfurt airport where there are almost daily observations. The models compare well with the observations in the surface layer and boundary layer except during the period of the 2003 heatwave which is discussed in more detail below. In the upper troposphere the models overestimate the amount of ozone, with the control generally performing better. This can be seen more clearly in the monthly averaged profile for February 2003 as shown in Figure 3.2.17. The models underestimate ozone in the surface layer and boundary layer. Throughout the free troposphere, the reanalysis underestimates ozone, and in the upper troposphere the reanalysis overestimates ozone.

In the upper troposphere the control run usually does better than the reanalysis as seen in Figure 3.2.18 showing Osaka and New York six months apart. During the winter months, when the tropopause mixing layer is lower, the models have difficulty in capturing the gradient of ozone. In the summer months, the mixing layer is encountered less frequently and hence the models do not reproduce the sharp gradient around the tropopause. The better behaviour by the control run over that with assimilation is a result also seen in the operational CAMS forecasts (o-suite), and has been described by Gaudel et al., (2015) in a study based on the MACC reanalysis.

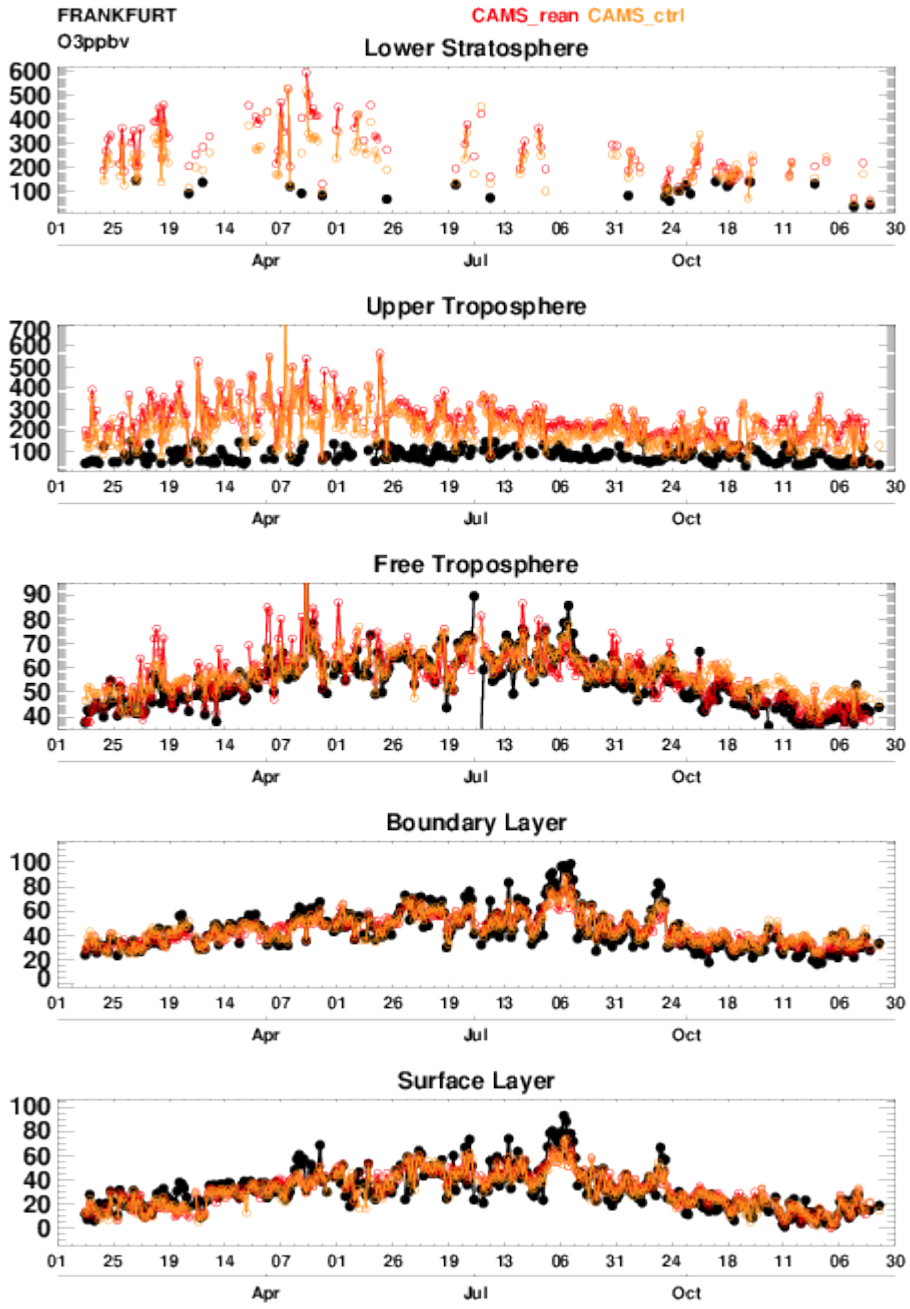

Figure 3.2.16. Timeseries for 2003 of ozone at Frankfurt from IAGOS (MOZAIC) observations in black and for the control run (orange) and reanalysis (red). Units: ppbv.

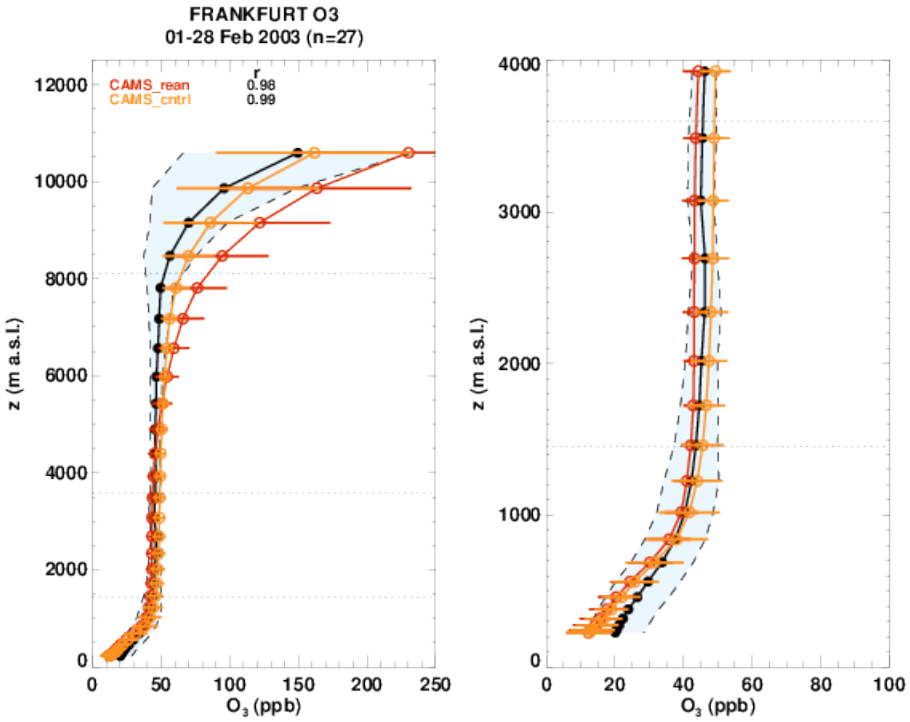

Figure 3.2.17. Monthly averaged ozone over Frankfurt for February 2003. The solid black line of the observations and the dashed black line shows the standard deviation of the observations.

Heatwave in summer 2003

The main event of 2003 was the major heatwave over northern Europe, concerning particularly the period 2-14 August. The heatwave was studied with IAGOS (MOZAIC) measurements in detail by Tressol et al. (2008). In Figure 3.2.19 we show the monthly averaged profile for August over Frankfurt. In the UTLS the control run performs very well. The monthly averaged amount of ozone in the surface and boundary layers during the heatwave as seen by the IAGOS aircraft, is higher than usual, reaching 65 ppbv. These amounts are underestimated by the reanalysis. The timeseries (Fig. 3.2.20), shows this underestimation more clearly. During the heatwave, the three runs underestimate ozone, but outside of this period they perform quite well. There is an improvement by the CAMS reanalysis compared with the MACC reanalysis in the surface and boundary layers, but in the upper troposphere, this is strikingly reversed.

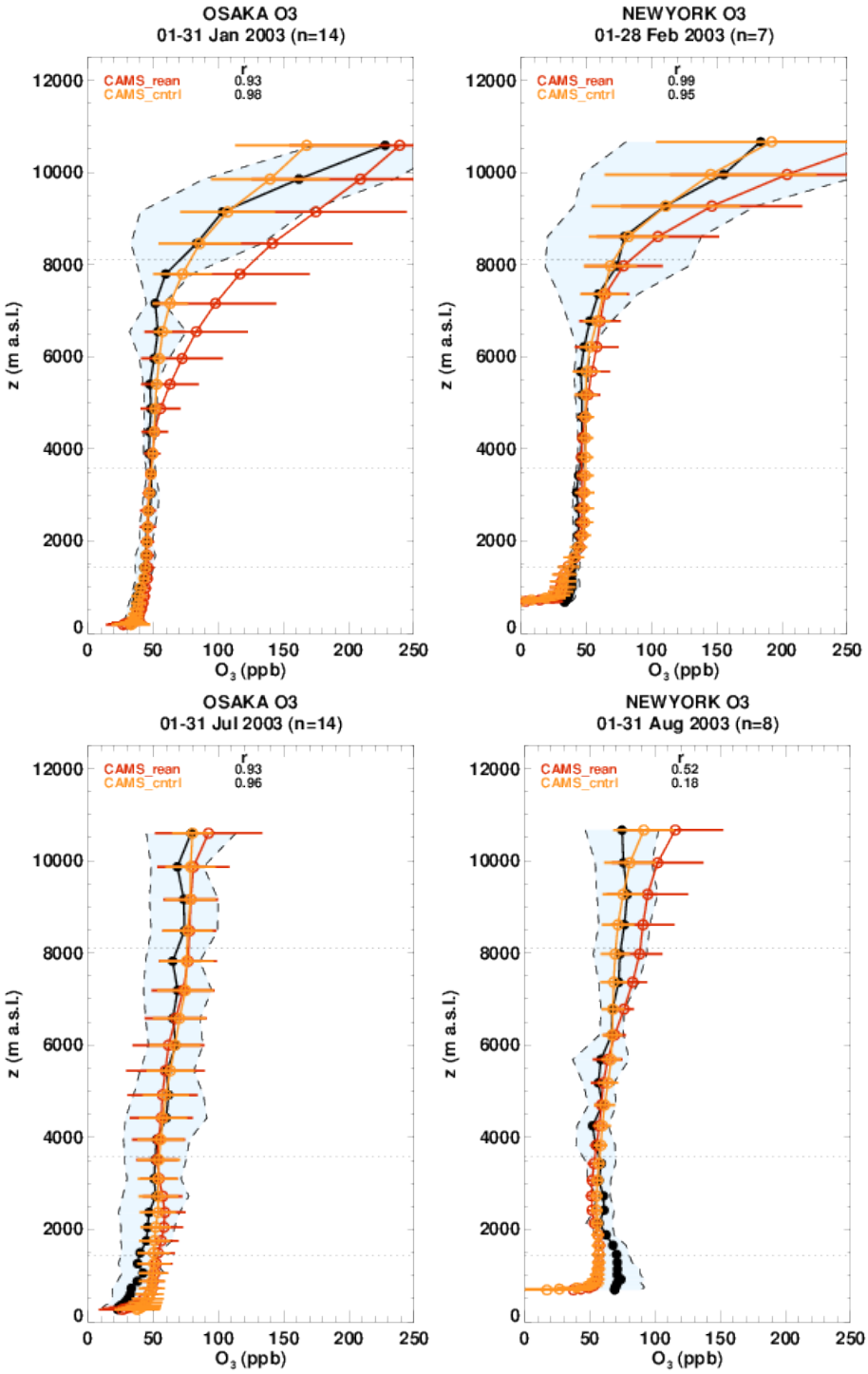

Figure 3.2.18. Monthly averaged ozone over Osaka for January and July, and for New York in February and August 2003. The solid black line if the observations and the dashed black line shows the standard deviation of the observations.

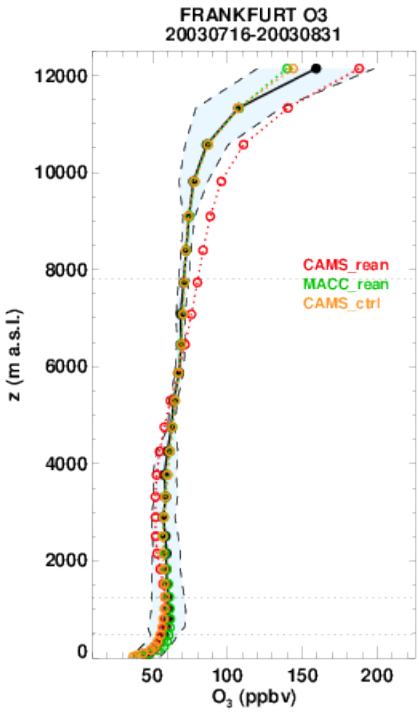

Figure 3.2.19. Ozone averaged of the period of the heatwave 16 July-30 August 2003. The CAMS reanalysis is in red, the MACC reanalysis in green and the CAMS control in orange. The solid black line if the observations and the dashed black line shows the standard deviation of the observations.

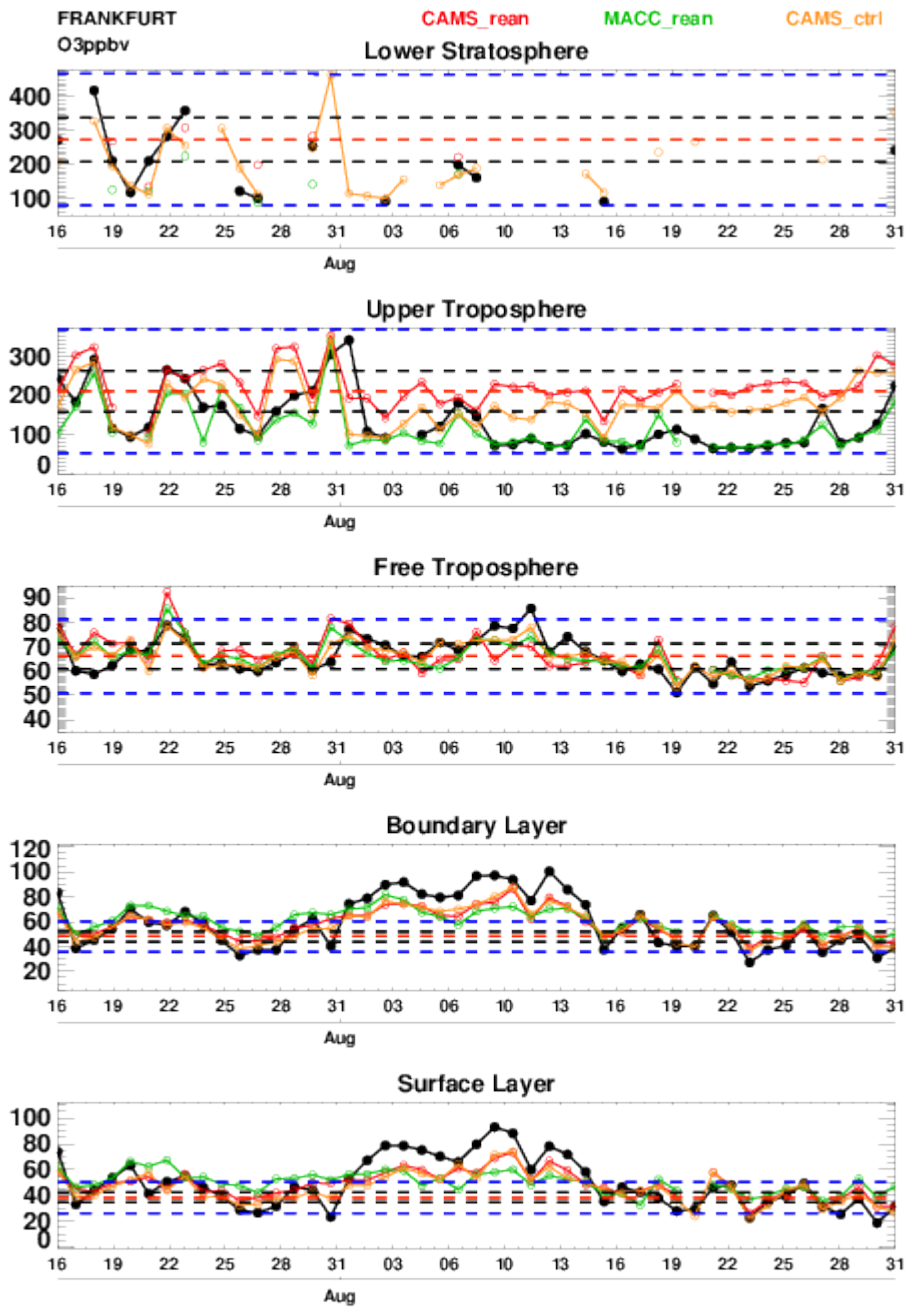

Figure 3.2.20. Timeseries of ozone over Frankfurt for the period of the intense heatwave over Europe 16 July-31 August. Observations are in black, the CAMS reanalysis is in red, the CAMS control in orange and the MACC reanalysis in green. The red dashed line is the mean of the observations from 2003-2012 the black dashed line is 1 sigma from the mean, and the blue dashed line is 3 sigmas from the mean.

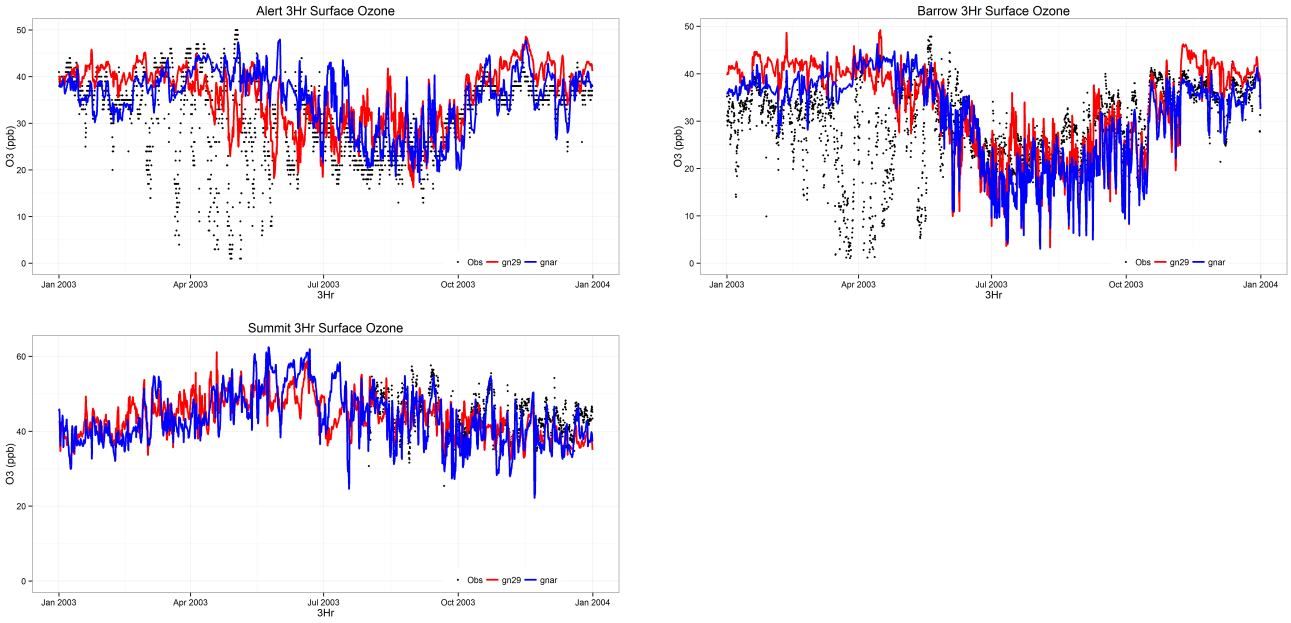

Figure 3.2.21. Time series for gn29 (red) and gnar (blue) compared to observations (black dots) at Alert, Nunavut, Canada; Barrow, Alaska, USA and Summit in central Greenland.

3.2.5 Verification with ozone surface data in the Arctic

Validation with IASOA surface observations

The reanalysis simulations are evaluated against measured surface ozone concentrations at three Arctic sites: Alert, Nunavut, Canada; Barrow, Alaska, USA and Summit in central Greenland. Measurements are only available for 5 months for Summit, Fig. 3.2.21. Ozone depletion events at the two coastal stations in March – June 2003 are not captured by the model simulations during spring. These events are related to halogen chemistry reactions that are not represented in the model simulations.

The simulations are on average in good agreement with the observations apart from the spring depletion events. There is a positive bias for both simulations at Alert and Barrow due to the overestimation in spring. The gn29 simulation tend to overestimate the O3 concentrations at Alert and Barrow in autumn and winter, while the gnar simulation is in better agreement with observations in these periods. The short-term variability is well captured with a correlation coefficient of r = 0.32-0.55 for the gn29 and r = 0.28-0.78 for the gnar run, although the correlation coefficient is off-set by the spring depletion events at Alert and Barrow (Table 3.2.1).

		NMB	R
Alert	gn29	0.14	0.55
	gnar	0.12	0.42
Barrow	gn29	0.12	0.32
	Gnar	0.04	0.28
Summit	gn29	-0.06	0.49
	Gnar	-0.07	0.78

Table 3.2.1. Normalised Mean Bias (NMB) and correlation coefficient (r) of the gn29 and the gnar simulations for the Alert, Nunavut, Canada; Barrow, Alaska, USA and Summit in central Greenland for 2003.

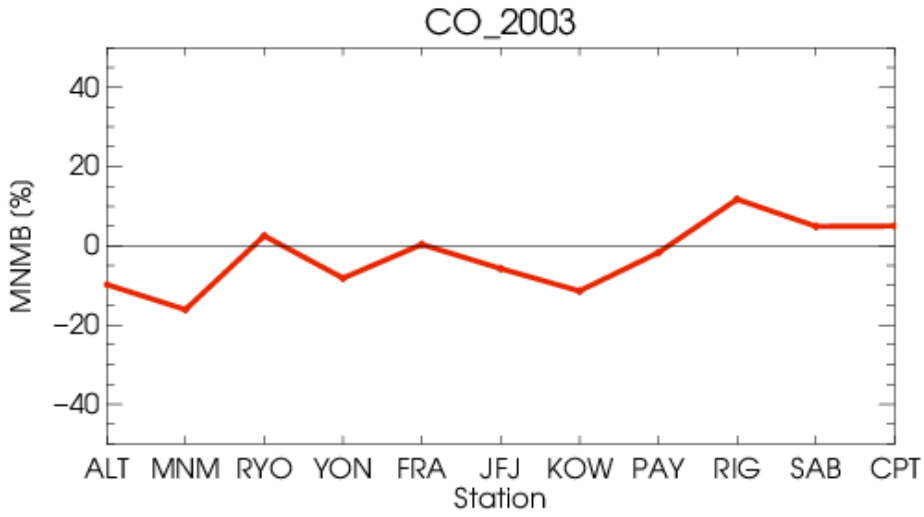

Figure 3.3.1. MNMBs for CO for GAW stations

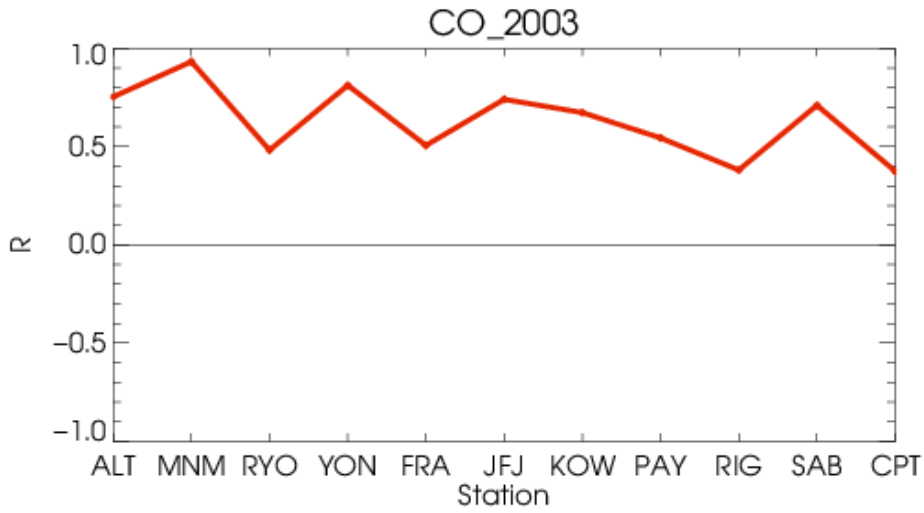

Figure 3.3.2. Rs for CO for GAW stations.

3.3 Carbon monoxide

3.3.1 Validation with Global Atmosphere Watch (GAW) Surface Observations

Surface CO for GAW stations is mostly slightly underestimated (with MNMBs between -16% and 12%) by the reanalysis. For single stations (RYO and FRA) spikes in CO appear that do not seem to correspond to the measurements (fire signal?), see Fig. 3.3.6 (RYO, FRA). Correlation coefficients (Fig. 3.3.2) are between 0.37 and 0.90 (on average 0.67).

The calculation of MNMBs for each month (Fig. 3.3.3) shows that MNMBs are more negative during the northern winter months (Jan, Feb, Nov, Dec) than during the summer. Correlation coefficients (Fig. 3.3.4), however, are higher during the winter months.

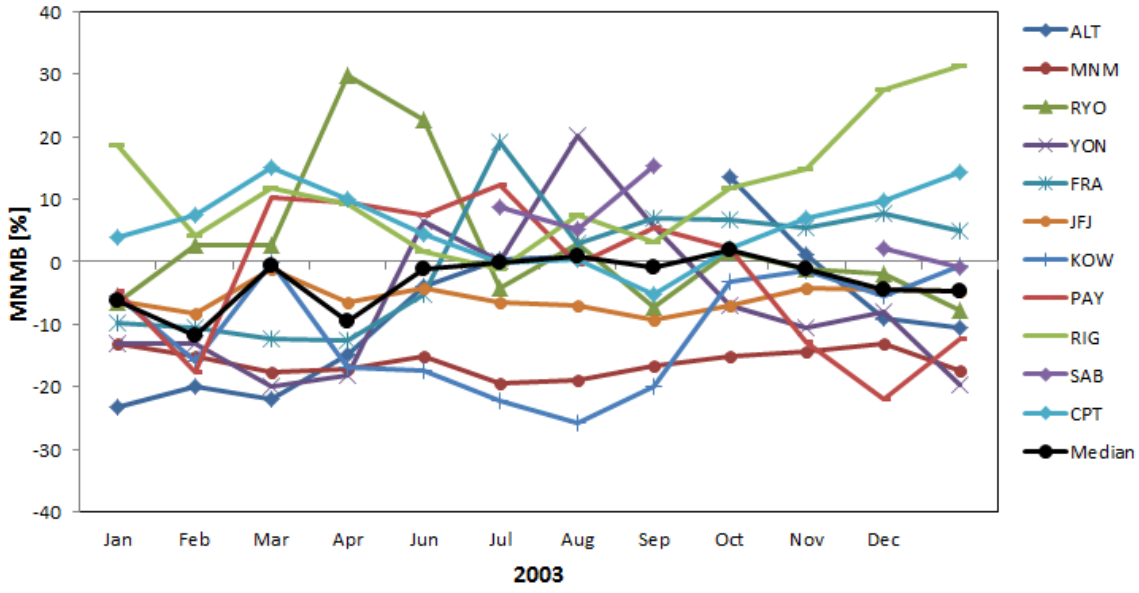

Figure 3.3.3. MNMBs calculated for each month for CO for GAW stations

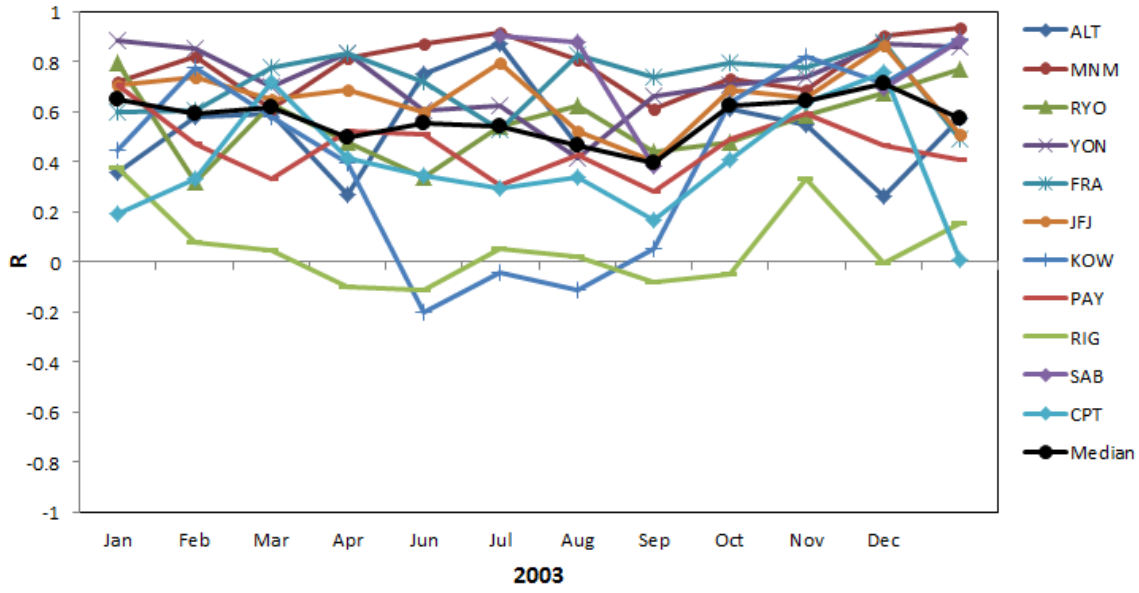

Figure 3.3.4. Rs calculated for each month for CO for GAW stations

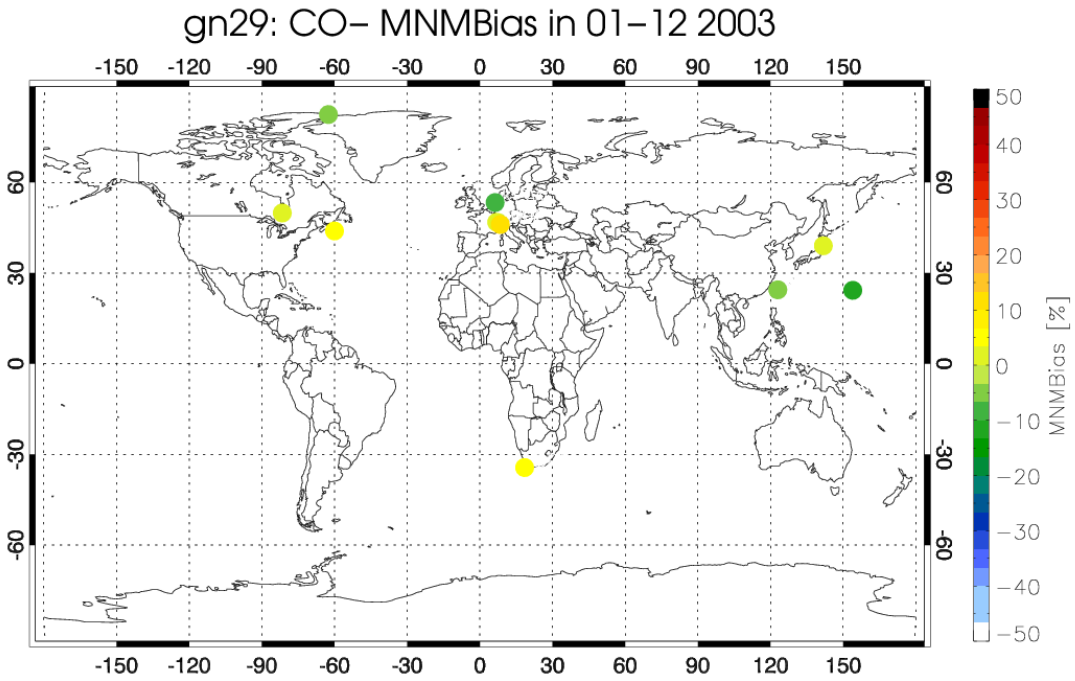

Figure 3.3.5. Distribution of overall MNMBs for CO for 2003 for GAW stations

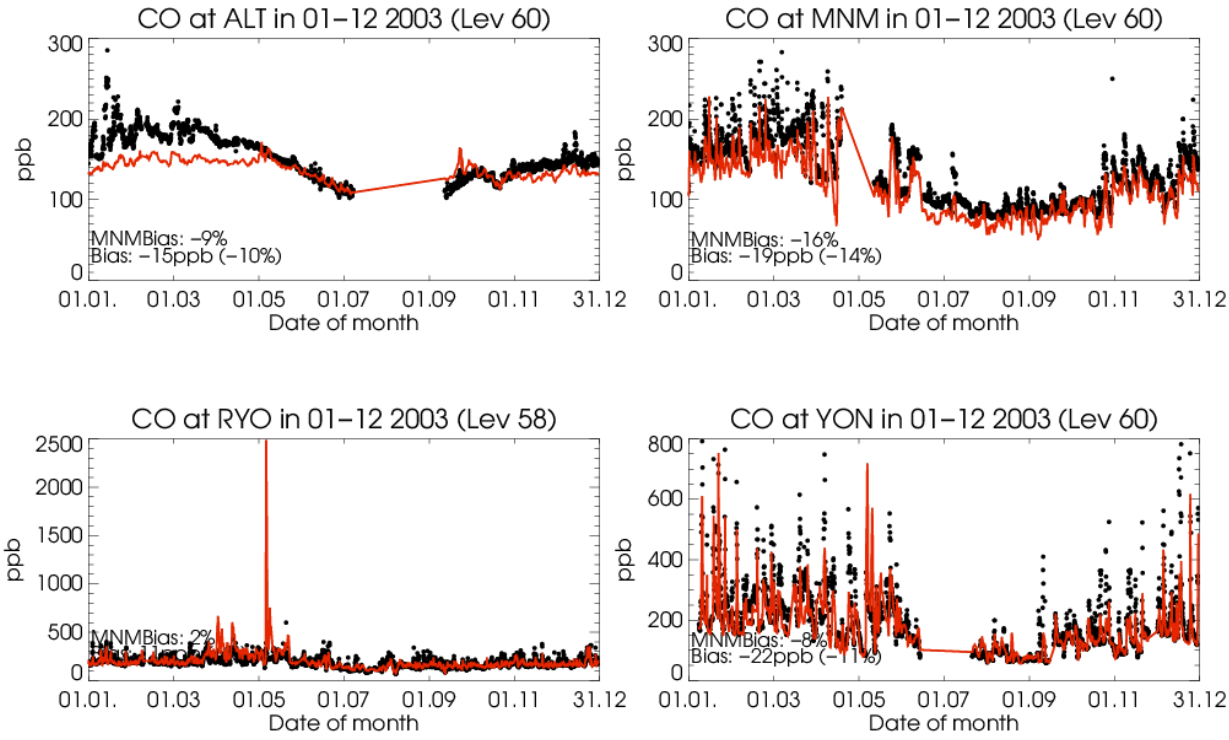

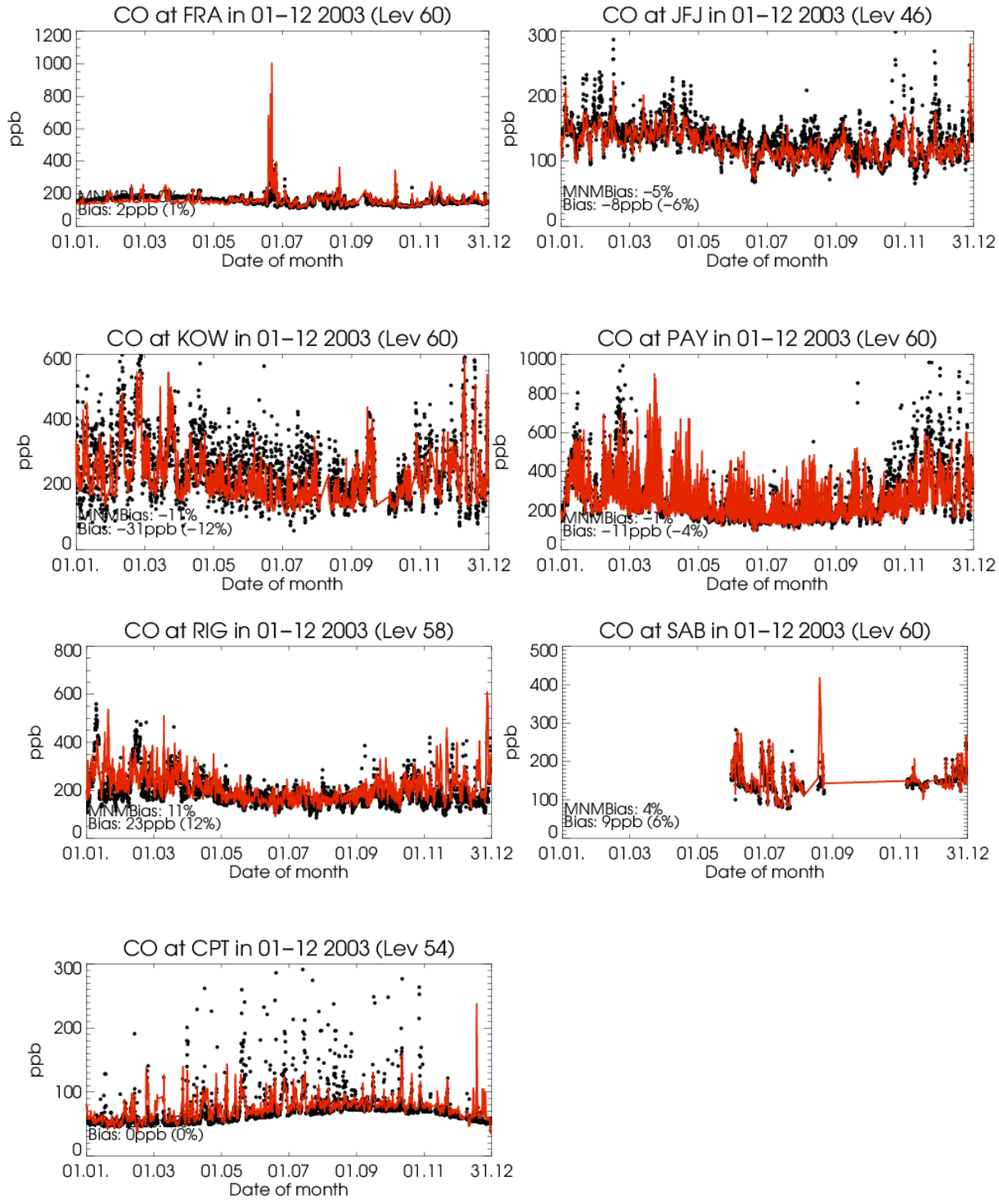

Figure 3.3.6. Timeseries plots for CO for GAW stations in the period 01-12 2003.

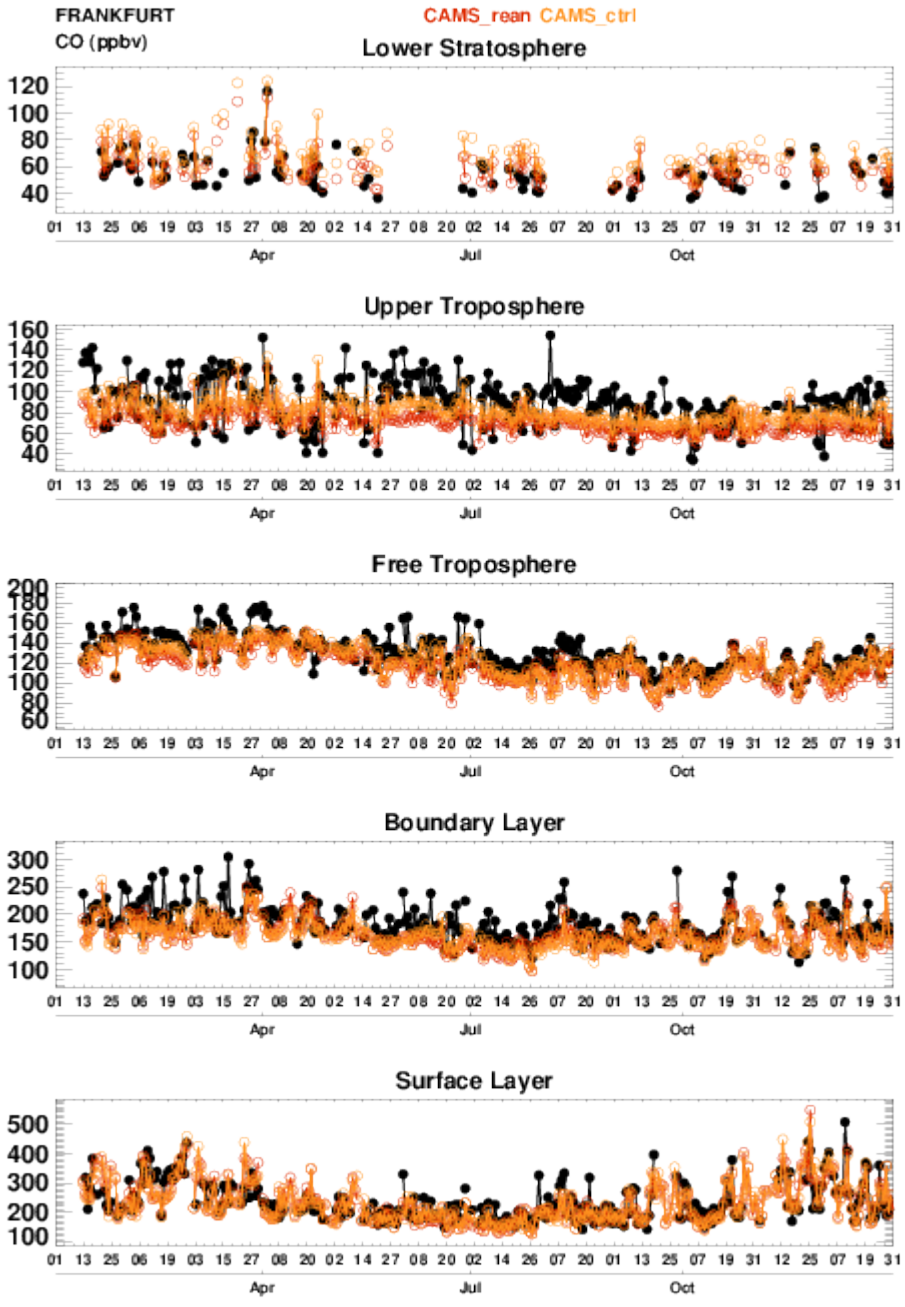

Figure 3.3.7. Timeseries for 2003 of CO at Frankfurt from IAGOS (MOZAIC) observations in black and for the control run (orange) and reanalysis in red.

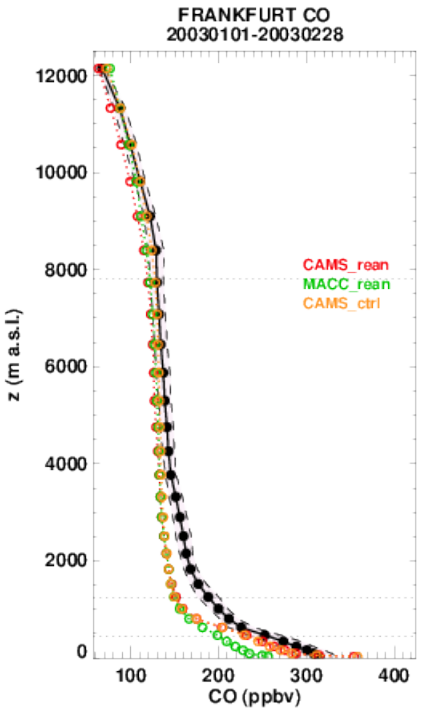

Figure 3.3.8. CO over Frankfurt during January and February. The CAMS reanalysis is in red, the MACC reanalysis in green and the CAMS control in orange. The solid black line if the observations and the dashed black line shows the standard deviation of the observations.

3.3.2 IAGOS Aircraft observations

Figure 3.3.7 shows the timeseries for Frankfurt for 2003. In the surface layer, boundary layer and free troposphere the models slightly underestimate CO, with this underestimation being more pronounced in the upper troposphere. The CAMS and the MACC reanalysis systematically underestimated CO in the surface layer, particularly in the northern hemisphere in winter. Stein et al., (2014) attributed this to an underestimation of traffic emissions. The CAMS reanalysis appears to be better at capturing the high concentrations of CO in the surface layer over European airports (Frankfurt, Paris, Vienna, Munich) during winter 2003. (Fig. 3.3.9 shows profiles at Frankfurt, Paris and Munich and Vienna) Fig. 3.3.8 show the profile of CO for Frankfurt averaged for January and February. There is a clear improvement of the CAMS reanalysis compared with the old MACC reanalysis. In the upper troposphere the three runs behave similarly.

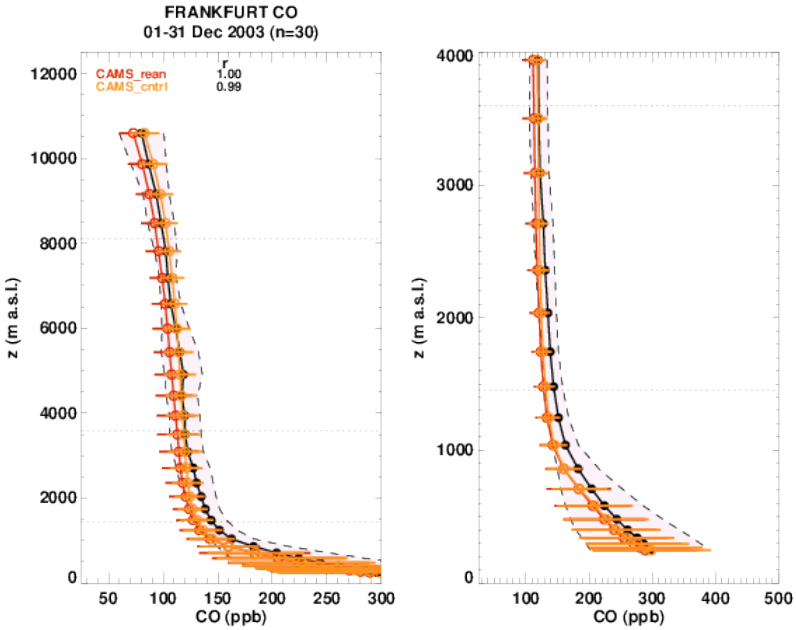
FRANKFURT CO
01-31 Dec 2003 (n=30)
CAMS_rean
CAMS_cntrl
r
1.00
0.99
z (m a.s.l.)
CO (ppb)

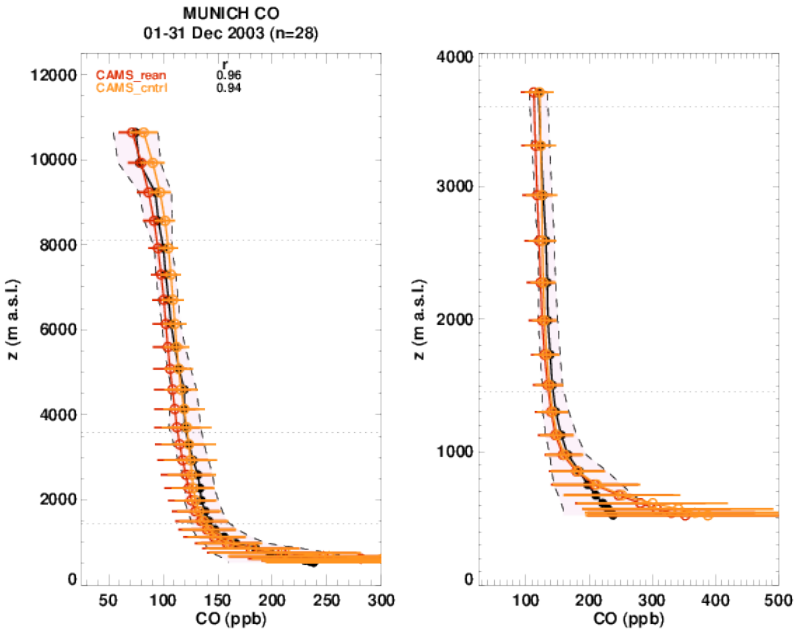
MUNICH CO
01-31 Dec 2003 (n=28)
CAMS_rean
CAMS_cntrl
r
0.96
0.94
z (m a.s.l.)
CO (ppb)

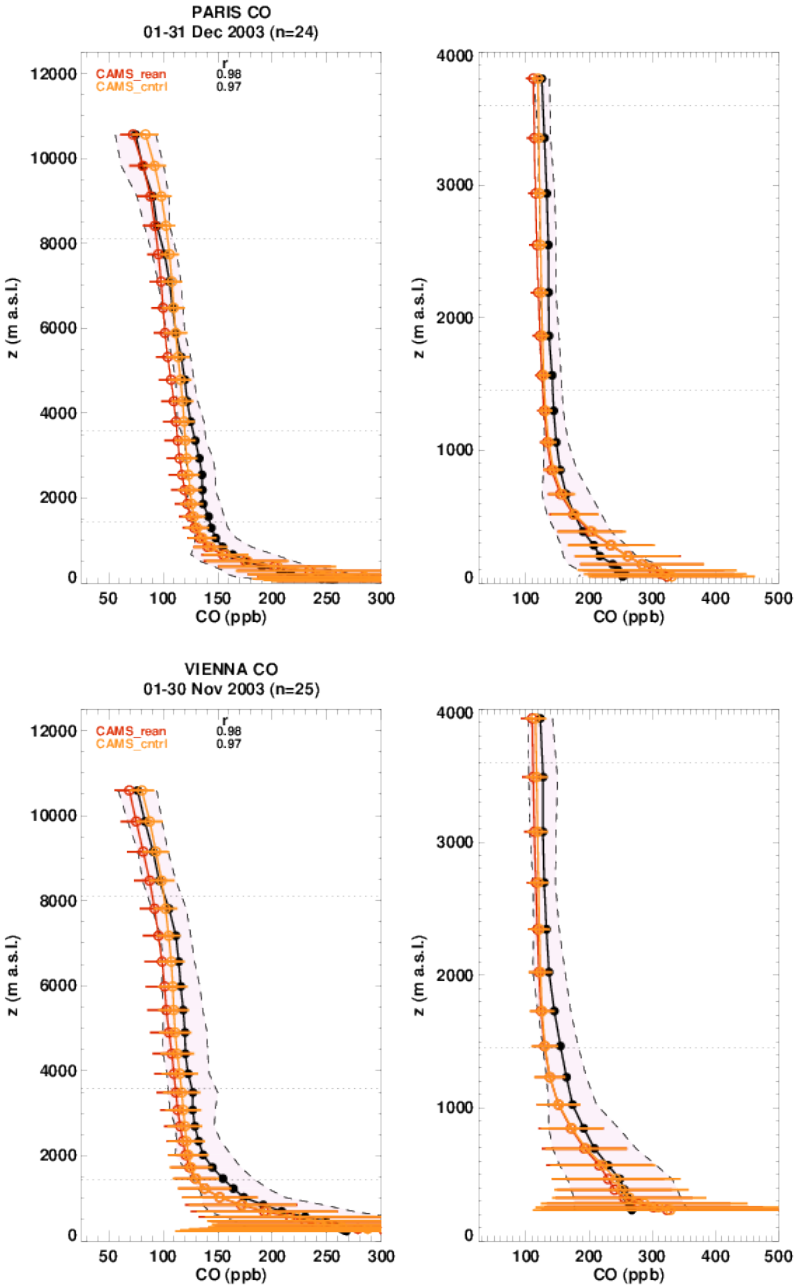

Figure 3.3.9. Monthly averaged ozone over Frankfurt, Munich Paris for December 2003 and Vienna for November 2003. The solid black line if the observations and the dashed black line shows the standard deviation of the observations.

		DJF 2003			MAM 2003			JJA 2003			SON 2003		
		MB	stddev	nobs	MB	stddev	nobs	MB	stddev	nobs	MB	stddev	nobs
rean	Kiruna	-7.09	2.12	21	-9.87	2.88	43	-9.94	2.75	46	-4.55	5.94	32
	Zugspit	-6.54	3.92	237	-3.49	4.79	281	-9.89	5.60	199	-6.62	4.46	285
	Izana	-5.77	2.56	11	-7.98	4.29	54	-9.61	4.45	50	-7.25	4.35	36
		DJF 2004			MAM 2004			JJA 2004			SON 2004		
		MB	stddev	nobs	MB	stddev	nobs	MB	stddev	nobs	MB	stddev	nobs
rean	Kiruna	-8.53	2.52	14	-11.25	1.81	60	-9.20	3.20	34	-	-	-
	Zugspit	-5.55	4.08	37	-7.18	3.16	115	-9.58	5.36	145	-	-	-
	Izana	-7.10	3.06	24	-7.22	3.16	23	0.76	5.98	12	-	-	-

Table 3.3.1 Seasonal relative mean bias (MB, %), standard deviation (STD, %) for the considered period and number of observations used (NOBS), compared to NDACC FTIR observations at Kiruna, Zigspitze and Izana (mean bias and stddev in %). The overall uncertainty for the CO measurements is approximately 5%.

3.3.3 FTIR tropospheric CO observations, Validation against FTIR observations from the NDACC network

In this section, we compare the CO profiles of the CAMS reanalysis model with FTIR measurements Kiruna (68°N) (left), Zugspitze (47°N) and Izana (28°N). These ground-based, remote-sensing instruments are sensitive to the CO abundance in the troposphere and lower stratosphere, i.e. between the surface and up to 20 km altitude. Tropospheric CO profiles and columns are validated (up to 10km). A description of the instruments and applied methodologies can be found at http://nors.aeronomie.be.

Table 3.3.1 and figure 3.3.10 show that the day to day variation of the tropospheric columns of CO agree well. The reanalysis underestimates CO at all three sites with values around 10%, which is larger than the reported measurement uncertainty range (6%).

- The number of NDACC stations in 2003-3004 is limited
- The difference between the analysis and the 1d forecast run is negligible
- The observed biases are comparable to the biases for 2010 seen in gls8

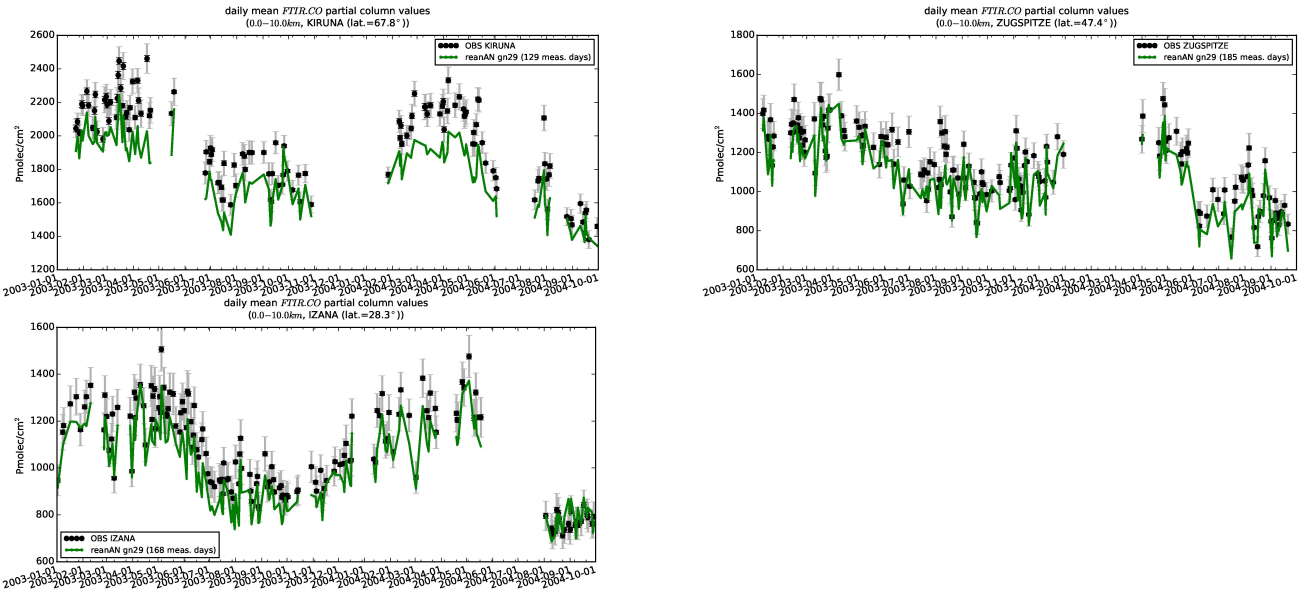

Figure 3.3.10. Daily mean values of rean tropospheric CO columns (till 10km) compared to NDACC FTIR data at Kiruna (68°N) (left), Zugspitze (47°N) and Izana (28°N) for the period 2003-October 2004. The number of measurement days is indicated in the legend.

3.3.4 Comparison CAMS reanalysis 2003 (gn29) with MOPITTv6/v7 CO

Timeseries of CO total columns from the CAMS 2003 reanalysis are compared with CO total column retrievals from MOPITT version 6 and version 7 (thermal infrared radiances) (Emmons et. al., 2009) over eight selected regions. As the processing and deliveries of the MOPITT Version 5 products, used in the previous reports, concluded at the end of 2016, we use MOPITT version 6 and version 7 products. For the comparison with MOPITT, the modelled CO concentrations were transformed using MOPITT v6 averaging kernels.

The CO total column seasonality in different regions is well reproduced by the model. CO total columns are slightly underestimated by the model compared to the satellite retrievals in Europe and the US (up to 10%) and in East Asia, Alaskan and Siberian fire regions during June to October (5-10%), with the exception of May 2003 in the Siberian fire region, where CAMS reanalysis is higher than the satellite retrievals by ~15%.

Figure 3.3.11 CO total columns for satellite retrievals (black) MOPITT V6 and V7 and reanalysis data (red) over selected regions for 2003.

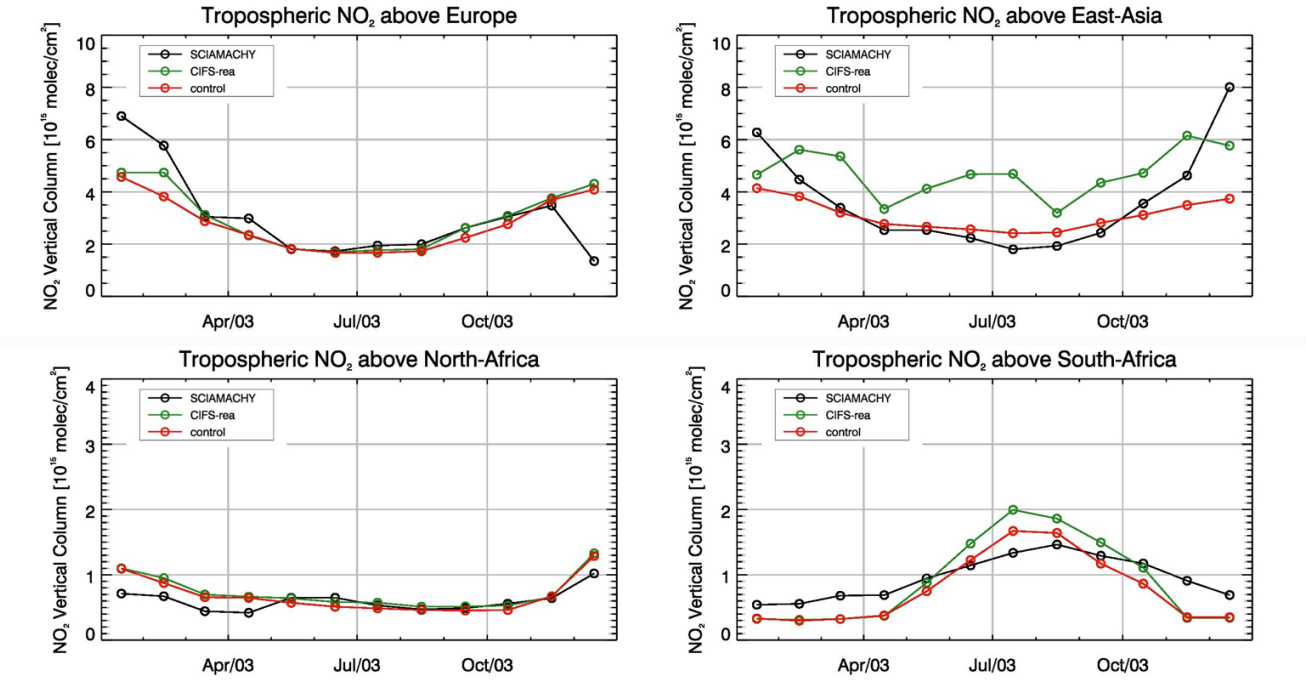

Figure 3.4.1. Comparison of time series of tropospheric NO_2 columns from SCIAMACHY to model results over selected regions. Upper panels represent regions dominated by anthropogenic emissions, lower panels represent those dominated by biomass burning.

3.4 Tropospheric nitrogen dioxide

3.4.1 Evaluation against SCIAMACHY NO2 retrievals

In this section, model columns of tropospheric NO_2 are compared to SCIAMACHY/Envisat NO_2 satellite retrievals (IUP-UB v0.7) [Richter et al., 2005]. This satellite data provides excellent coverage in space and time and very good statistics. However, only integrated tropospheric columns are available and the satellite data is always taken at the same local time, roughly 10:00 LT for SCIAMACHY, and at clear sky only. Therefore, model data are vertically integrated, interpolated in time and then sampled to match the satellite data. Specifically, SCIAMACHY data were gridded to model resolution (i.e. 0.75° deg x 0.75° deg). Model data were treated with the same reference sector subtraction approach as the satellite data. Uncertainties in NO_2 satellite retrievals are large and depend on the region and season. Winter values in mid and high latitudes are usually associated with larger error margins. As a rough estimate, systematic uncertainties in regions with significant pollution are on the order of 20% – 30%.

The seasonal variation of tropospheric NO_2 in some selected regions is shown in Fig. 3.4.1. Apart from East-Asia, the seasonality and magnitude of satellite values is reasonably well represented by the CAMS reanalysis for the regions investigated. Over East Asia, the control agrees much better with SCIAMACHY, but underestimates wintertime values leading to an underestimation of the seasonal cycle. The CAMS reanalysis shows a strong variation of values from month to another over East-Asia and completely fails to reproduce the observed sesonality. Satellite observations in winter have larger uncertainties, but inaccuracies in winter NOx emissions and NO_2 lifetime in the highly polluted atmosphere over China could lead to larger model uncertainties during winter. The control is a bit closer to SCIAMACHY over South Africa.

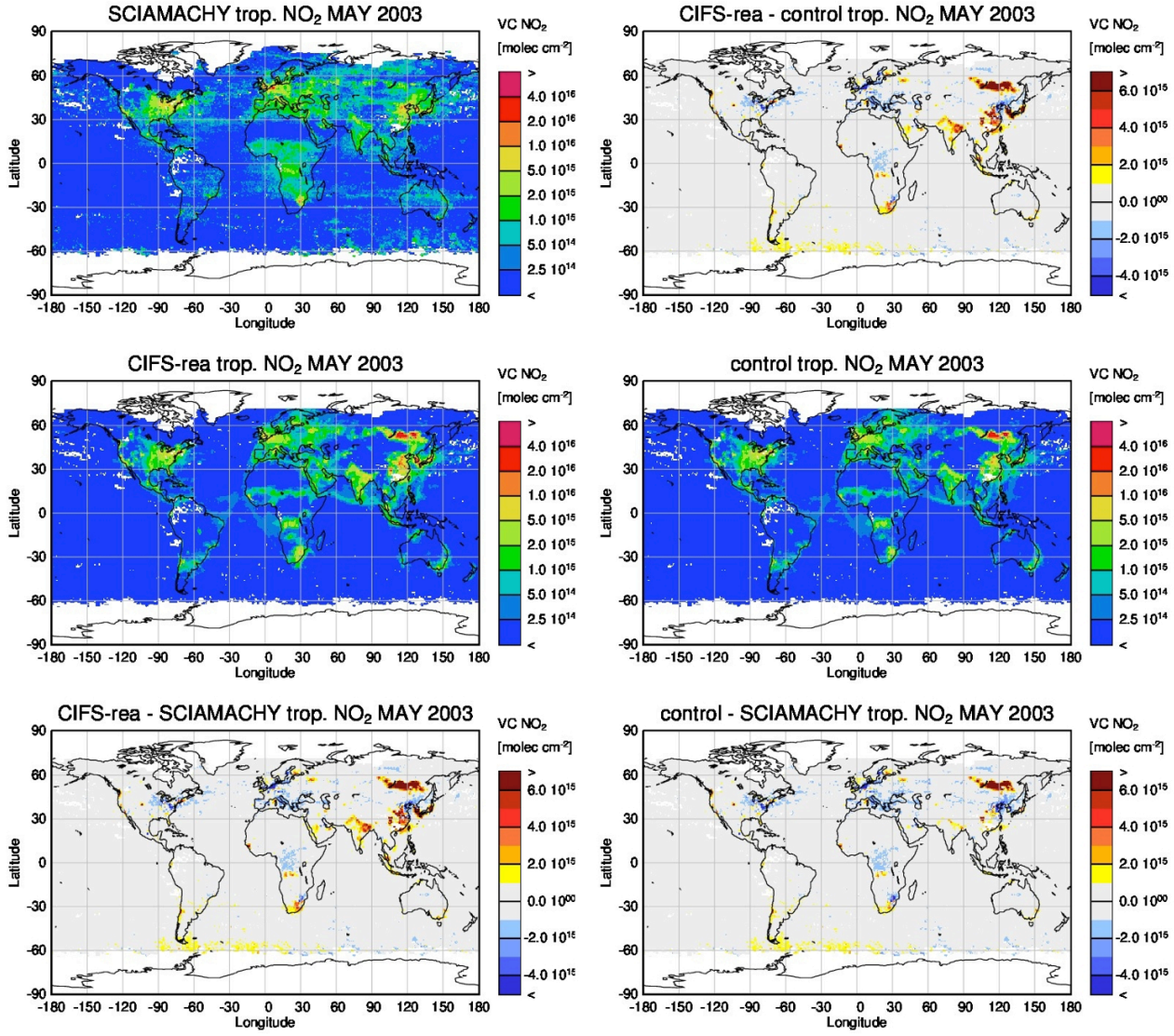

Figure 3.4.2. Global map comparisons of satellite retrieved and model simulated tropospheric NO_2 columns [molec cm^{-2}] for May 2003. The top row shows monthly mean tropospheric NO_2 columns retrieved by SCIAMACHY as well as the difference between the CAMS reanalysis and control, the second row shows the corresponding tropospheric NO_2 columns for model simulated averages. The third row shows differences of monthly means between models and SCIAMACHY. SCIAMACHY data were gridded to model resolution (i.e. 0.75° deg x 0.75° deg). Model data were treated with the same reference sector subtraction approach as the satellite data. Check panels

Global monthly mean map comparisons (see Fig. 3.4.2 for an example for May 2003) show that the overall spatial distribution and magnitude of tropospheric NO_2 is well reproduced by both model runs, indicating that emission patterns and NO_x photochemistry are reasonably represented. Some differences are apparent between observations and simulations, with generally larger shipping signals simulated by the models. Boreal forest fire emissions are overestimated for example over Siberia in May 2003. The reanalysis tends to show larger differences from SCIAMACHY than the control over Indonesia and East-Asia.

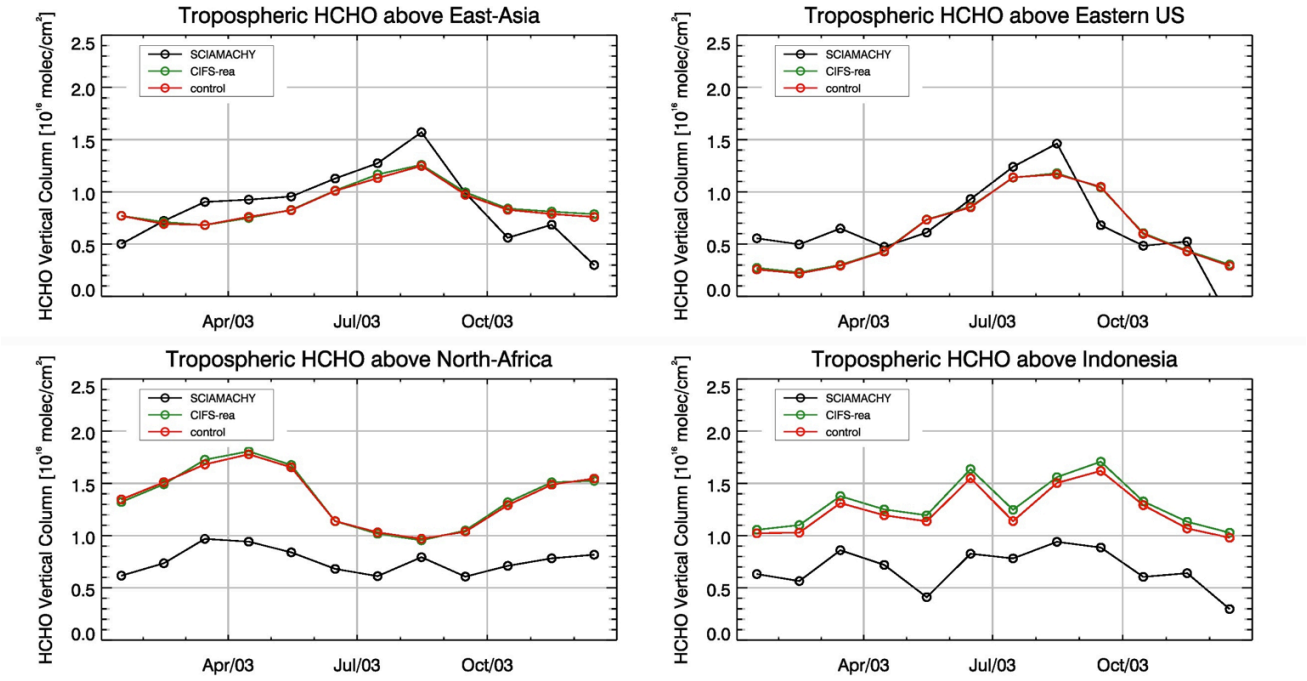

Figure 3.5.1. Comparison of time series of tropospheric HCHO columns from SCIAMACHY and model results over selected regions. The regions differ from those used for NO_2 to better focus on HCHO hotspots: East Asia (25-40°N, 110-125°E), Eastern US (30-40°N, 75-90°W), Northern Africa (0-15°N, 15°W-25°E) and Indonesia (5°S-5°N, 100-120°E). Negative satellite retrieved values over Eastern US are due to a lack of data during Northern Hemisphere winter months for this region.

3.5 Formaldehyde

3.5.1 Validation against SCIAMACHY HCHO satellite data

In this section, simulations of tropospheric formaldehyde are compared to SCIAMACHY/Envisat HCHO satellite retrievals (IUP-UB v1.0) [Wittrock et al., 2006]. As the retrieval is performed in the UV part of the spectrum where less light is available and the HCHO absorption signal is smaller than that of NO_2, the uncertainty of monthly mean HCHO columns is relatively large (20% – 40%) and both noise and systematic offsets have an influence on the results. However, absolute values and seasonality are retrieved more accurately over HCHO hotspots.

The time series in Fig. 3.5.1 show different cases for HCHO: regions dominated by biogenic emissions with some anthropogenic input (East Asia, Eastern US) and regions with both biogenic and pyrogenic sources (North-Africa and Indonesia). The CAMS reanalysis reproduces satellite observations for East Asia and Eastern US with respect to absolute values and seasonality. The reanalysis shows a positive offset compared to satellite retrievals for North-Africa and Indonesia, while the seasonality is in agreement with the retrievals. It is not clear if this is due to a low bias in the satellite data or to a model overestimation of HCHO in these regions. There is almost no difference between the reanalysis and the control for all regions, except for Indonesia where the control shows slightly lower values compared to the reanalysis.

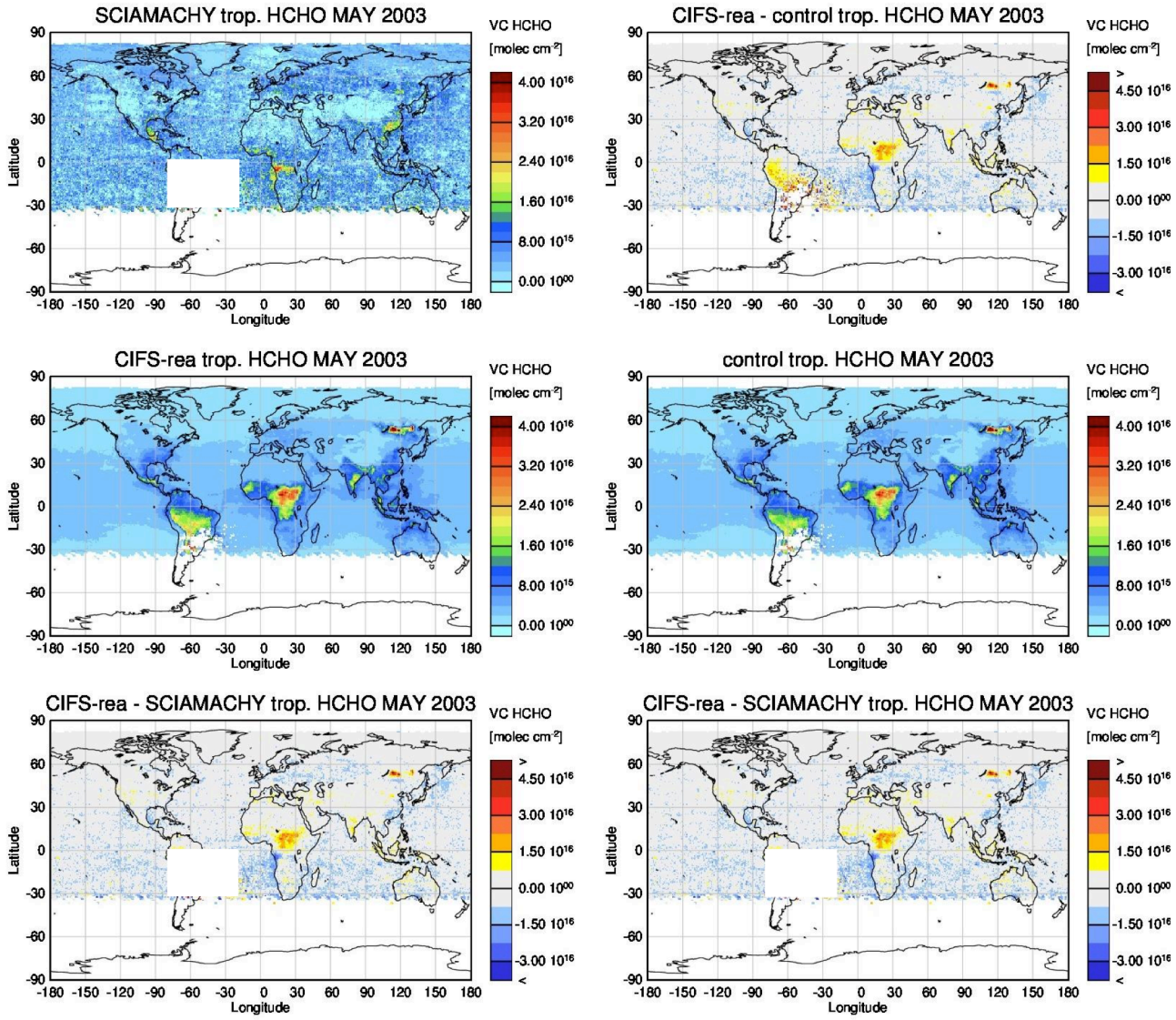

Figure 3.5.2. Global map comparisons of satellite retrieved and model simulated tropospheric HCHO columns [molec cm-2] for May 2003. The top row shows monthly mean tropospheric HCHO columns retrieved by SCIAMCHAY, the second row shows the same but for model simulated averages. The third row shows differences of monthly means between models and SCIAMACHY. SCIAMACHY data were gridded to model resolution (i.e. 0.75° deg x 0.75° deg). Model data were treated with the same reference sector subtraction approach as the satellite data. Satellite retrieved values in the region of the South Atlantic anomaly are not valid and therefore masked out (white boxes in all images except those which show model results only).
Check panels

Global monthly mean map comparisons (see Fig. 3.5.2 example for May 2003) show that the magnitude of oceanic and continental background values and the overall spatial distribution are well represented by the reanalysis and control. Compared to SCIAMACHY satellite retrievals, there is an overestimation of values for Central Africa during the whole season as well as Northern Australia during autumn and winter. Values over Europe are underestimated during spring, and there is an overestimation of values for boreal forest fires possibly pointing to problems regarding the emissions e.g. in May 2003 (as for tropospheric NO_2).

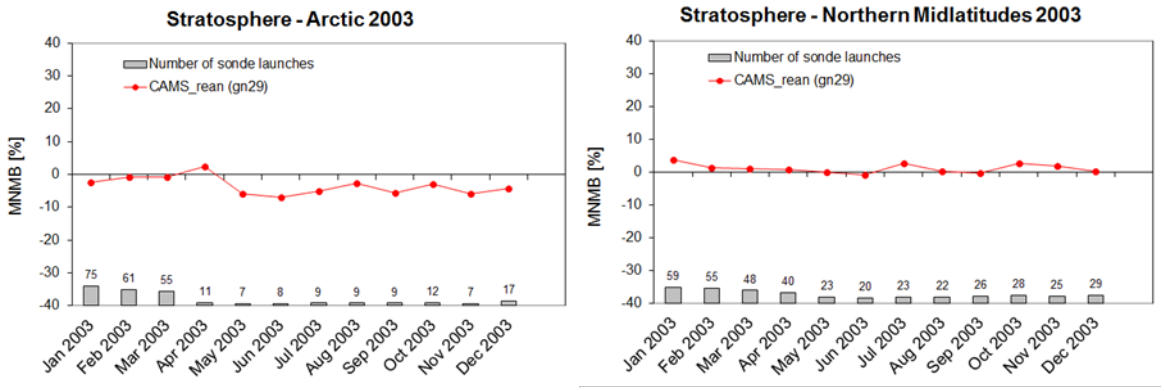

Figure 3.6.1: MNMBs, reanalysis minus ozone sonde, over the Arctic and Northern midlatitudes.

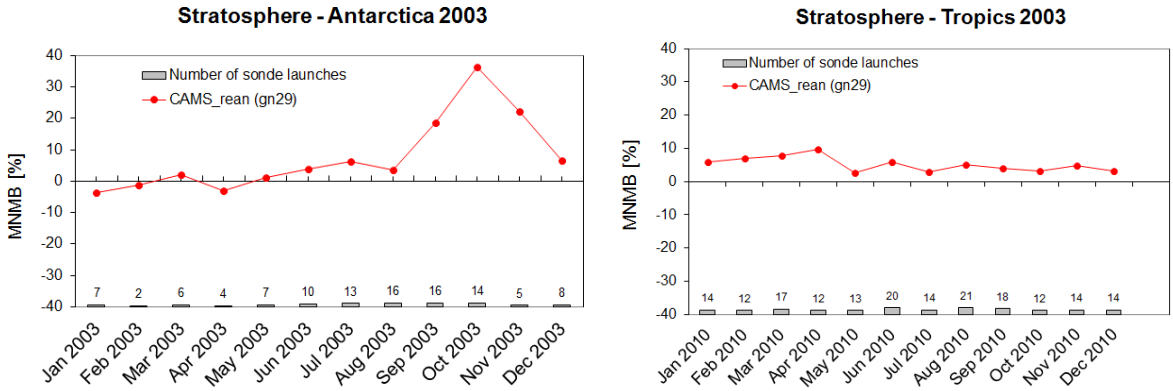

Figure 3.6.2: MNMBs, reanalysis minus ozone sonde, over the Antarctic and the Tropics

3.6 Stratospheric ozone

3.6.1 Validation against ozone sondes

In what follows, we present the results of the stratospheric ozone evaluation against ozone soundings from the NDACC, WOUDC, NILU and SHADOZ databases. The sondes have a precision of 3-5% (~10% in the troposphere for Brewer Mast) and an uncertainty of 5-10%. For further details see Cammas et al. (2009), Deshler et al. (2008) and Smit et al (2007). Model profiles of the reanalysis are compared to balloon sondes measurement data of 44 stations for the period January-December 2003. The validation covers the vertical range between 90 and 10hPa , (for the Tropics 60 and 10hPa). A description of the applied methodologies and a map with the sounding stations can be found in Eskes et al. (2016).

Over the over the **Northern Midlatitudes** O_3 partial pressures are reproduced correctly with MNMBs between -1 and 3.6%, see Fig. 3.6.1. Over the **Arctic**, O_3 partial pressures are slightly underestimated (MNMBs are between -7 and 2.5%). Over the **Tropics**, stratospheric Ozone is slightly overestimated throughout 2003 (MNMBs between 2.5 and 10%). Over the **Antarctic**, MNMBs are between -4 and 7%, except during the peak of the ozone hole season (October 2003), where MNMBs reach up to 36%; this needs further investigation and might be related to the use of

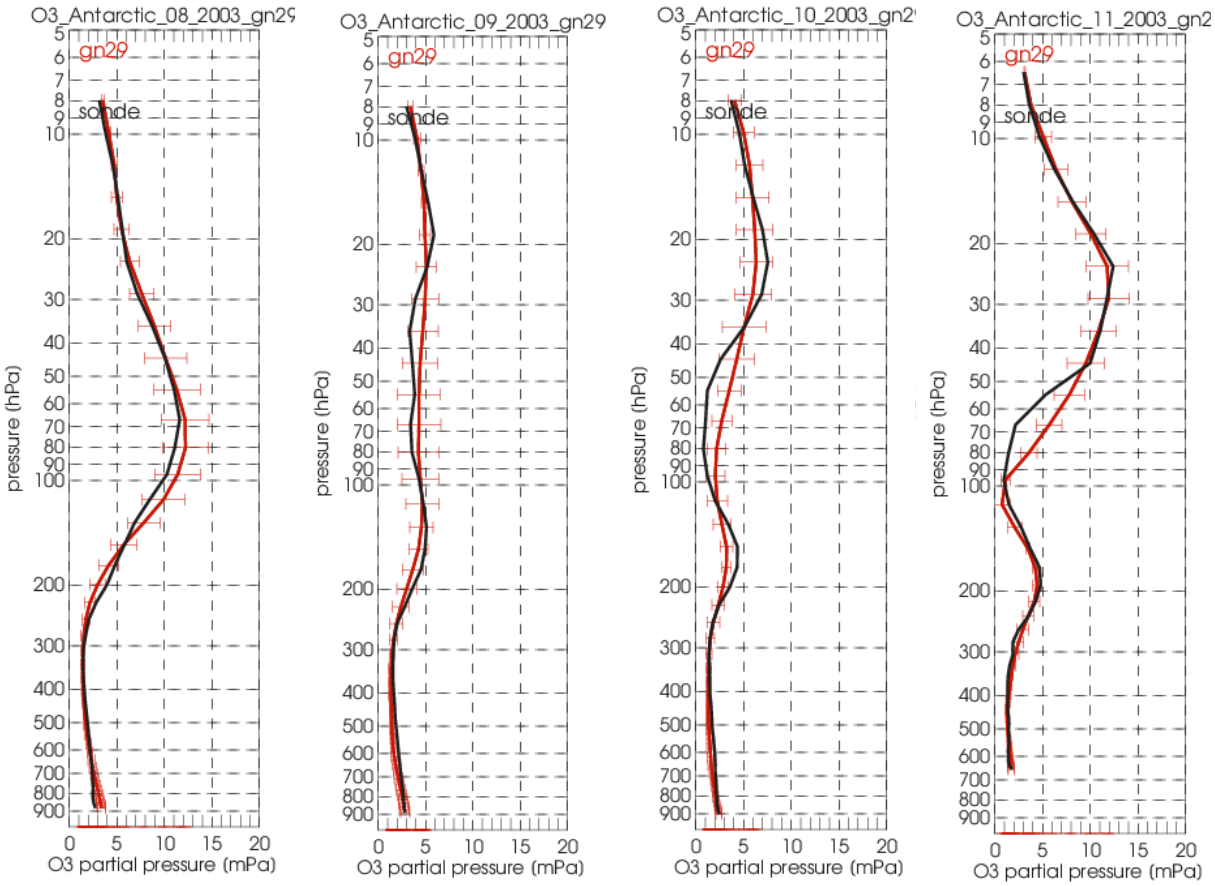

Figure 3.6.3: Mean profiles for Aug, Sep, Oct and Nov 2003 over Antarctica (monthly mean of soundings of the stations Neumayer and South Pole)

the 21L v8.6 SBUV/2 data. Stratospheric ozone is overestimated especially between 90-30 hPa during the ozone hole season, see Fig. 3.6.2 and Fig. 3.6.3.

3.6.2 Validation against ozone observations from the NDACC network (MWR, LIDAR)

In this section we present a comparison between the CAMS reanalysis model against MWR and LIDAR observations from the NDACC network. A detailed description of the instruments and applied methodologies for all NDACC instruments can be found at http://nors.aeronomie.be.

MWR (microwave) at Mauna Loa (19.5°N, mountain station) and Bern (47°N, 7°E, northern midlatitude station). LIDAR at Lauder, New Zeeland (46°S, 169.7°E, altitude 370m) and Hohenpeissenberg, Germany (47°N, 11°E, altitude 1km)

From table 3.6.1, the upper stratospheric partial column bias at Bern during MAM 2003 is highest and significant (bias=12%) compared to the 6% uncertainty on the partial column. However, note that during MAM only limited measurements are available at Bern and that the bias is determined by measurements during the first week of April 2003 (see Fig. 3.6.4). At Mauna Loa, the observed bias falls within the measurements uncertainty. For the operational CAMS system (o-suite), the typical bias at Bern is below 1%.

Table 3.6.1: Seasonal relative mean bias (MB, %), standard deviation (STD, %) of the partial (upper stratospheric 25km – 65km) ozone column for the considered period and number of observations used (NOBS), compared to NDACC microwave observations at Bern and Mauna Loa (mean bias and stddev in %).

		DJF 2003			MAM			JJA			SON		
		MB	stddev	nobs	MB	stddev	nobs	MB	stddev	nobs	MB	stddev	nobs
rean	Bern	3.23	3.96	23	12.22	8.67	16	6.00	4.62	62	5.43	4.26	54
	Mauna	-8.17	2.47	5	-6.24	2.61	7	-5.53	1.66	4	-6.79	3.90	7

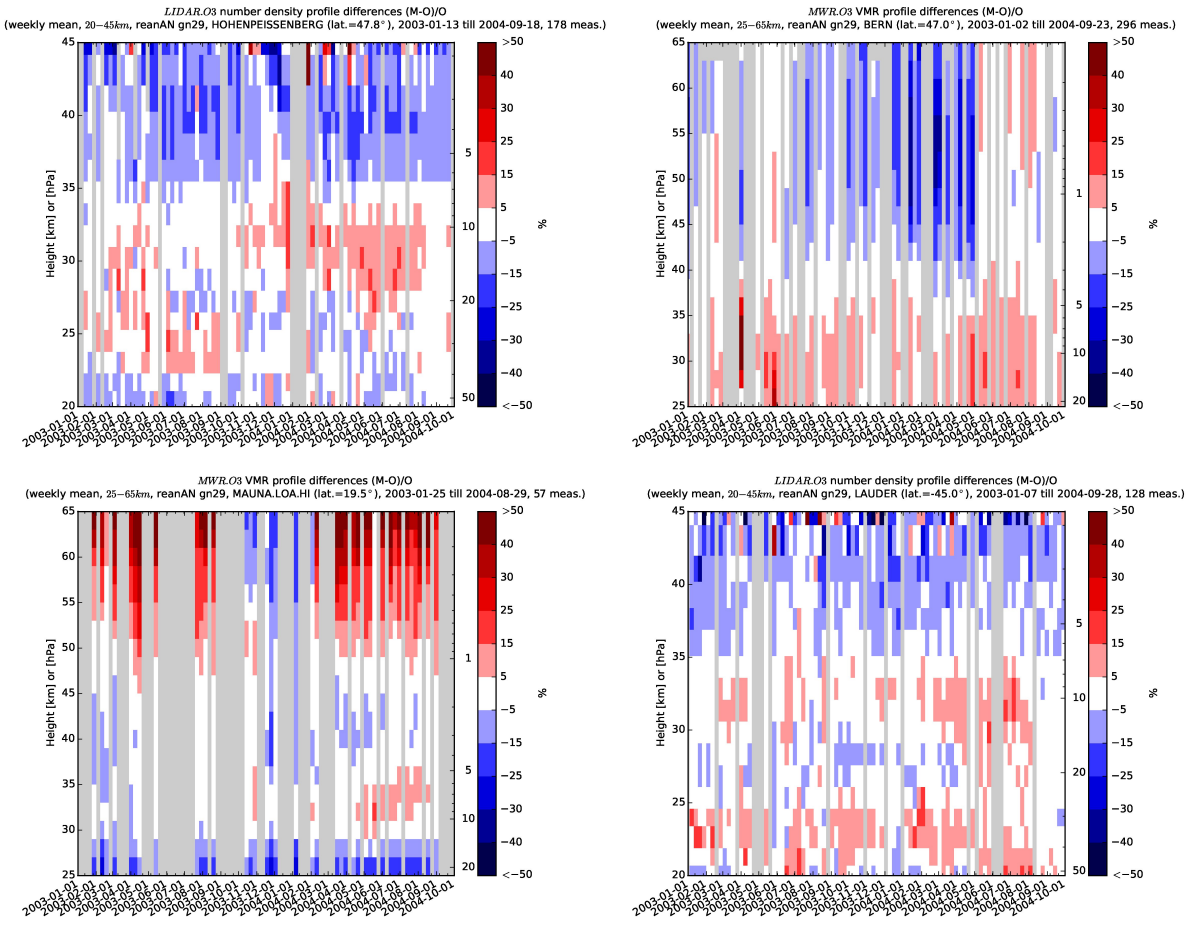

Figure 3.6.4: Comparison of the weekly mean profile bias between the O_3 mixing ratios of o-suite and the NDACC station at Hohenpeissenberg (LIDAR), Bern (MWR), Mauna Loa (MWR) and Lauder (LIDAR). For the LIDAR stations, the measurement uncertainty above 35km is comparable to the observed profile bias.

From the profile differences in Fig. 3.6.4 we see that the overestimation at Bern is located between 30km and 35km, and this is confirmed by the LIDAR profiles at Hohenpeissenberg. At Lauder and Hohenpeissenberg (LIDAR), the reanalysis corresponds with the observed ozone between 25km and 35km: slightly underestimating below 30km and slightly overestimating between 30 and 35km.

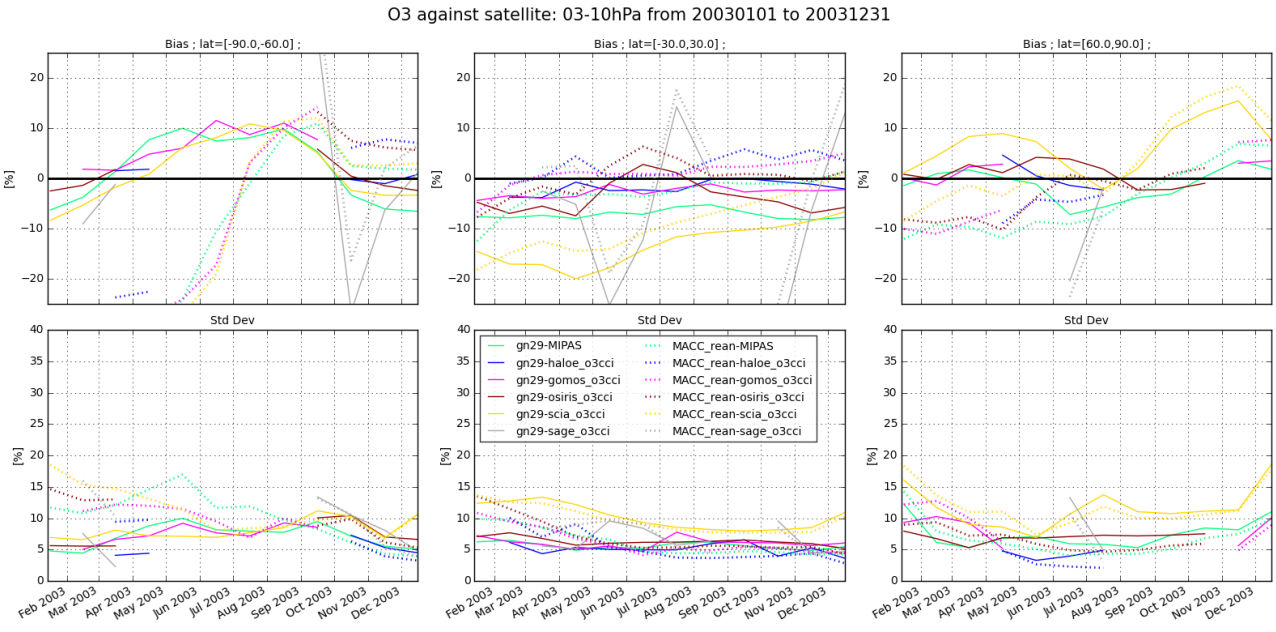

Figure 3.6.5: Time series comparing ozone from CAMS reanalyses (gn29) and MACC reanalyses with observations from MIPAS, HALOE, GOMOS, OSIRIS, SCIAMACHY and SAGE for the period 2003-01-01 to 2003-12-31 in the upper stratosphere (3-10hPa averages): top row, normalized mean bias (model-obs)/obs (%); bottom row, standard deviation of relative differences (%).

The uncertainty on the LIDAR concentration increases with altitude and above 35km the observed differences are comparable to the measurement uncertainty (>10%, see http://nors.aeronomie.be/projectdir/PDF/NORS_D4.2_DUG.pdf).

3.6.3 Comparison with observations by limb-scanning satellites

This section compares the model output with observations by limb-scanning satellite instruments: MIPAS, HALOE, GOMOS, OSIRIS, SCIAMACHY, SAGE II and ODIN/SMR. In order to keep the processing uniform, the ESA CCI harmonized dataset of ozone profiles from satellite limb and occultation measurements was chosen, see Sofieva et al. (2013). The only exception is MIPAS where we use the MIPAS-ESA v6 dataset.

All datasets are averaged over all longitudes and over the three most interesting latitude bands for stratospheric ozone: Antarctic (90°S-60°S), Tropics (30°S-30°N) and Arctic (60°N-90°N).

For reference, we also include the MACC reanalysis, which has been validated during the preoperational phase of CAMS, see Benediktow et al. (2014).

The satellite observations are affected by biases which depend on latitude range and altitude, and may have also long-term stability problem, see Hubert et al. (2016). Globally the SMR instrument has inconsistent values with respect to the others and present a high variability; it has been eliminated from this validation. In the following figures, we present the mean bias against the instruments and in the second row the standard deviation on the biases.

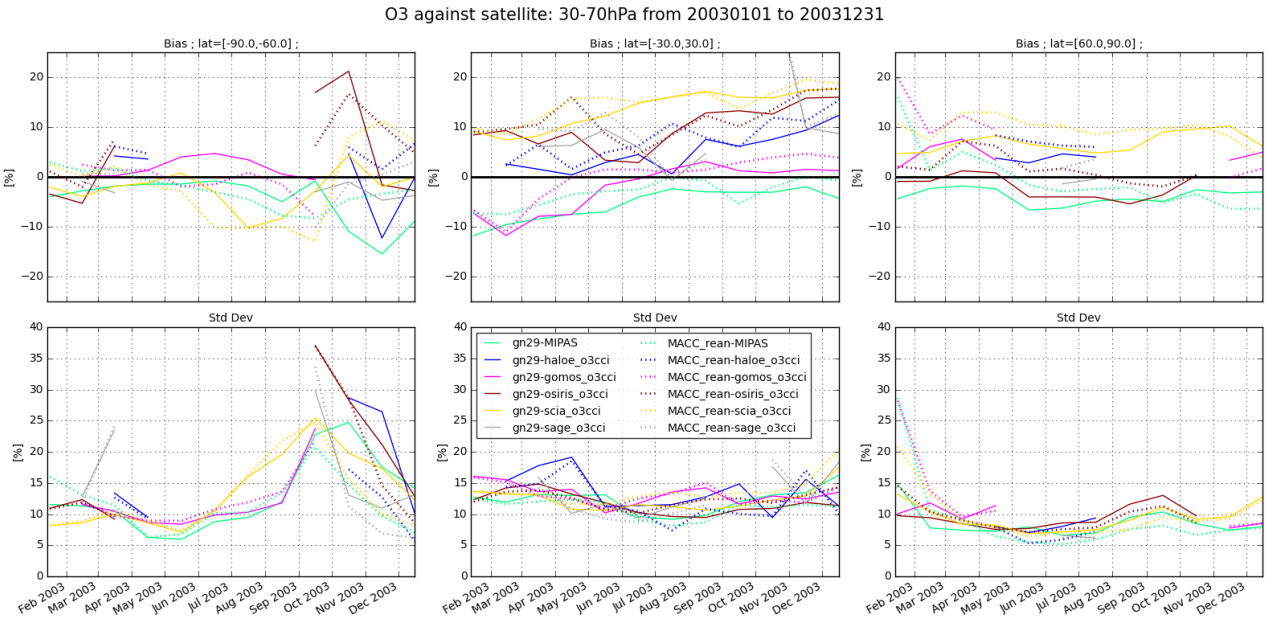

Figure 3.6.6: Time series comparing ozone from CAMS reanalyses (gn29) and MACC reanalyses with observations from MIPAS, HALOE, GOMOS, OSIRIS, SCIAMACHY and SAGE II for the period 2003-01-01 to 2003-12-31 in the lower stratosphere (30-70hPa averages): top row, normalized mean bias (model-obs)/obs (%); bottom row, standard deviation of relative differences (%).

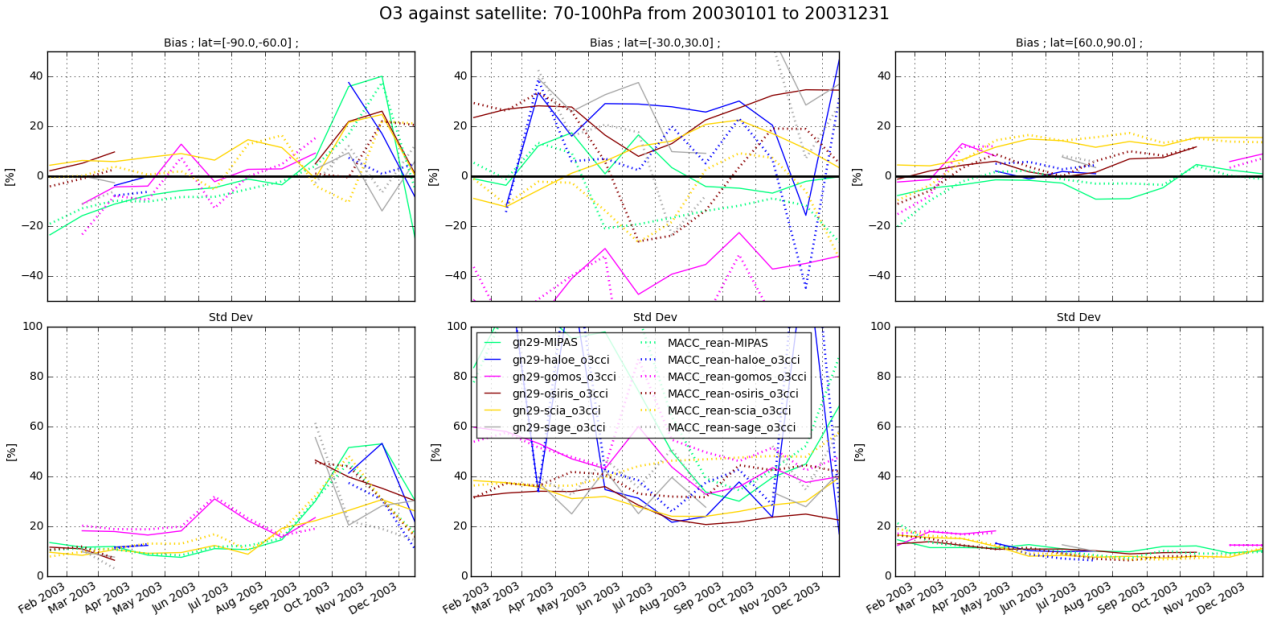

Figure 3.6.7: Time series comparing ozone from CAMS reanalyses (gn29) and MACC reanalyses with observations from MIPAS, HALOE, GOMOS, OSIRIS, SCIAMACHY and SAGE II for the period 2003-01-01 to 2003-12-31 in the UTLS (70-100hPa averages): top row, normalized mean bias (model-obs)/obs (%); bottom row, standard deviation of relative differences (%).

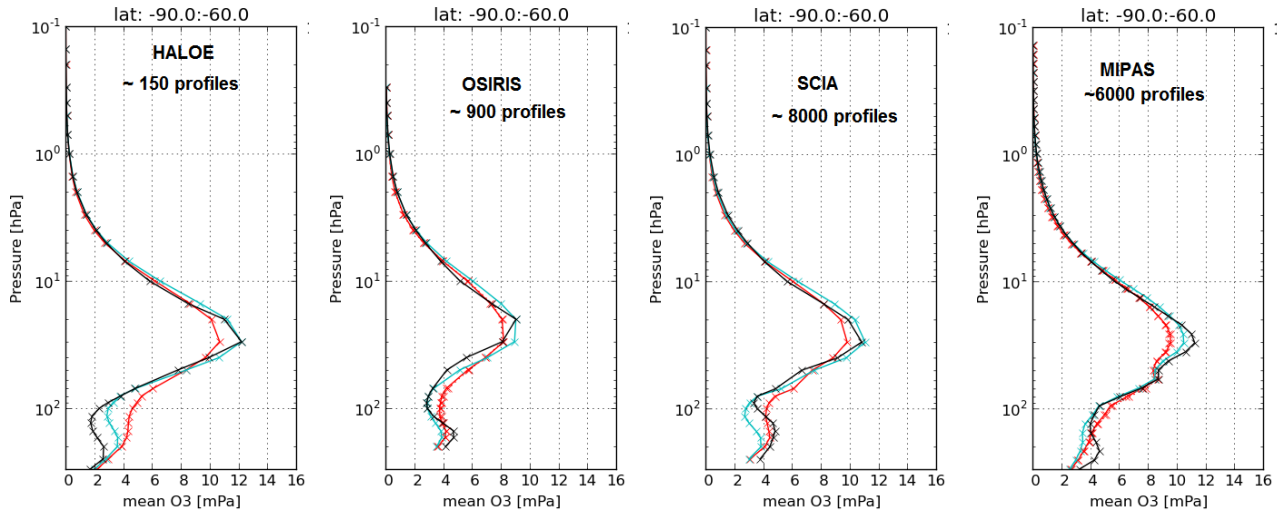

Figure 3.6.8: Mean profiles for October 2003 over the South Pole latitude band (90°S-60°S): reanalysis gn29 (red) and MACC (cyan) versus satellite observations (black) using, from left to right: HALOE, OSIRIS, SCIAMACHY and MIPAS.

In the upper stratosphere (3-10hPa, see Fig. 3.6.5), there is a clear improvement in the polar regions, compared to the MACC reanalysis. In the tropics, the bias is generally negative (with an amplitude depending on the instrument) and lower than the MACC reanalysis. In this altitude range, the SAGE II instrument has inconsistent measurements relative to the others.

Globally, except for SCIAMACHY and SAGE II, the absolute value of the bias is < 10%.

In the middle lower stratosphere (30-70hPa, see Fig. 3.6.6), in the south polar region, the October overestimation with respect to ozonesondes is confirmed by OSIRIS, SCIA and HALOE but it is not as severe (20%, 5% and 5% respectively). Unexpectedly, this overestimation is not confirmed by MIPAS. The difference with ozonesonde findings is due to the different sampling of the vortex: ozonesondes are available only at Neumayer and South Pole.

In the tropics the bias is slightly positive (0-10%) except for MIPAS where it is slightly negative (-10 to 0%).

Globally the absolute value of the mean bias is < 15% except for SCIAMACHY and OSIRIS during the ozone hole episode and at the Tropics during the second half of the year.

In the lower stratosphere and UTLS (70-100hPa, see Fig. 3.6.7), only the measurement in the polar regions can be used, as the biases relative to the instruments in the tropics are totally inconsistent. In the Antarctic, a high bias (>20%) is reported for the months of October and November. Except for this ozone hole episode, globally the absolute value of the bias is <15%.

The ozone hole episode was studied with profiles of partial pressures averaged over October 2003 for 90°S-60°S, separately for each available instrument (figure 3.6.8). Qualitatively speaking the conclusion is the same as with ozonesondes (figure 3.6.3): the vertical profiles of the reanalysis gn29 are smoother than the observations, which was not the case with the MACC reanalysis. This holds also in the comparison with MIPAS, even though that dataset was assimilated.

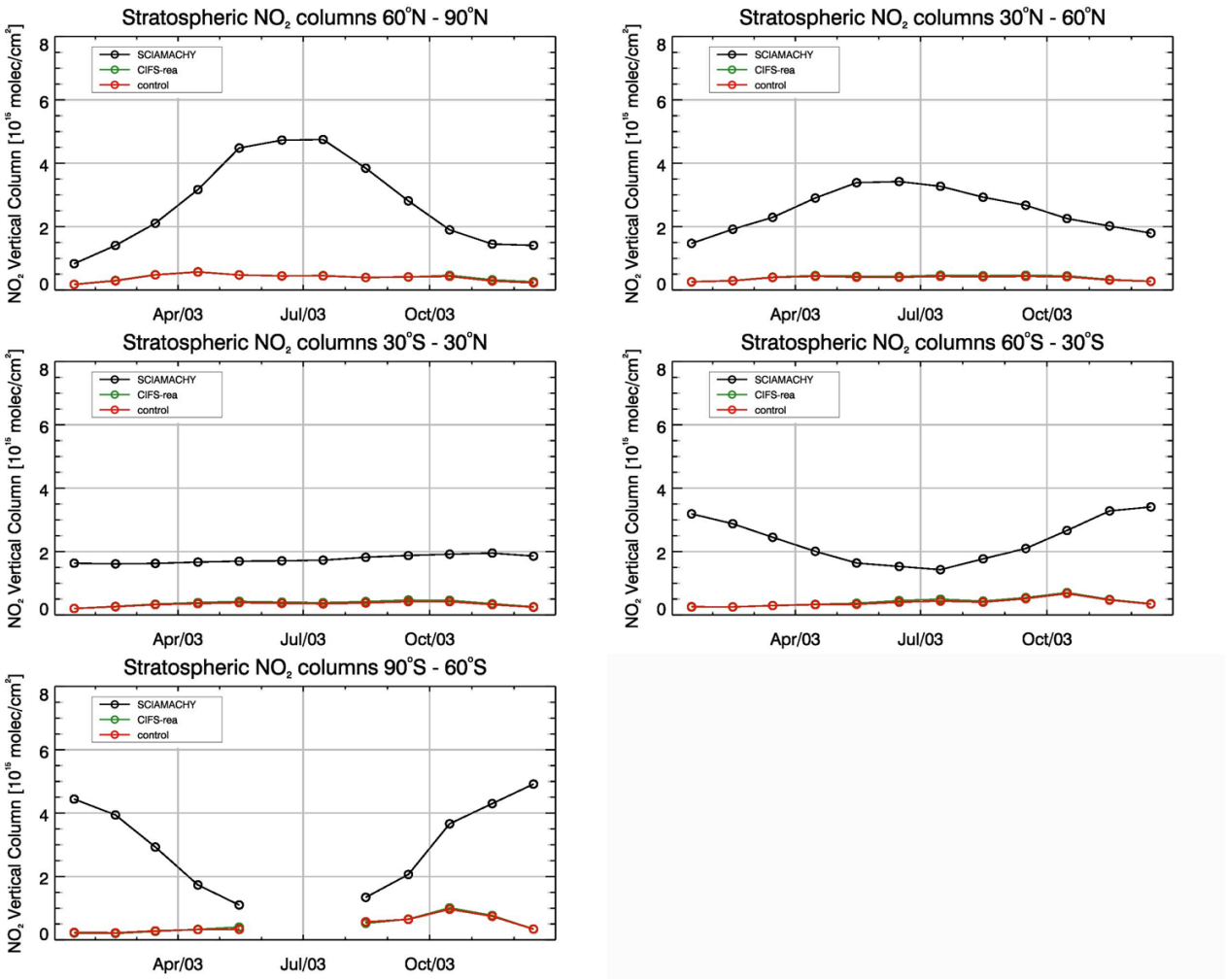

Figure 3.7.1. Time series of average stratospheric NO_2 columns [10^{15} molec cm^{-2}] from SCIAMACHY compared to model results for different latitude bands.

3.7 Stratospheric NO_2

3.7.1 Comparison with observation from the NDACC network (FTIR)

All NDACC FTIR stations (Ny Alesund 79N, Kiruna 68N, Jungfraujoch 47N, Izana 28N and Reunion 21S) show a strong underestimation of the stratospheric NO_2 column with biases between 70 and 80%. For the experimental reanalysis gls8, typical biases in 2010 were between 30 and 40%.

3.7.2 Comparison with SCIAMACHY satellite observations

Nitrogen dioxide from SCIAMACHY/Envisat satellite retrievals (IUP-UB v0.7) were compared to simulated stratospheric NO_2 columns. As expected, time series for different latitude bands (Fig. 3.7.1) show that the reanalysis and control fail to reproduce observed stratospheric NO_2 columns, due to the missing stratospheric chemistry in C-IFS.

4. Validation results for greenhouse gases

4.1 CO_2 validation against ICOS observations

In this section, we compare the CO_2 simulations of the CAMS reanalysis model with surface in-situ measurements. The ICOS infrastructure was not available in 2003, and consequently the access to the data is not straightforward. In this report we have used three stations maintained by LSCE: Amsterdam Island (37.8°S, 77.5°E, 70m asl), Mace Head (53.3°N, 9.9°W, 25m asl) and Puy de dôme (45.7°N, 3°E, 1465 m asl). The measurement protocols are described in the WDCGG web site.

The model underestimates the CO_2 diurnal cycles (Figure 4.1.1) at the two coastal stations (AMS, MHD), probably due to the influence of local sources not well represented in the emission distribution maps. At the mountain station of PUY (France) the CO_2 signal is pretty well simulated, despite a 1 to 2 hours delay in the daytime CO_2 drawdown.

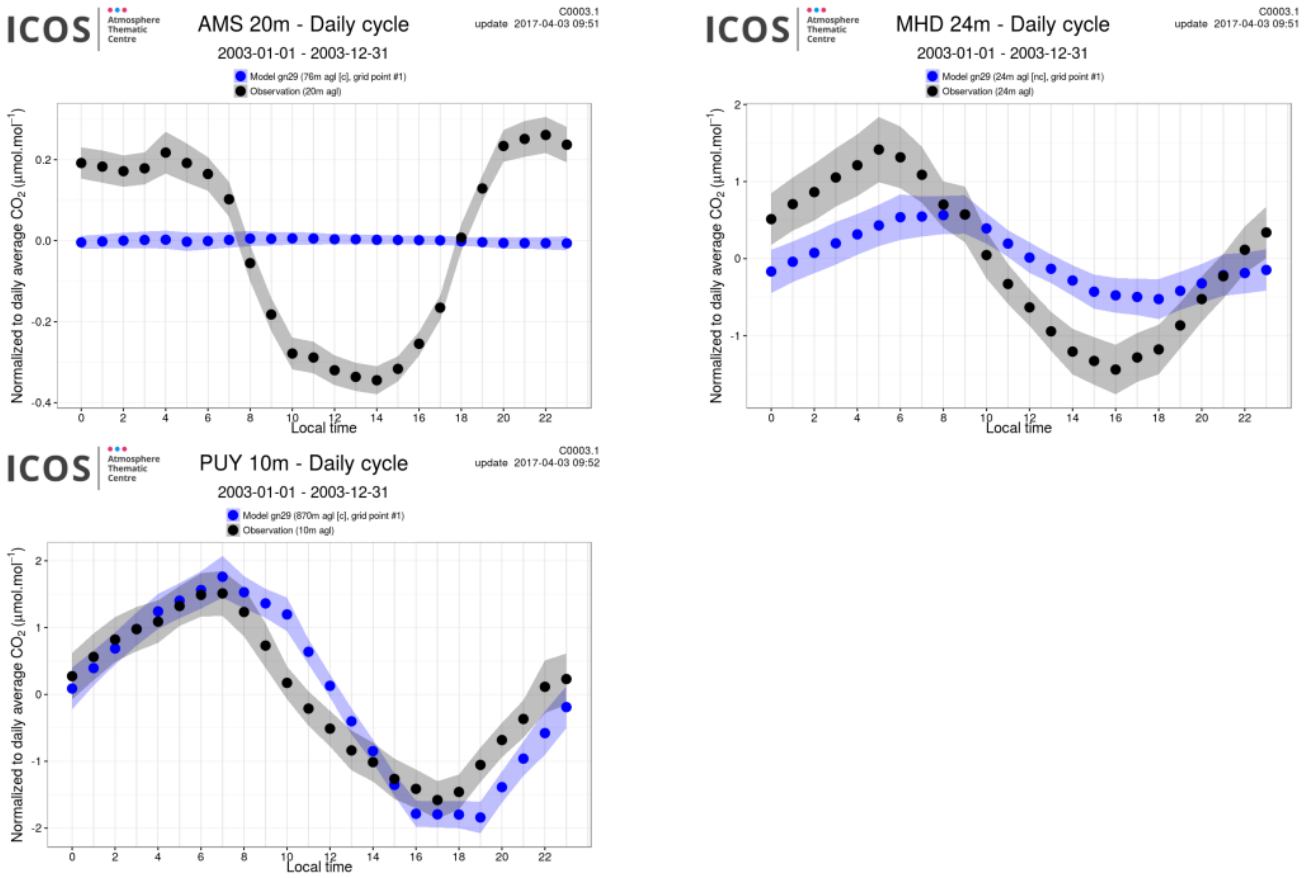

Fig. 4.1.1. Comparison of the mean CO_2 diurnal cycles at the three surface sites (AMS, MHD, PUY).

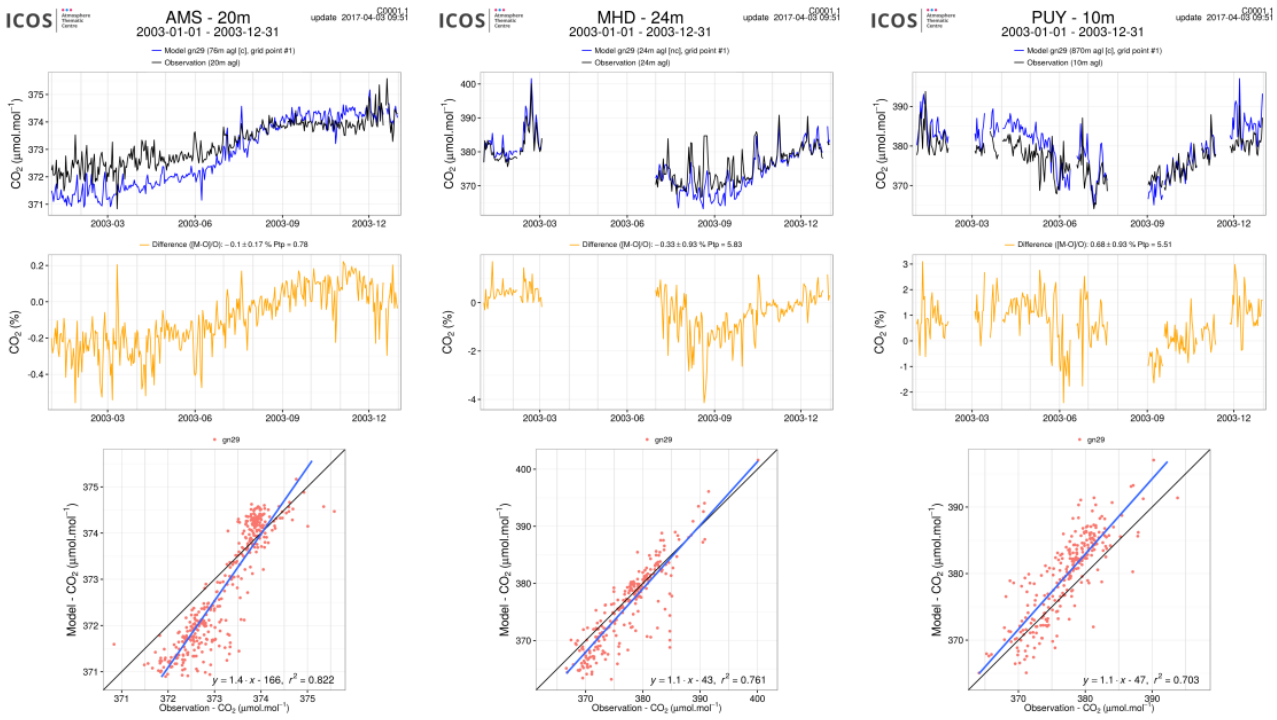

Fig. 4.1.2. Comparison of the CO_2 daily averages at the three surface sites (AMS, MHD, PUY)

At the synoptic scale, the model captures relatively well the phase and amplitude of the synoptic events. One can observe for example an excellent representation of a continental air mass signature at Mace Head in February 2003 (Figure 4.1.2). On the other hand the model overestimates the amplitude of the seasonal cycle by about 0.3% in the southern hemisphere, and 1 to 2% in the northern hemisphere with too high concentrations in the end of winter and too low in the end of summer. It should be noted that the biases are slightly higher for nighttime periods (Figure 4.1.3). The correlation coefficients remain relatively constant over the season, and for day versus night time periods (Figure 4.1.3).

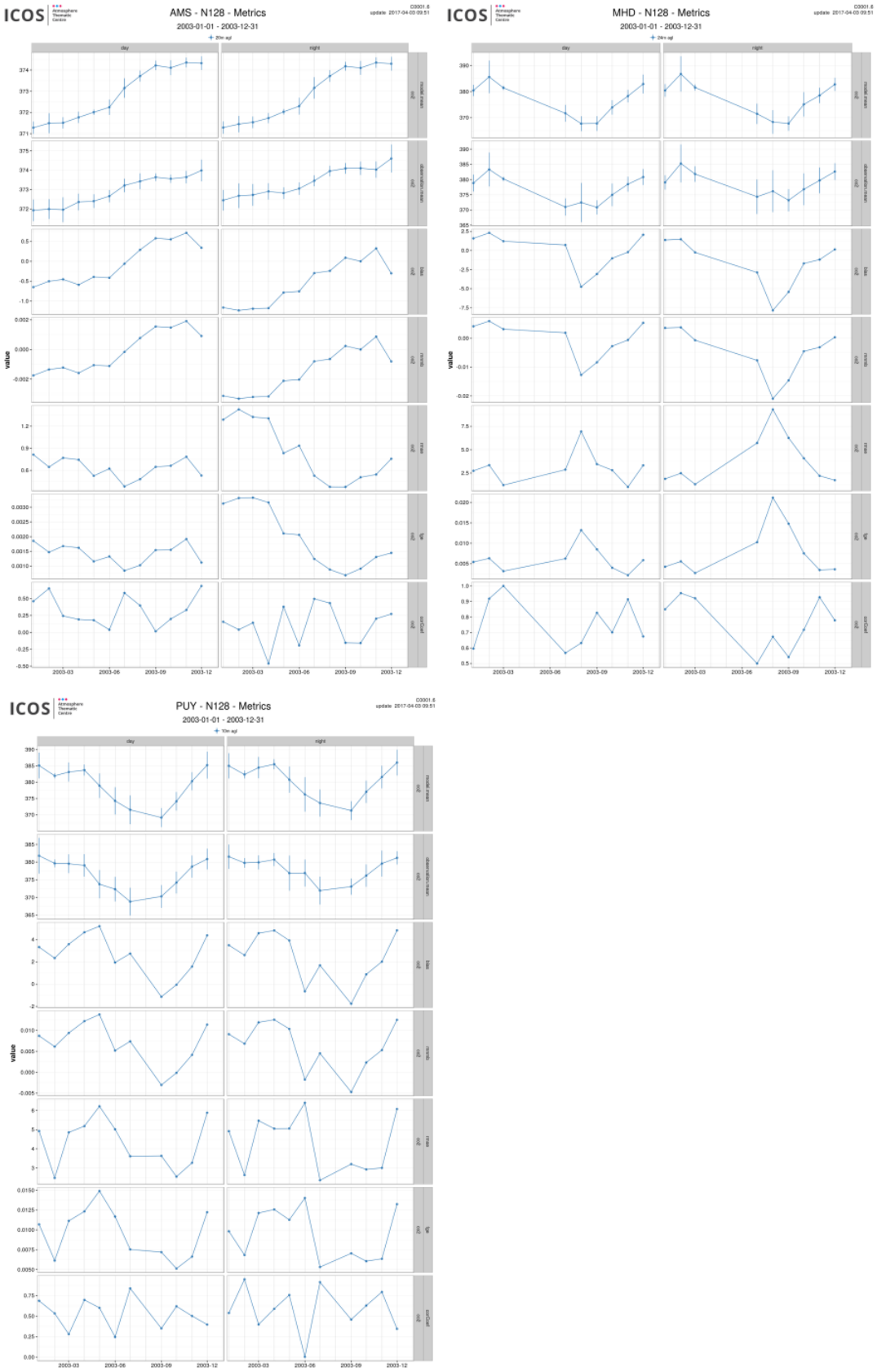

Fig. 4.1.3. Monthly means metrics of CO_2 simulations for the three sites (AMS, MHD, PUY), for daytime (left) and nighttime (right) periods.

5. References

Agustí-Panareda, A., Massart, S., Chevallier, F., Boussetta, S., Balsamo, G., Beljaars, A., Ciais, P., Deutscher, N. M., Engelen, R., Jones, L., Kivi, R., Paris, J.-D., Peuch, V.-H., Sherlock, V., Vermeulen, A. T., Wennberg, P. O., and Wunch, D.: Forecasting global atmospheric CO_2, Atmos. Chem. Phys., 14, 11959-11983, doi:10.5194/acp-14-11959-2014, 2014.

Agustí-Panareda, A., Massart, S., Chevallier, F., Balsamo, G., Boussetta, S., Dutra, E., and Beljaars, A.: A biogenic CO_2 flux adjustment scheme for the mitigation of large-scale biases in global atmospheric CO_2 analyses and forecasts, Atmos. Chem. Phys., 16, 10399-10418, doi:10.5194/acp-16-10399-2016, 2016.

Agusti-Panareda, A., Diamantakis, M., Bayona, V., Klappenbach, F., and Butz, A.: Improving the inter-hemispheric gradient of total column atmospheric CO_2 and CH_4 in simulations with the ECMWF semi-Lagrangian atmospheric global model, Geosci. Model Dev., 10, 1-18, doi:10.5194/gmd-10-1-2017, 2017.

Benedetti, A., J.-J. Morcrette, O. Boucher, A. Dethof, R. J. Engelen, M. Fisher, H. Flentjes, N. Huneeus, L. Jones, J. W. Kaiser, S. Kinne, A. Mangold, M. Razinger, A. J. Simmons, M. Suttie, and the GEMS-AER team: Aerosol analysis and forecast in the ECMWF Integrated Forecast System. Part II : Data assimilation, J. Geophys. Res., 114, D13205, doi:10.1029/2008JD011115, 2009.

Benedictow, A., A.M. Blechschmidt, I. Bouarar, E. Botek, S. Chabrillat, Y. Christophe, E. Cuevas, H. Clark, H. Flentje, A. Gaudel, J. Griesfeller, V. Huijnen, N. Huneeus, L. Jones, J. Kapsomenakis, S. Kinne, B. Langerock, K. Lefever, M. Razinger, A. Richter, M. Schulz, W. Thomas, V. Thouret, M. Vrekoussis, A. Wagner, C. Zerefos: Validation report of the MACC reanalysis of global atmospheric composition, MACC-II Deliverable D_83.6 (available from http://macc.copernicus-atmosphere.eu/services/aqac/global_verification/validation_reports)

Bergamaschi, P., et al. (2013), Atmospheric CH_4 in the first decade of the 21st century: Inverse modeling analysis using SCIAMACHY satellite retrievals and NOAA surface measurements, J. Geophys. Res. Atmos., 118, 7350–7369, doi:10.1002/jgrd.50480.

Cammas, J.P., Brioude J., Chaboureau J.-P., Duron J., Mari C., Mascart P., Nédélec P., Smit H., Pätz H.-W., Volz-Thomas A., Stohl A., and Fromm M., Injection in the lower stratosphere of biomass fire emissions followed by long-range transport: a MOZAIC case study. Atmos. Chem. Phys., 9, 5829-5846, 2009

Cariolle, D. and Teyssèdre, H.: A revised linear ozone photochemistry parameterization for use in transport and general circulation models: multi-annual simulations, Atmos. Chem. Phys., 7, 2183-2196, doi:10.5194/acp-7-2183-2007, 2007.

Dee, D. P. and S. Uppala, Variational bias correction of satellite radiance data in the ERA-Interim reanalysis. Quart. J. Roy. Meteor. Soc.,135, 1830-1841, 2009.

Deshler, T., J.L. Mercer, H.G.J. Smit, R. Stubi, G. Levrat, B.J. Johnson, S.J. Oltmans, R. Kivi, A.M. Thompson, J. Witte, J. Davies, F.J. Schmidlin, G. Brothers, T. Sasaki (2008) Atmospheric comparison of electrochemical cell ozonesondes from different maufacturers, and with different cathode solution strengths: The Balloon Experiment on Standards for Ozonsondes. J. Geophys. Res.113, D04307, doi:10.1029/2007JD008975

Emmons, L. K., D. P. Edwards, M. N. Deeter, J. C. Gille, T. Campos, P. Nédélec, P. Novelli, and G. Sachse, Measurements of Pollution In The Troposphere (MOPITT) validation through 2006 Atmos. Chem. Phys., 9, 1795-1803, 2009

Errera, Q., Daerden, F., Chabrillat, S., Lambert, J. C., Lahoz, W. A., Viscardy, S., Bonjean, S., and Fonteyn, D., 4D-Var Assimilation of MIPAS chemical observations: ozone and nitrogen dioxide analyses, Atmos. Chem. Phys., 8, 6169-6187, 2008.

Eskes, H., Huijnen, V., Arola, A., Benedictow, A., Blechschmidt, A.-M., Botek, E., Boucher, O., Bouarar, I., Chabrillat, S., Cuevas, E., Engelen, R., Flentje, H., Gaudel, A., Griesfeller, J., Jones, L., Kapsomenakis, J., Katragkou, E., Kinne, S., Langerock, B., Razinger, M., Richter, A., Schultz, M., Schulz, M., Sudarchikova, N., Thouret, V., Vrekoussis, M., Wagner, A., and Zerefos, C.: Validation of reactive gases and aerosols in the MACC global analysis and forecast system, Geosci. Model Dev., 8, 3523-3543, doi:10.5194/gmd-8-3523-2015, 2015.

Eskes, H.J., V. Huijnen, S, Basart, A. Benedictow, A.-M. Blechschmidt, S. Chabrillat, H. Clark, Y. Christophe, E. Cuevas, H. Flentje, K. M. Hansen, J. Kapsomenakis, B. Langerock, M. Ramonet, A. Richter, M. Schulz, A. Wagner, T. Warneke, C. Zerefos: Observations characterisation and validation methods document. Copernicus Atmosphere Monitoring Service (CAMS) report, CAMS84_2015SC1_D84.8.1_2016Q2_201603, March 2016. Available from: http://atmosphere.copernicus.eu/user-support/validation/verification-global-services

Flemming, J., Huijnen, V., Arteta, J., Bechtold, P., Beljaars, A., Blechschmidt, A.-M., Diamantakis, M., Engelen, R. J., Gaudel, A., Inness, A., Jones, L., Josse, B., Katragkou, E., Marecal, V., Peuch, V.-H., Richter, A., Schultz, M. G., Stein, O., and Tsikerdekis, A.: Tropospheric chemistry in the Integrated Forecasting System of ECMWF, Geosci. Model Dev., 8, 975-1003, doi:10.5194/gmd-8-975-2015, 2015.

Flemming, J., Benedetti, A., Inness, A., Engelen, R. J., Jones, L., Huijnen, V., Remy, S., Parrington, M., Suttie, M., Bozzo, A., Peuch, V.-H., Akritidis, D., and Katragkou, E.: The CAMS interim Reanalysis of Carbon Monoxide, Ozone and Aerosol for 2003–2015, Atmos. Chem. Phys., 17, 1945-1983, doi:10.5194/acp-17-1945-2017, 2017.

Granier, C. et al.: Evolution of anthropogenic and biomass burning emissions of air pollutants at global and regional scales during the 1980–2010 period. Climatic Change (109), 2011

Hubert, D., Lambert, J.-C., Verhoelst, T., Granville, J., Keppens, A., Baray, J.-L., Bourassa, A. E., Cortesi, U., Degenstein, D. A., Froidevaux, L., Godin-Beekmann, S., Hoppel, K. W., Johnson, B. J., Kyrölä, E., Leblanc, T., Lichtenberg, G., Marchand, M., McElroy, C. T., Murtagh, D., Nakane, H., Portafaix, T., Querel, R., Russell III, J. M., Salvador, J., Smit, H. G. J., Stebel, K., Steinbrecht, W., Strawbridge, K. B., Stübi, R., Swart, D. P. J., Taha, G., Tarasick, D. W., Thompson, A. M., Urban, J., van Gijsel, J. A. E., Van Malderen, R., von der Gathen, P., Walker, K. A., Wolfram, E., and Zawodny, J. M.: Ground-based assessment of the bias and long-term stability of 14 limb and occultation ozone profile data records, Atmos. Meas. Tech., 9, 2497-2534, doi:10.5194/amt-9-2497-2016, 2016.

Huijnen, V., et al.: The global chemistry transport model TM5: description and evaluation of the tropospheric chemistry version 3.0, Geosci. Model Dev., 3, 445-473, doi:10.5194/gmd-3-445-2010, 2010.

Huijnen, V., H.J. Eskes, A. Wagner, M. Schulz, Y. Christophe, M. Ramonet, S. Basart, A. Benedictow, A.-M. Blechschmidt, S. Chabrillat, H. Clark, E. Cuevas, H. Flentje, K.M. Hansen, U. Im, J. Kapsomenakis, B. Langerock, A. Richter, N. Sudarchikova, V. Thouret, T. Warneke, C. Zerefos, Validation report of the CAMS near-real-time global atmospheric composition service. System evolution and performance statistics; Status up to 1 June 2016, Copernicus Atmosphere Monitoring Service (CAMS) report, CAMS84_2015SC1_D.84.1.4_2016Q3_201609, September 2016.

Inness, A., Blechschmidt, A.-M., Bouarar, I., Chabrillat, S., Crepulja, M., Engelen, R. J., Eskes, H., Flemming, J., Gaudel, A., Hendrick, F., Huijnen, V., Jones, L., Kapsomenakis, J., Katragkou, E., Keppens, A., Langerock, B., de Mazière, M., Melas, D., Parrington, M., Peuch, V. H., Razinger, M., Richter, A., Schultz, M. G., Suttie, M., Thouret, V., Vrekoussis, M., Wagner, A., and Zerefos, C.: Data assimilation of satellite-retrieved ozone, carbon

monoxide and nitrogen dioxide with ECMWF's Composition-IFS, Atmos. Chem. Phys., 15, 5275-5303, doi:10.5194/acp-15-5275-2015, 2015.

Kaiser, J. W., Heil, A., Andreae, M. O., Benedetti, A., Chubarova, N., Jones, L., Morcrette, J.-J., Razinger, M., Schultz, M. G., Suttie, M., and van der Werf, G. R.: Biomass burning emissions estimated with a global fire assimilation system based on observed fire radiative power, Biogeosciences, 9, 527-554, doi:10.5194/bg-9-527-2012, 2012.

Lefever, K., van der A, R., Baier, F., Christophe, Y., Errera, Q., Eskes, H., Flemming, J., Inness, A., Jones, L., Lambert, J.-C., Langerock, B., Schultz, M. G., Stein, O., Wagner, A., and Chabrillat, S.: Copernicus stratospheric ozone service, 2009–2012: validation, system intercomparison and roles of input data sets, Atmos. Chem. Phys., 15, 2269-2293, doi:10.5194/acp-15-2269-2015, 2015.

Massart, S., Agusti-Panareda, A., Aben, I., Butz, A., Chevallier, F., Crevoisier, C., Engelen, R., Frankenberg, C., and Hasekamp, O.: Assimilation of atmospheric methane products into the MACC-II system: from SCIAMACHY to TANSO and IASI, Atmos. Chem. Phys., 14, 6139-6158, doi:10.5194/acp-14-6139-2014, 2014.

Massart, S., Agustí-Panareda, A., Heymann, J., Buchwitz, M., Chevallier, F., Reuter, M., Hilker, M., Burrows, J. P., Deutscher, N. M., Feist, D. G., Hase, F., Sussmann, R., Desmet, F., Dubey, M. K., Griffith, D. W. T., Kivi, R., Petri, C., Schneider, M., and Velazco, V. A.: Ability of the 4-D-Var analysis of the GOSAT BESD XCO_2 retrievals to characterize atmospheric CO_2 at large and synoptic scales, Atmos. Chem. Phys., 16, 1653-1671, doi:10.5194/acp-16-1653-2016, 2016.

Morcrette, J.-J., O. Boucher, L. Jones, D. Salmond, P. Bechtold, A. Beljaars, A. Benedetti, A. Bonet, J. W. Kaiser, M. Razinger, M. Schulz, S. Serrar, A. J. Simmons, M. Sofiev, M. Suttie, A. M. Tompkins, and A. Untch: Aerosol analysis and forecast in the ECMWF Integrated Forecast System. Part I: Forward modelling, J. Geophys. Res., 114, D06206, doi:10.1029/2008JD011235, 2009.

Richter, A., Burrows, J. P., Nüß, H., Granier, C, Niemeier, U.: Increase in tropospheric nitrogen dioxide over China observed from space, Nature, 437, 129-132, doi: 10.1038/nature04092, 2005

Sindelarova, K., Granier, C., Bouarar, I., Guenther, A., Tilmes, S., Stavrakou, T., Müller, J.-F., Kuhn, U., Stefani, P., and Knorr, W.: Global data set of biogenic VOC emissions calculated by the MEGAN model over the last 30 years, Atmos. Chem. Phys., 14, 9317-9341, doi:10.5194/acp-14-9317-2014, 2014.

Smit, H.G.J., W. Straeter, B.J. Johnson, S.J. Oltmans, J. Davies, D.W. Tarasick, B. Hoegger, R. Stubi, F.J. Schmidlin, T. Northam, A.M. Thompson, J.C. Witte, I. Boyd: Assessment of the performance of ECC-ozonesondes under quasi-flight conditions in the environmental simulation chamber: Insights from the Juelich Ozone Sonde Intercomparison Experiment (JOSIE), J. Geophys. Res. 112, D19306, doi:10.1029/2006JD007308, 2007.

Sofieva, V. F., Rahpoe, N., Tamminen, J., Kyrölä, E., Kalakoski, N., Weber, M., Rozanov, A., von Savigny, C., Laeng, A., von Clarmann, T., Stiller, G., Lossow, S., Degenstein, D., Bourassa, A., Adams, C., Roth, C., Lloyd, N., Bernath, P., Hargreaves, R. J., Urban, J., Murtagh, D., Hauchecorne, A., Dalaudier, F., van Roozendael, M., Kalb, N., and Zehner, C.: Harmonized dataset of ozone profiles from satellite limb and occultation measurements, Earth Syst. Sci. Data, 5, 349-363, doi:10.5194/essd-5-349-2013, 2013, http://www.earth-syst-sci-data.net/5/349/2013/.

Stein, O., Schultz, M. G., Bouarar, I., Clark, H., Huijnen, V., Gaudel, A., George, M., and Clerbaux, C.: On the wintertime low bias of Northern Hemisphere carbon monoxide found in global model simulations, Atmos. Chem. Phys., 14, 9295-9316, doi:10.5194/acp-14-9295-2014, 2014.

Tressol, M., C. Ordonez, R. Zbinden, J. Brioude, V. Thouret, C. Mari, P. Nedelec, J.-P. Cammas, H. Smit, H.-W. Patz, and A. Volz-Thomas, Air pollution during the 2003 European heat wave as seen by MOZAIC airliners,Atmos. Chem. Phys., 8, 2133-2150, doi:10.5194/acp-8-2133-2008, 2008.

van der A, R. J. , M. A. F. Allaart, and H. J. Eskes, Multi sensor reanalysis of total ozone, Atmos. Chem. Phys., 10, 11277–11294, doi:10.5194/acp-10-11277-2010, www.atmos- chem-phys.net/10/11277/2010/, 2010

van der A, R. J., Allaart, M. A. F., and Eskes, H. J.: Extended and refined multi sensor reanalysis of total ozone for the period 1970–2012, Atmos. Meas. Tech., 8, 3021-3035, doi:10.5194/amt-8-3021-2015, 2015.

Wittrock, F., A. Richter, H. Oetjen, J. P. Burrows, M. Kanakidou, S. Myriokefalitakis, R. Volkamer, S. Beirle, U. Platt, and T. Wagner, Simultaneous global observations of glyoxal and formaldehyde from space, Geophys. Res. Lett., 33, L16804, doi:10.1029/2006GL026310, 2006

Annex 1: Acknowledgements

Listed below are the authors contributing to the sections in this report. The authors contributing to the model description are also provided, as well as acknowledgements to the validation datasets.

Tropospheric reactive gases reactive gases

Annette Wagner, MPG (editor, O3 sondes, GAW data)
Hannah Clark, Valerie Thouret, CNRS-LA (IAGOS)
Harald Flentje, DWD (O3 sondes, GAW data)
Anne Blechschmidt and Andreas Richter, IUB Bremen (GOME-2 NO2, HCHO)
John Kapsomenakis, Christos Zerefos, AA (ESRL)
K. Petersen and N. Sudarchikova, satellite IR observations (MPG)
Kaj Hansen, Ulas Im, AU (Arctic theme)
Bavo Langerock, BIRA (NDACC)

Tropospheric aerosol

Michael Schulz, MetNo (editor, Aerocom, Aeronet)
Anna Benedictow, Jan Griesfeller, MetNo (Aerocom, Aeronet)
Sara Basart, M. Teresa Pay, Oriol Jorba, BSC-CNS (Aeronet, MODIS, AirBase, SDS-WAS NAMEE RC)
Emilio Cuevas, AEMET (Aeronet, MODIS, AirBase, SDS-WAS NAMEE RC)
Harald Flentje, DWD (Backscatter profiles)

Stratospheric reactive gases

Yves Christophe, Simon Chabrillat, BIRA (satellite observations)
Annette Wagner, MPI-M (O3 sondes)
Bavo Langerock, BIRA (NDACC FTIR, MWR, UVVIS DOAS, LIDAR)
Anne Blechschmidt and Andreas Richter, IUB-UB Bremen (SCIAMACHY NO2)

Greenhouse gases

Michel Ramonet, IPSL (ICOS)
Olivier Jossoud and Leonard Rivier, LSCE (ICOS)
Thorsten Warneke, UBC (TCCON)
Bavo Langerock, BIRA (TCCON)

Reactive gases and aerosol modeling

Antje Inness, Richard Engelen (ECMWF)
Vincent Huijnen (KNMI)

Acknowledgements for the validation datasets used

We are grateful to the numerous operators of the Aeronet network and to the central data processing facility at NASA Goddard Space Flight Center for providing the NRT sun photometer data, especially Ilya Slutker, David Giles and Brent Holben for sending the data.

The authors thank to all researchers, data providers and collaborators of the World Meteorological Organization's Sand and Dust Storm Warning Advisory and Assessment System (WMO SDS-WAS) for Northern Africa, Middle East and Europe (NAMEE) Regional Node. Also special thank to Canary Government as well as AERONET, MODIS, U.K. Met Office MSG, MSG Eumetsat and EOSDIS World Viewer principal investigators and scientists for establishing and maintaining data used in the activities of the WMO SDS-WAS NAMEE Regional Center (http://sds-was.aemet.es/).

We acknowledge the European Environment Information and Observation Network (Eionet) Air Quality portal which provides details relevant for the reporting of air quality information from EU Member States and other EEA member and co-operating countries. This information is submitted according to Directives 2004/107/EC and 2008/50/EC of the European Parliament and of the Council.

Also, we want to acknowledge the openair project (http://www.openair-project.org/) which is a Natural Environment Research Council (NERC) knowledge exchange project that aims to provide a collection of open-source tools for the analysis of air pollution data.

We wish to acknowledge the provision of ozone sonde data by the World Ozone and Ultraviolet Radiation Data Centre established at EC in Toronto (http://woudc.org), by the Data Host Facility of the Network for the Detection of Atmospheric Composition Change established at NOAA (http://ndacc.org), by the Norwegian Institute for Air Research and by the National Aeronautics and Space Administration (NASA).

We wish to thank the NDACC investigators for the provision of observations at Ny Alesund, Bern, Jungfraujoch, Izaña, Reunion Maido, Hohenpeissen, Mauna Loa, Lauder.

We wish to thank ESA for providing the HARMonized dataset of Ozone profiles (HARMOZ).

We acknowledge the strong support of the European Commission, Airbus, and the airlines (Lufthansa, Air France, Austrian, Air Namibia, Cathay Pacific, Iberia and China Airlines so far) which have carried the MOZAIC or IAGOS equipment and undertaken maintenance since 1994. In its last 10 years of operation, MOZAIC has been funded by INSU-CNRS (France), Météo-France, Université Paul Sabatier (Toulouse, France) and Research Center Jülich (FZJ, Jülich, Germany). IAGOS has been additionally funded by the EU projects IAGOS-DS and IAGOS-ERI. The MOZAIC–IAGOS database is supported by AERIS (CNES and INSU-CNRS).

The authors acknowledge the provision of Global Atmosphere Watch (GAW) data by the World Data Centre for Greenhouse Gases (WDCGG).

We wish to acknowledge the provision of ozone sonde data by the World Ozone and Ultraviolet Radiation Data Centre established at EC in Toronto (https//woudc.org), by the Data Host Facility of the Network for the Detection of Atmospheric Composition Change established at NOAA

(http://ndacc.org), by the Norwegian Institute for Air Research (http://www.nilu.no/) and by the National Aeronautics and Space Administration NASA (https://tropo.gsfc.nasa.gov/shadoz/).

The authors acknowledge the European Monitoring and Evaluation Programme (EMEP; http://www.emep.int/) for the provision of ground based ozone concentrations.

The MOPITT CO data were obtained from the NASA Langley Research Center ASDC. We acknowledge the LATMOS IASI group for providing IASI CO data.

SCIAMACHY lv1 radiances were provided to IUP-UB by ESA through DLR/DFD.

The authors acknowledge Environment and Climate Change Canada for the provision of Alert ozone data and Sara Crepinsek – NOAA for the provision of Tiksi ozone data. Surface ozone data from the Zeppelin Mountain, Svalbard are from www.luftkvalitet.info. Surface ozone data from the Villum Research Station, Station Nord (VRS) were financially supported by "The Danish Environmental Protection Agency" with means from the MIKA/DANCEA funds for Environmental Support to the Arctic Region. The Villum Foundation is acknowledged for the large grant making it possible to build VRS in North Greenland.

We acknowledge the University of Saskatchewan, Canada for providing the OSIRIS (http://osirus.usas.ca/) observations data and the Canadian Space Agency and science teams for providing validation observations by ACE-FTS on the Canadian satellite SCISAT-1.

We acknowledge the provision of CO_2/CH_4 data from SNO-RAMCES/ICOS network coordinated by LSCE/OVSQ (CEA-CNRS-UVSQ, Université Paris-Saclay), as well as Laboratorio de Física de la Atmósfera (UMSA, Bolivia), Environmental Chemical Processes Laboratory (ECPL/UoC, Greece), Station Géophysique de LAMTO, Ivory Coast), C-CAPS/NUIG/EPA (Ireland), BIRA-IASB (Belgium) and the following research institutes in France: LaMP/OPGC, P2OA/LA/OMP, OPE/ANDRA, OHP/PYTHEAS, OPAR/LACY/OSUR, UMR EcoFoG, IPEV, IRD.

Copernicus Atmosphere Monitoring Service

ECMWF - Shinfield Park, Reading RG2 9AX, UK

Contact: info@copernicus-atmosphere.eu